RESULTS AND DISCUSSION

SECTION (A)

STUDYING THE CORROSION BEHAVIOR OF COPPER BY THE WEIGHT LOSS METHOD

To evaluate the influence of quinazoline compounds on the corrosion of copper in 2M HNO_3 acid, the weight-loss technique was employed as the chemical testing technique.

3.1-CORROSION INHIBITION BEHAVIOR

The corrosion behavior of a metal in an aqueous environment is characterized by the extent to which it dissolves in the solution. This can be quantified by using the simple relationship:

$$W_o = W_B - W_A$$

where:

W_o= weight of metal loss in the corrosive solution.

W_B= weight of metal before exposure to the corrosive solution

$W_{A=}$ weight of metal after exposure to the corrosive solution

The degree of dissolution, of course, dependent on the surface area of the metal exposed and the time of exposure; hence the corrosion rate is given with respect to area and time.

$$\text{Corrosion rate} = \frac{W_o}{A\ t} \qquad (3.1)$$

where:

A: is the area of electrode in cm^2.

t :is the time immersion in min.

The weight-loss method is usually preferred because the quantity measured is directly related to the extent of corrosion and does not rely on any assumptions about reactions occurring during corrosion.

Figures (3.1-3.5) show the weight loss-time curves for copper in 2M nitric acid in absence and presence of different concentrations of quinazoline compounds. As shown from these Figs, by increasing the concentration of these compounds, the weight loss of copper samples are decreased. This means that the presence of these compounds retards the corrosion of copper in 2M nitric acid or in other words, these compounds act as inhibitors.

The percentage inhibition efficiencies (%IE) of quinazoline compounds were determined by using the equation:

$$\%IE = \left(1 - \frac{W_{inh}}{W_{free}}\right) \times 100 \qquad (3.2)$$

where:

W_{inh} : is the weight loss of the metal in presence of inhibitor.

W_{free}: is the weight loss of the metal in absence of inhibitor.

And the surface coverage (θ) can be calculated from the following equation

$$\theta = \frac{I.E}{100} \qquad (3.3)$$

From the calculated values of %IE given in Table (3.1), the order of the inhibition efficiencies of quinazoline compounds is as follow:

$$5 > 4 > 3 > 2 > 1$$

It is obvious from Table (3.1) that the inhibition efficiency of quinazoline compounds increases with increasing the concentration of these compounds.

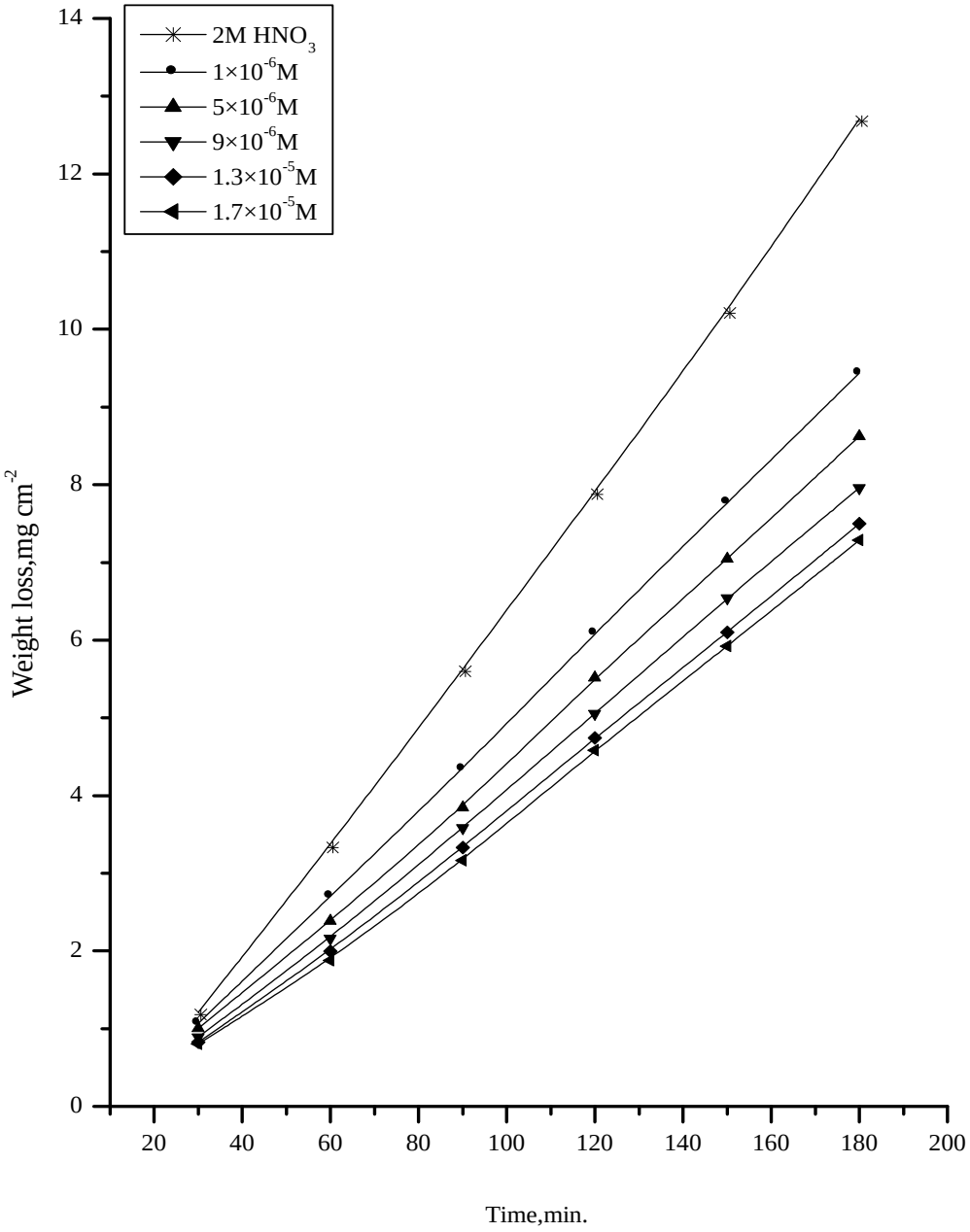

Fig.(3.1): Weight loss-time curves for copper in 2M HNO_3 in absence and presence of different concentrations of compound (1) at 30°C.

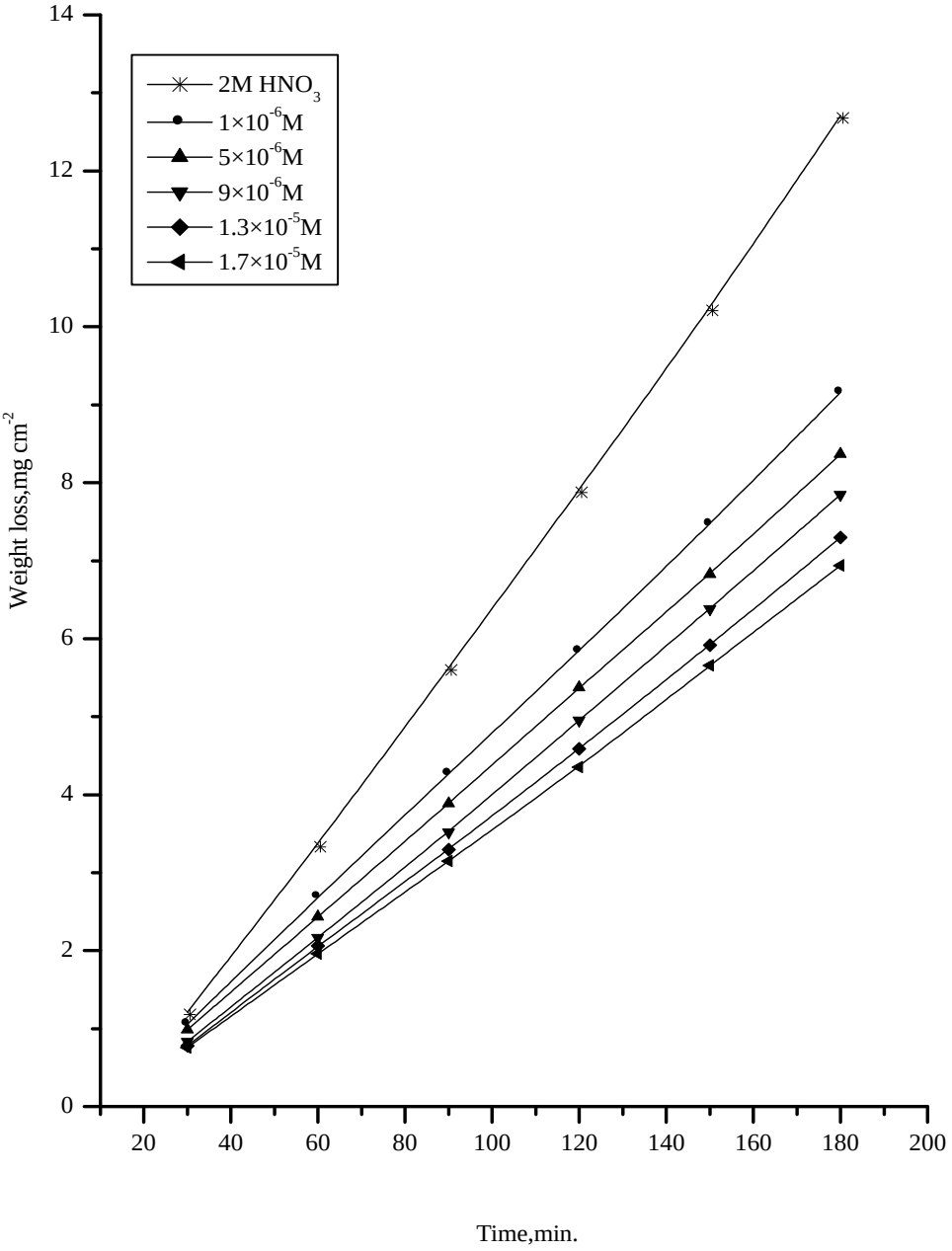

Fig.(3.2):Weight loss-time curves for copper in 2M HNO_3 in presence and absence of different concentration of compound (2) at 30 C.

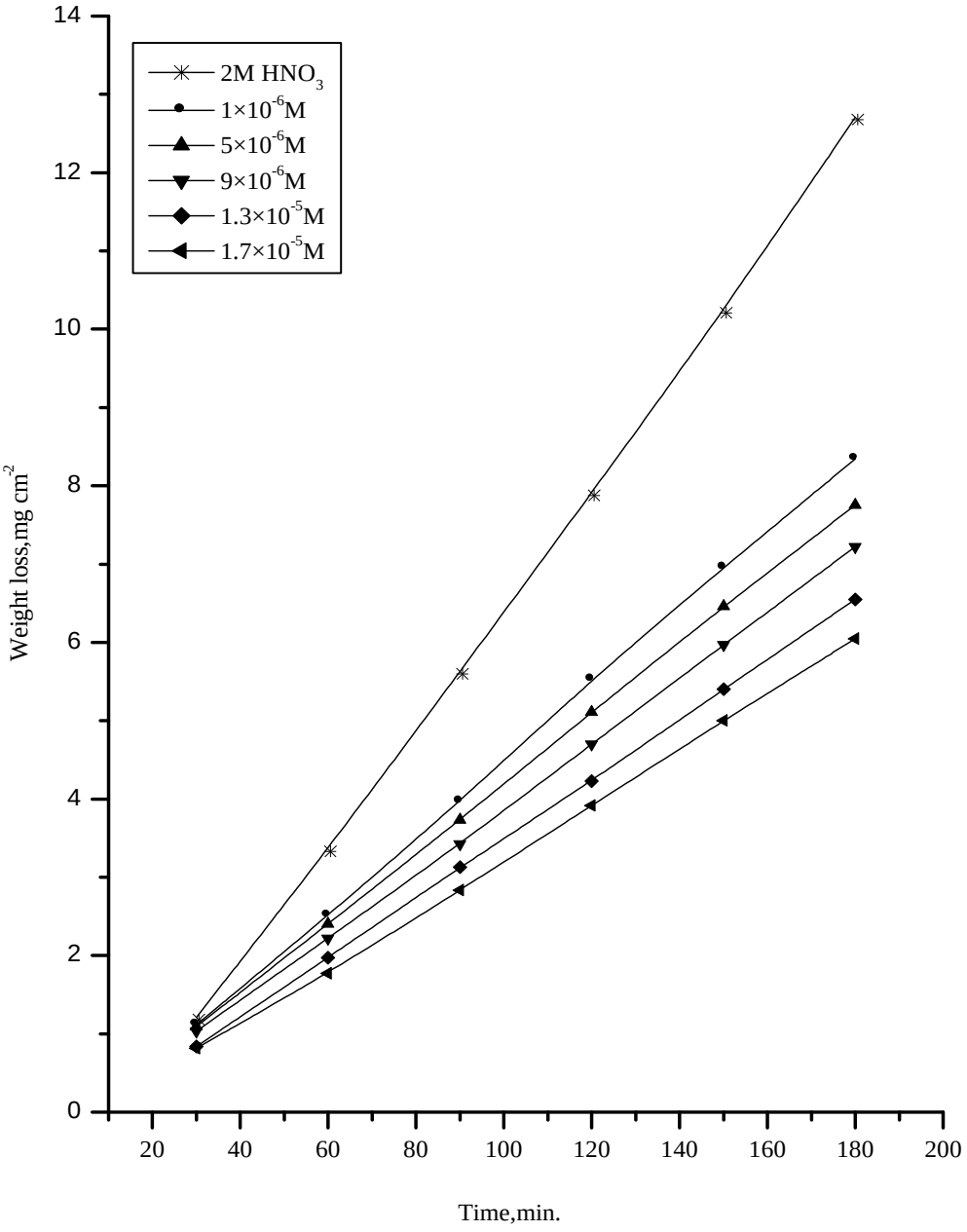

Fig.(3.3):Weight loss-time curves for copper in 2M HNO_3 in presence and absence of different concentration of compound (3) at 30°C.

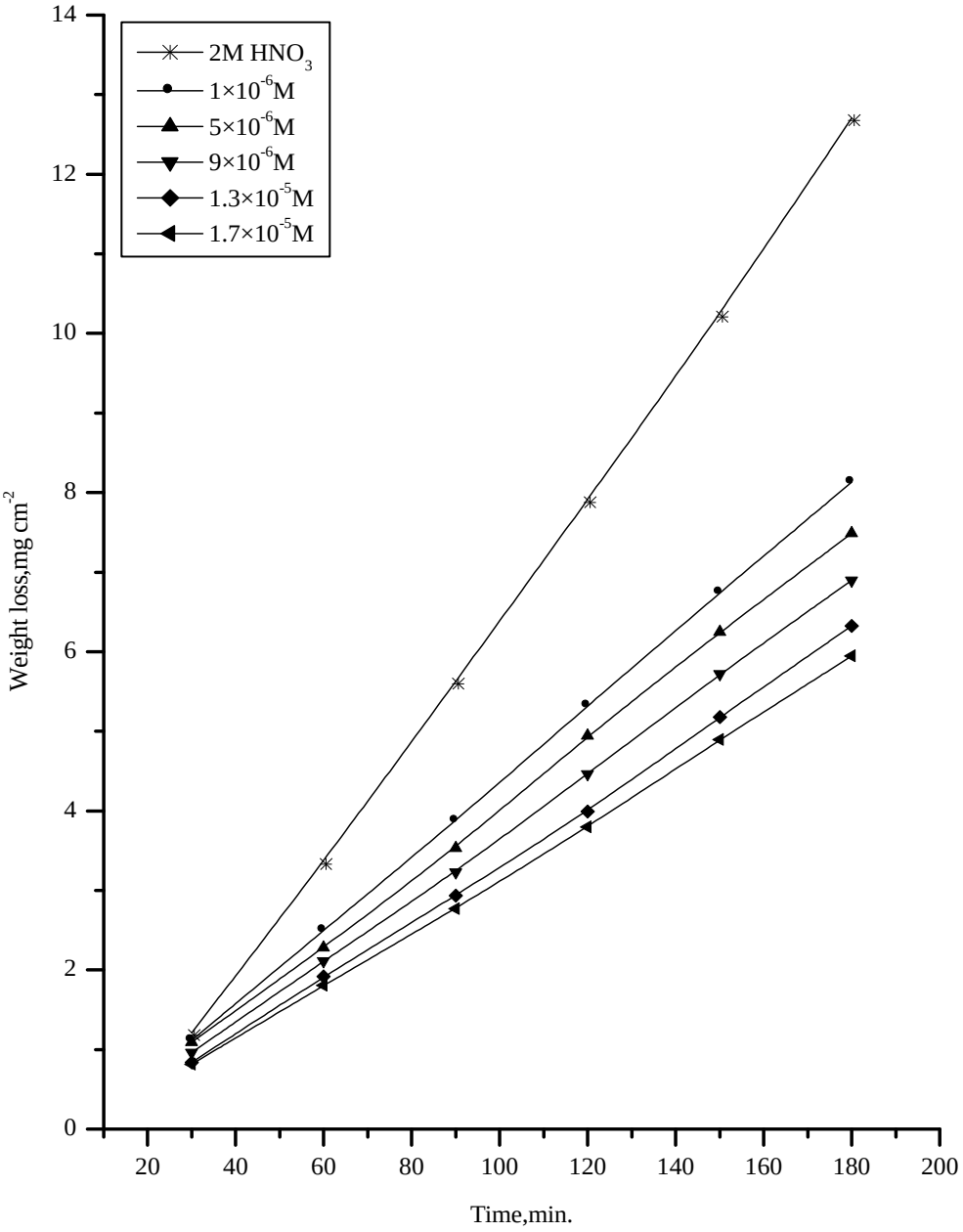

Fig.(3.4): Weight loss-time curves for copper in 2M HNO_3 in absence and presence of different concentrations of compound (4) at 30°C.

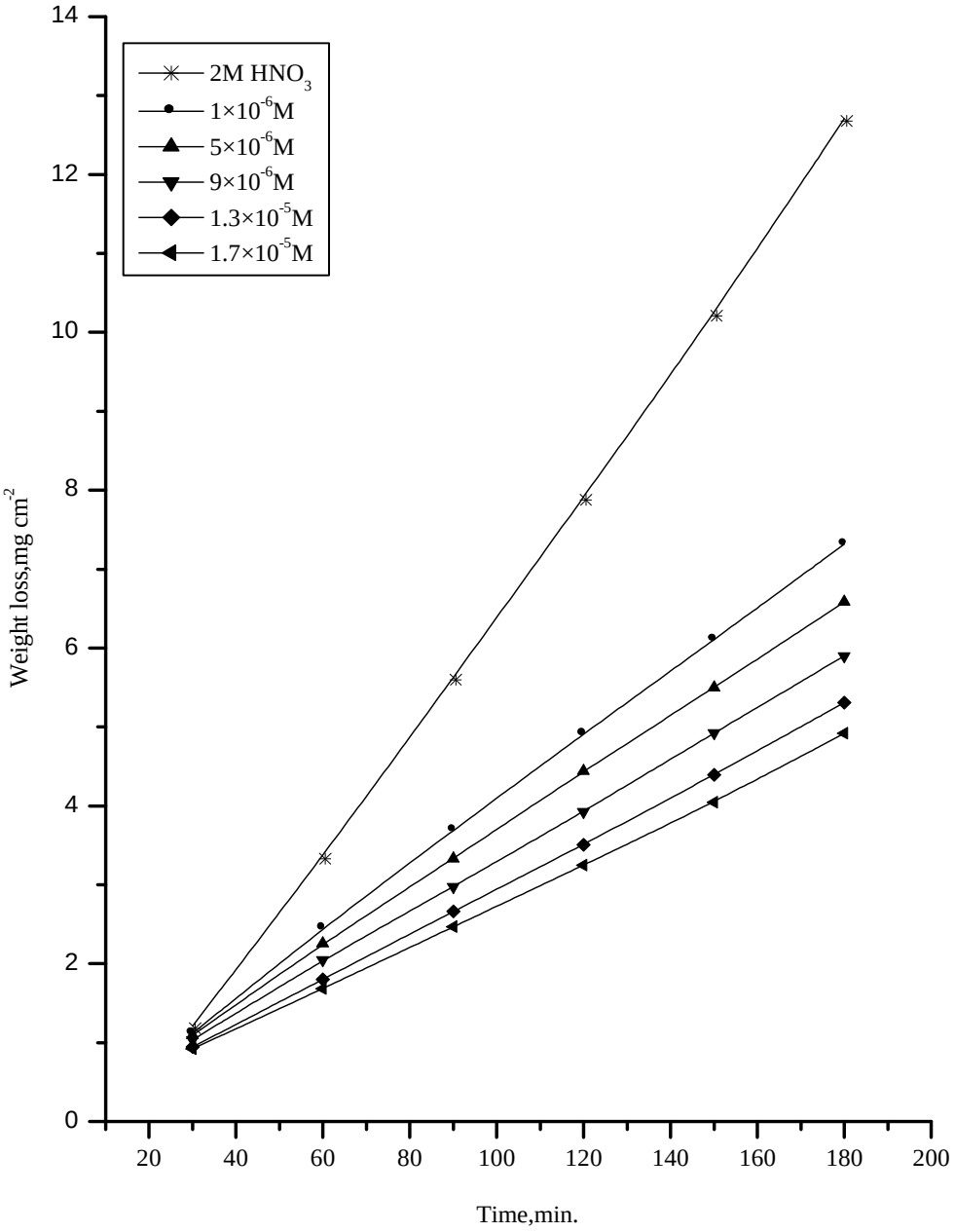

Fig.(3.5): Weight loss-time curves for copper in 2M HNO_3 in absence and presence of different concentrations of compound (5) at 30°C.

Table (3.1): Inhibition efficiency at different concentrations of inhibitors as determined from weight loss method at 30°C.

Conc., M	%Inhibition				
	Compound (1)	Compound (2)	Compound (3)	Compound (4)	Compound (5)
$1x10^{-6}$	23.00	26.09	30.09	32.67	37.85
$5x10^{-6}$	30.25	32.06	35.36	37.50	43.82
$9x10^{-6}$	36.08	37.32	40.55	43.50	50.35
$1.3x10^{-5}$	40.00	42.00	46.50	49.50	55.60
$1.7x10^{-5}$	42.01	44.98	50.50	52.01	58.90

3.2-ROLE OF ANIONS IN CORROSION-INHIBITION OF COPPER IN ACIDIC SOLUTIONS AND SYNERGISTIC EFFECT.

The effect of Cl^- and Br^- ions on the corrosion inhibition of copper in 2M HNO_3 solution in presence and absence of the quinazoline compounds was studied by weight loss method. Figs. (3.6-3.15) represents the weight loss - time curves for copper dissolution in 2M HNO_3 in presence of $1x10^{-4}$M Cl^-, Br^- and also in presence of different concentrations of quinazoline compounds.

The values of inhibition efficiency (%IE) for various concentrations of inhibitors in the presence of specific concentrations of these anions ($1x10^{-4}$M Cl^-, Br^-) are given in Tables (3.2 and 3.4).

It is observed that %IE of the inhibitors increases by the addition of these different anions due to synergistic effect [53].The strong chemisorption of these ions in combination with cation of the inhibitor. The cation is then adsorbed by coulombic attraction on the metal surface where these anions are already adsorbed by chemisorption. Stabilization of these adsorbed anions with cations leads to greater surface coverage and therefore greater inhibition.

The synergistic inhibition effect was evaluated using a parameter, S_θ, obtained from the surface coverage values (θ) of the anion, cation, and both.

Aramaki and Hackerman [54] calculated the synergism parameter S_θ using the following equation.

$$S_\theta = 1-\theta_{1+2} / 1-\theta`_{1+2} \quad (3.9)$$

Where:

$\theta_{1+2} = (\theta_1 + \theta_2) - (\theta_1\theta_2)$

θ_1 = surface coverage by anions.

θ_2 = surface coverage by cations.

$\theta`_{1+2}$ = measured surface coverage by both the anion and cations.

We calculate synergism parameters for various concentrations of inhibitors in the presence of specific concentrations of (1x10-4M Cl-, Br-) from the above equation and their corresponding values are shown in Tables (3.3) and (3.5). As can be seen from this table, value of S_θ are nearly equal to unity, which suggests that the enhanced inhibition efficiencies caused by the addition of chloride and bromide ions to quinazoline compounds is due mainly to the synergistic effect.

The net increment of inhibition efficiency shows a synergistic effect of KBr and KCl with quinazoline compounds.

The synergistic effect depends on the type and concentration of anions. The adsorption ability on the copper surfaces was in the order KBr> KCl.

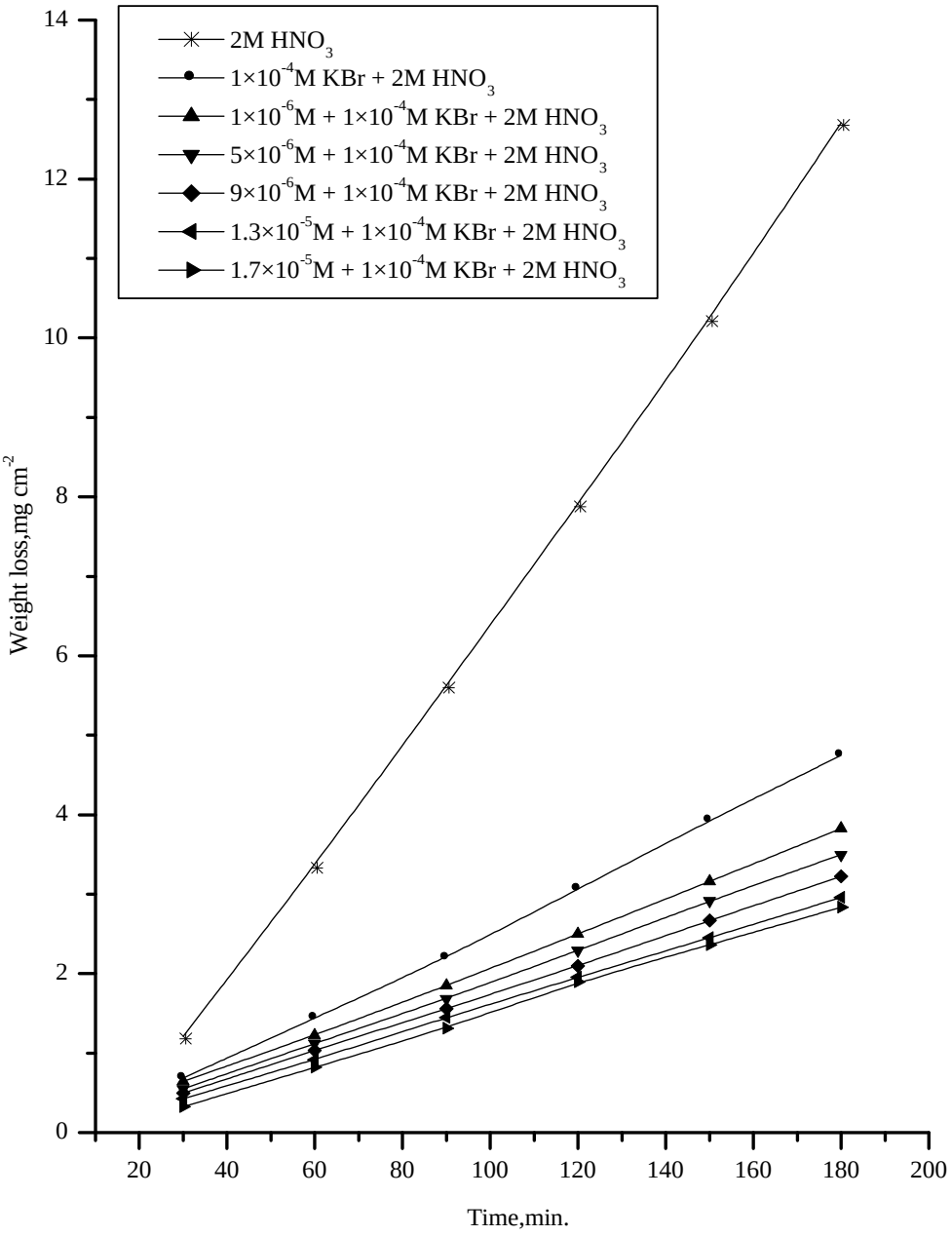

Fig.(3.6): Weight loss-time curves for copper in 2M HNO_3 in absence and presence of different concentrations of compound (1) and 1X10-4 M KBr at 30°C.

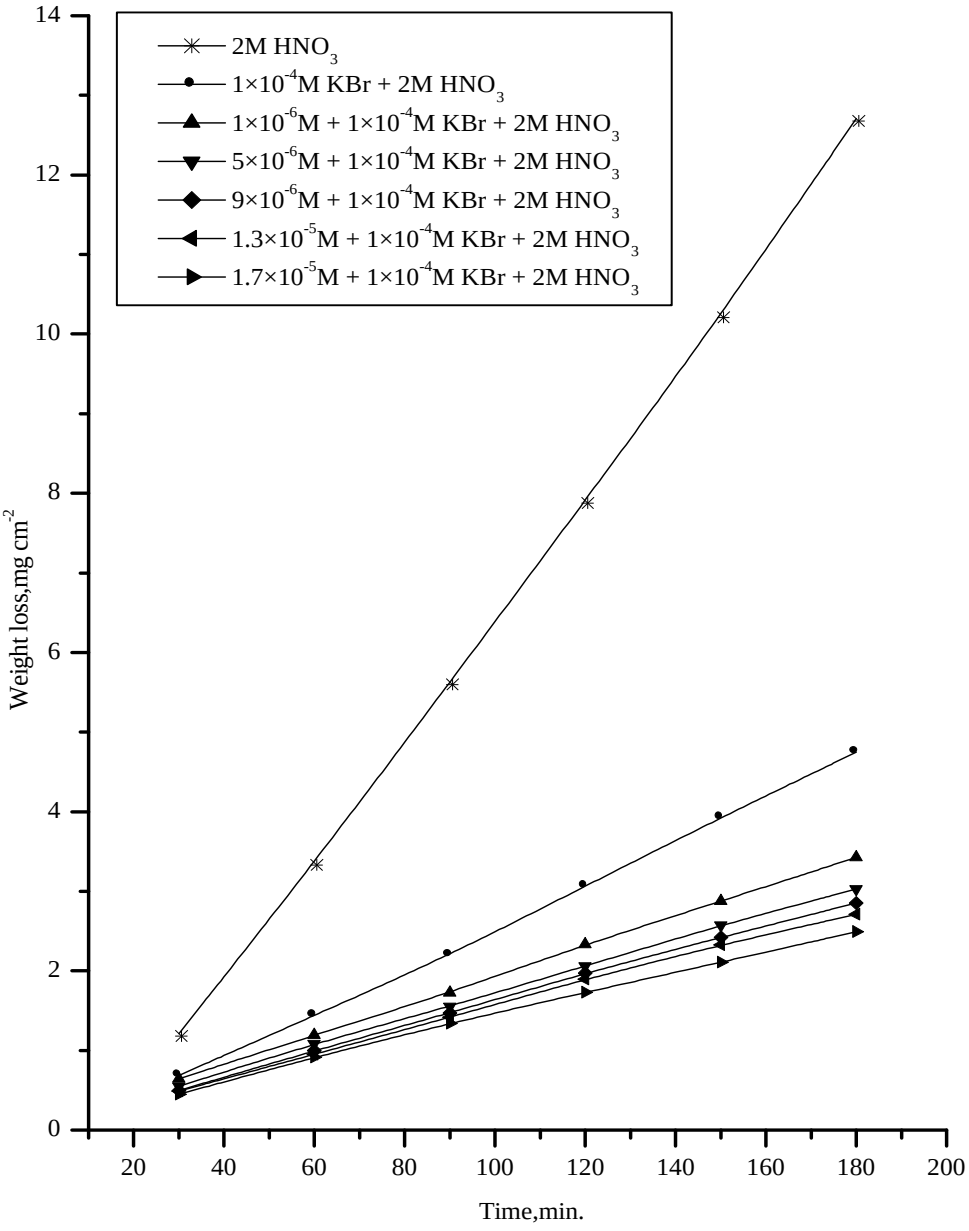

Fig.(3.7): Weight loss-time curves for copper in 2M HNO_3 in absence and presence of different concentrations of compound (2) and 1X10-4 M KBr at 30°C.

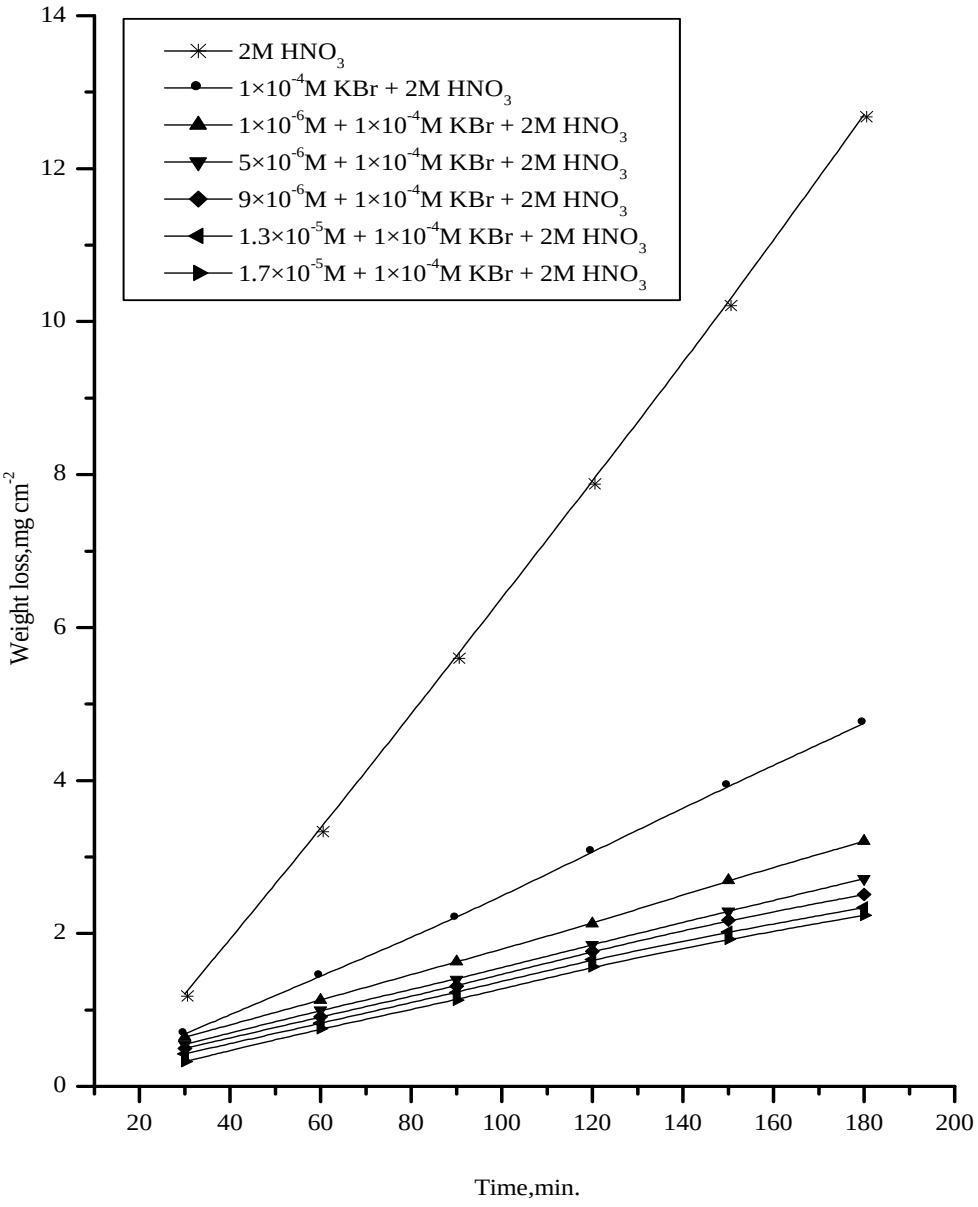

Fig.(3.8): Weight loss-time curves for copper in 2M HNO_3 in absence and presence of different concentrations of compound (3) and 1X10-4 M KBr at 30°C.

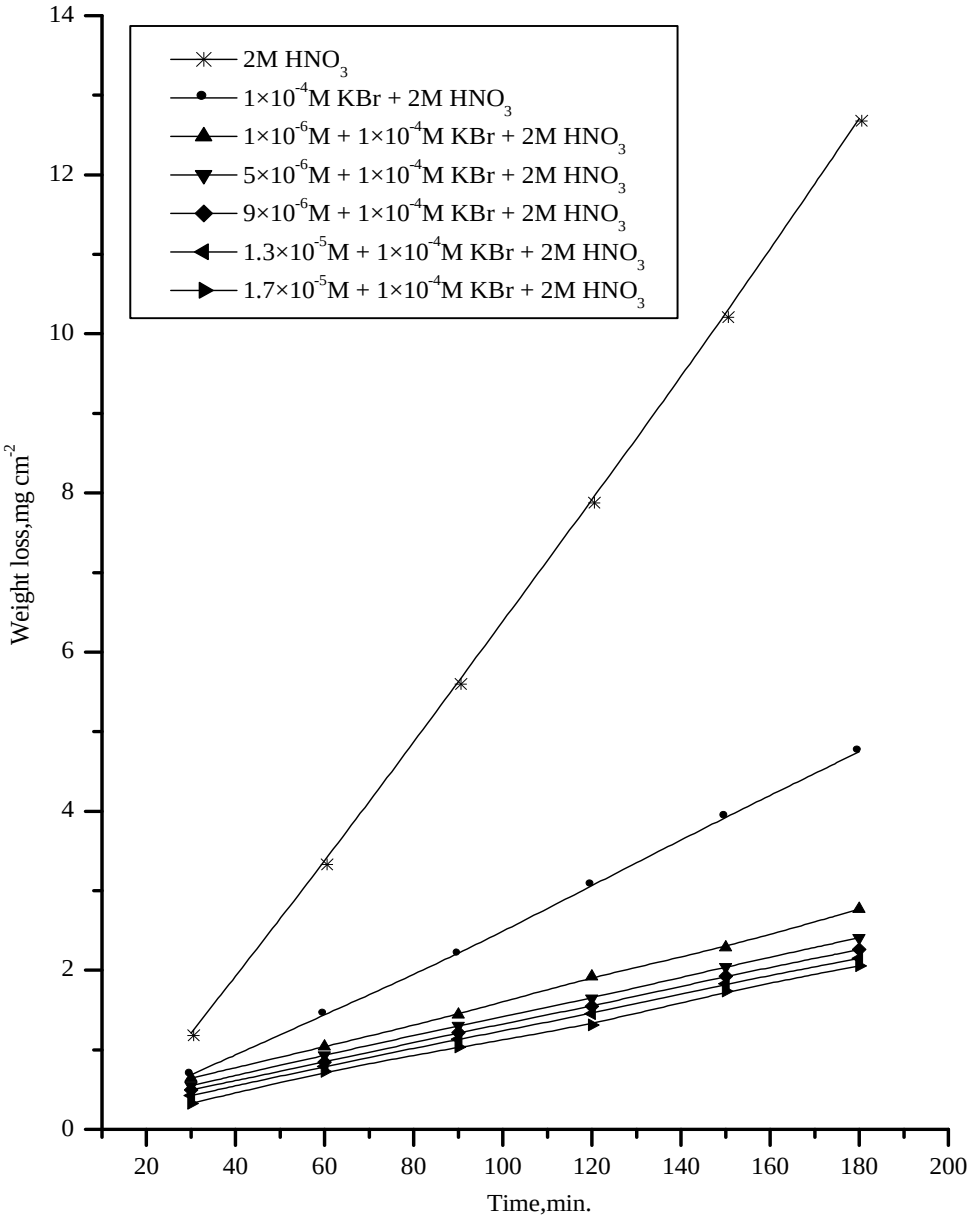

Fig.(3.9): Weight loss-time curves for copper in 2M HNO_3 in absence and presence of different concentrations of compound (4) and 1X10-4 M KBr at 30°C.

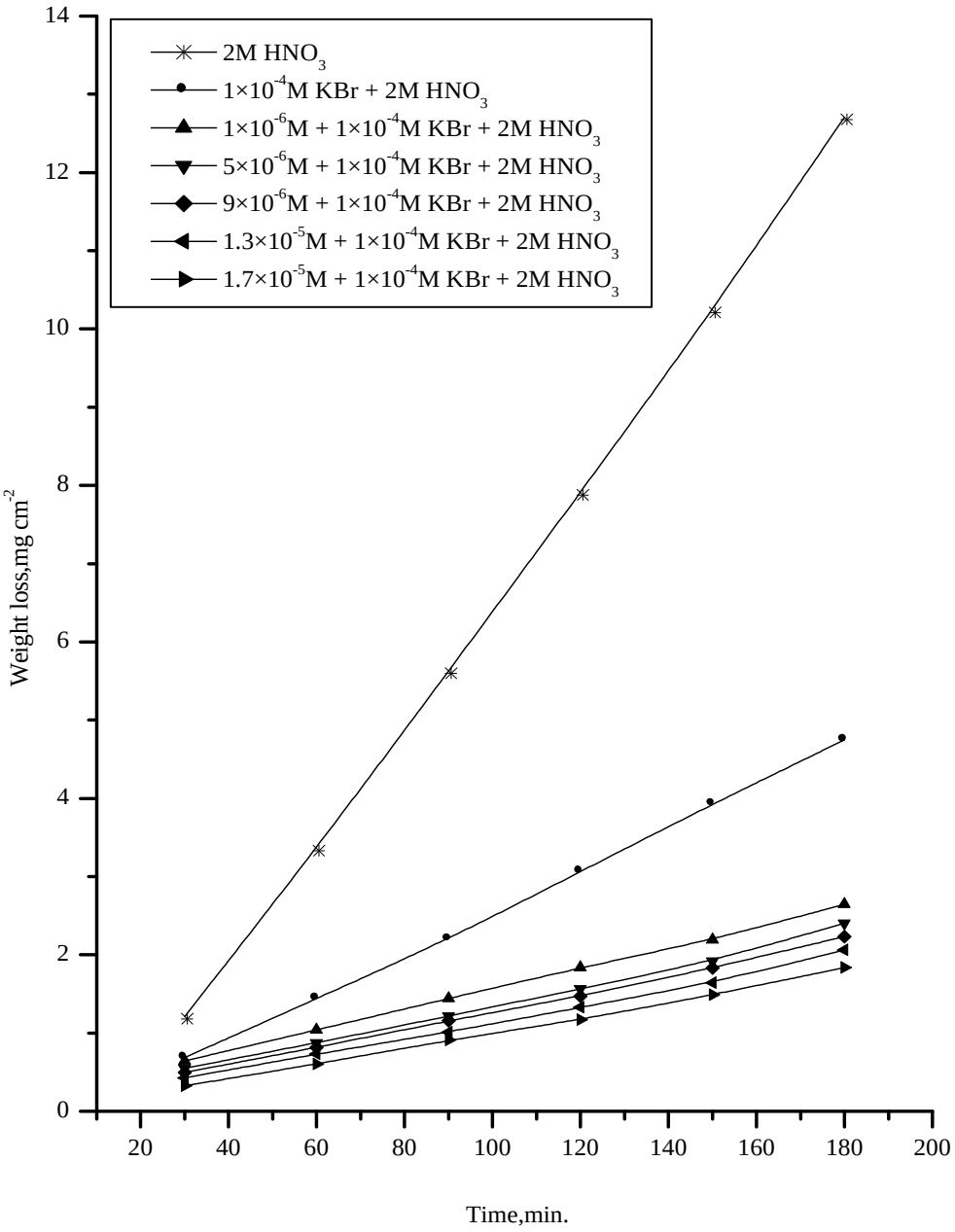

Fig.(3.10): Weight loss-time curves for copper in 2M HNO_3 in absence and presence of different concentrations of compound (5) and $1X10^{-4}$ M KBr at 30°C.

Table (3.2): Inhibition efficiency at different concentrations of inhibitors + 1 x 10^{-4} M KBr as determined from weight loss method at 30°C.

Conc., M	%Inhibition				
	Compound (1)	Compound (2)	Compound (3)	Compound (4)	Compound (5)
$1x10^{-6}$	68.38	70.48	73.12	75.76	76.81
$5x10^{-6}$	71.05	73.91	76.55	79.18	80.24
$9x10^{-6}$	73.48	75.08	77.69	80.45	81.38
$1.3x10^{-5}$	75.27	75.99	79.01	81.63	83.22
$1.7x10^{-5}$	76.02	78.13	80.24	83.40	85.24

Table (3.3): Synergistic parameter (S_θ) at different concentrations of all investigated inhibitors in 2M HNO_3 in presence of $1x10^{-4}$ M of KBr.

Conc., M	S_θ				
	Compound (1)	**Compound (2)**	**Compound (3)**	**Compound (4)**	**Compound (5)**
$1x10^{-6}$	0.94	0.93	0.99	1.05	1.09
$5x10^{-6}$	0.92	0.98	1.08	1.14	1.20
$9x10^{-6}$	0.93	0.96	1.04	1.12	1.17
$1.3x10^{-5}$	0.94	0.94	0.99	1.07	1.17
$1.7x10^{-5}$	0.91	0.92	0.97	1.06	1.19

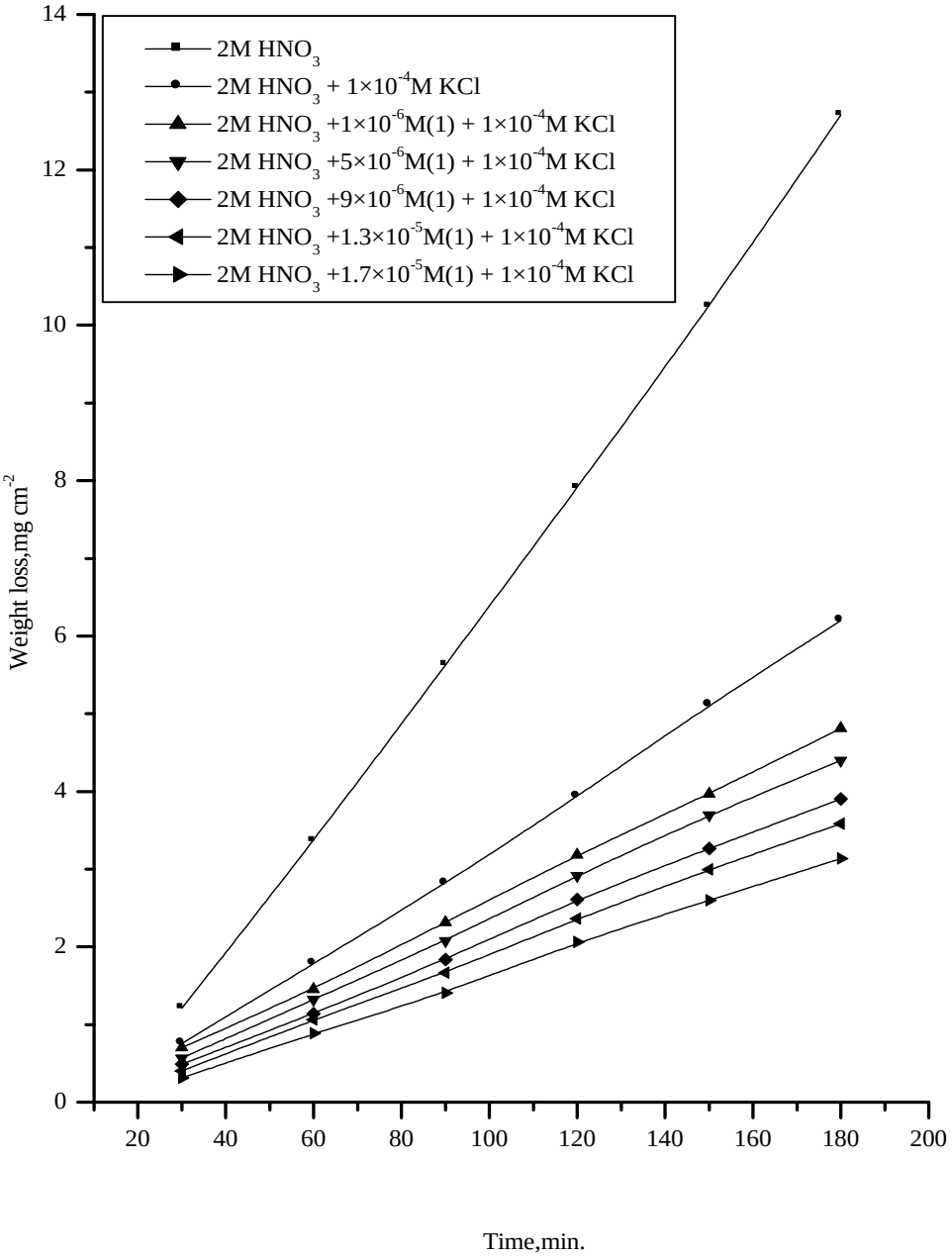

Fig.(3.11): Weight loss-time curves for copper in 2M HNO_3 in absence and presence of different concentrations of compound (1) and $1X10^{-4}$ M KCl at 30°C.

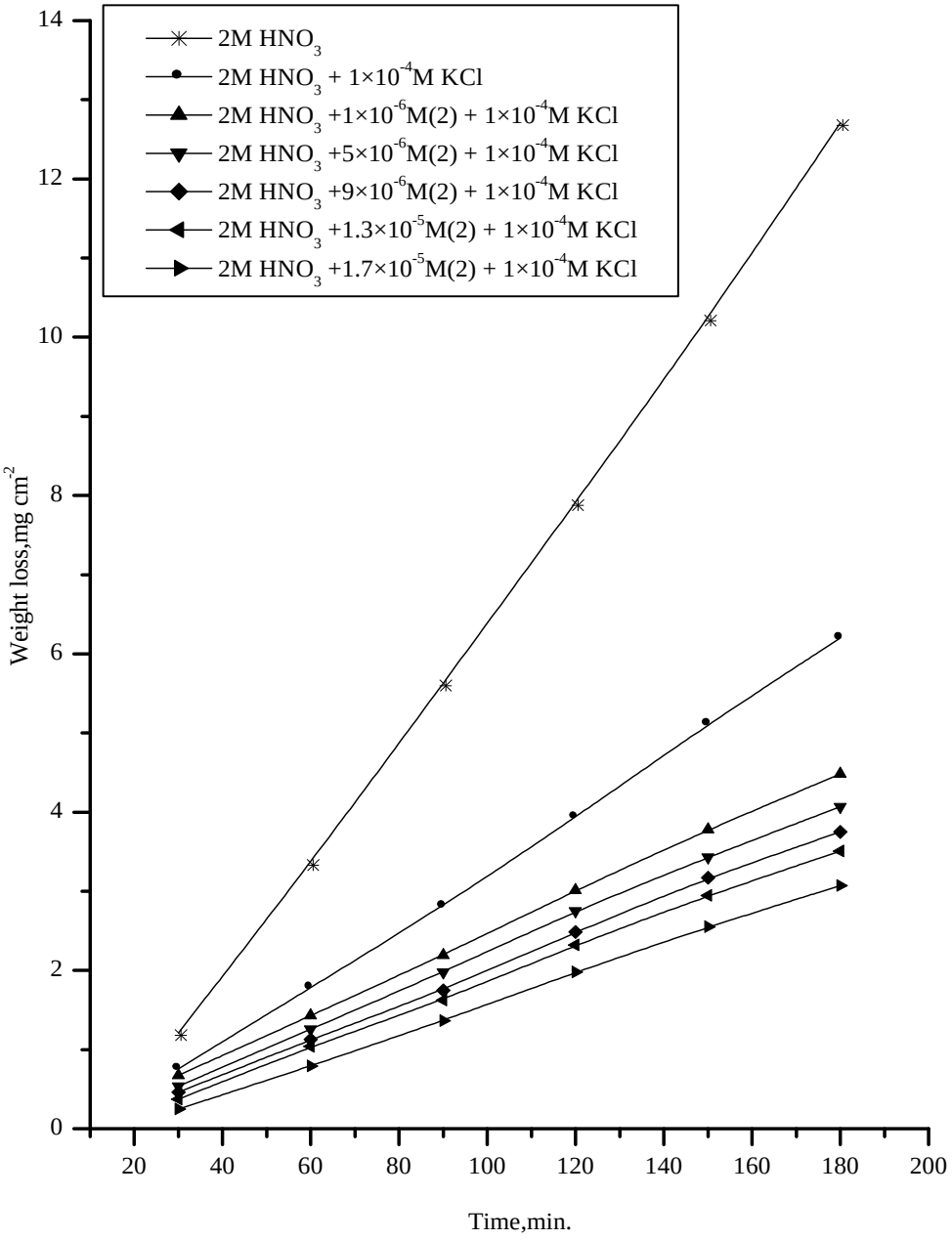

Fig.(3.12): Weight loss-time curves for copper in 2M HNO_3 in absence and presence of different concentrations of compound (2) and $1X10^{-4}$ M KCl at 30°C.

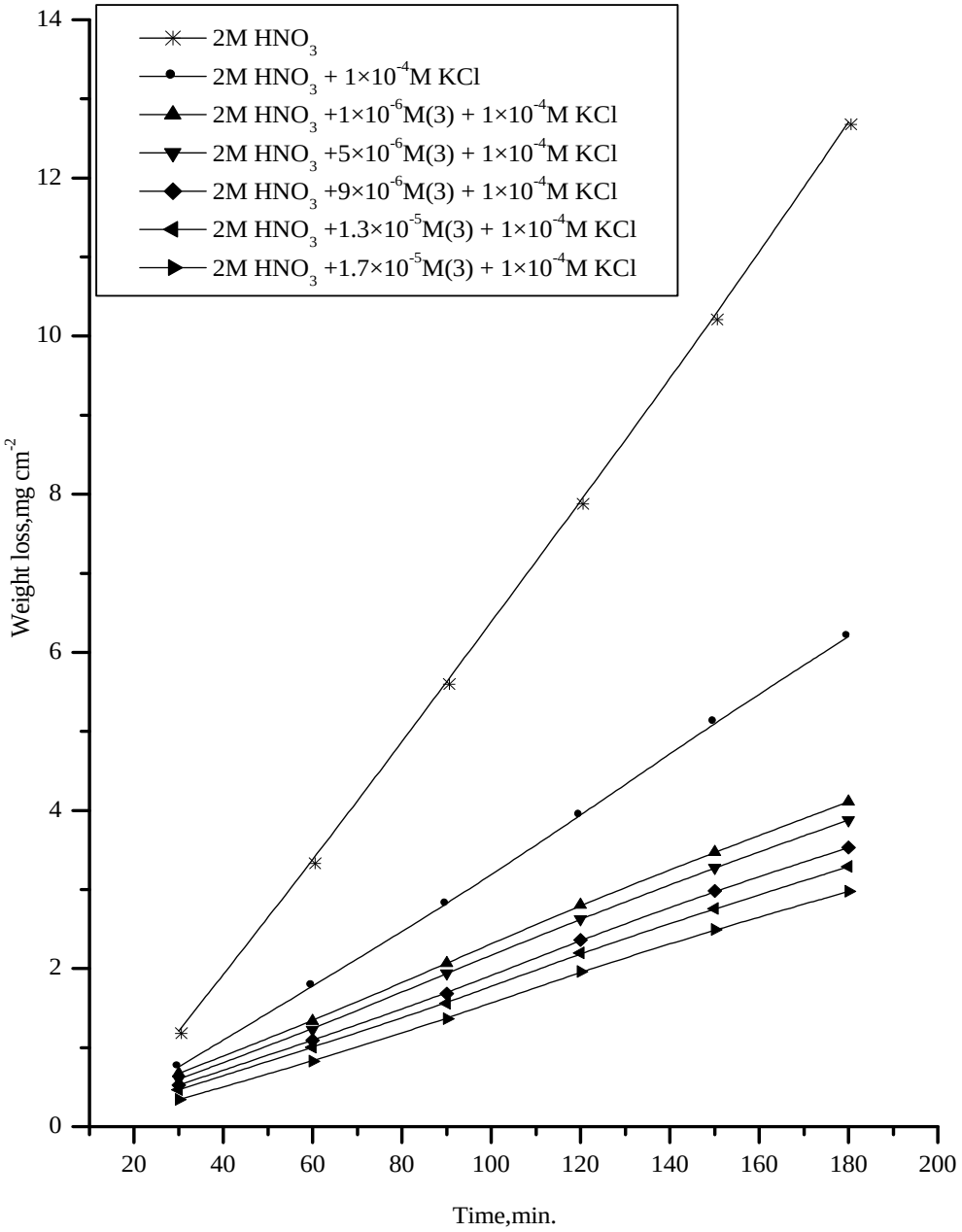

Fig.(3.13): Weight loss-time curves for copper in 2M HNO_3 in absence and presence of different concentrations of compound (3) and $1X10^{-4}$ M KCl at 30°C.

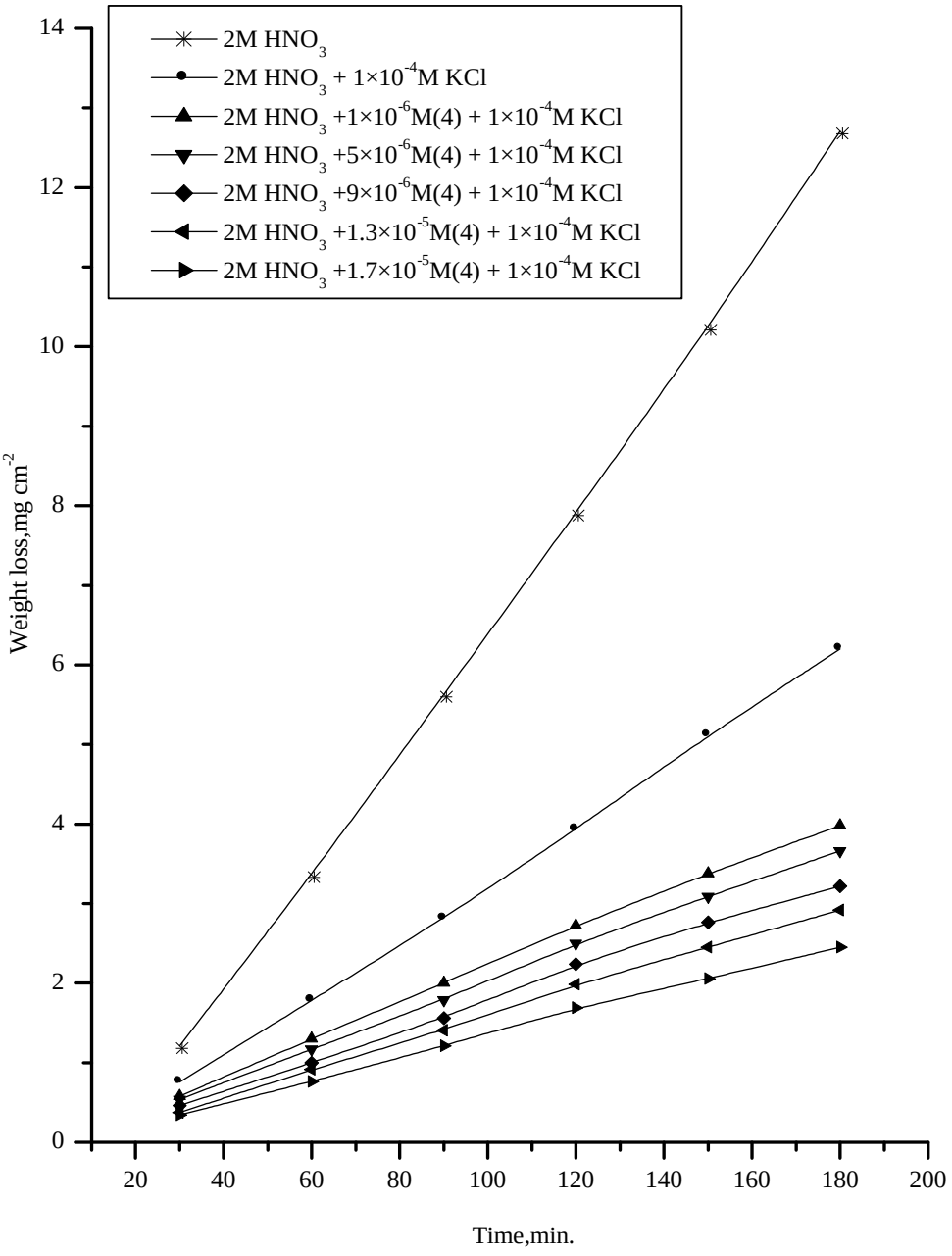

Fig.(3.14): Weight loss-time curves for copper in 2M HNO_3 in absence and presence of different concentrations of compound (4) and $1X10^{-4}$ M KCl at 30°C.

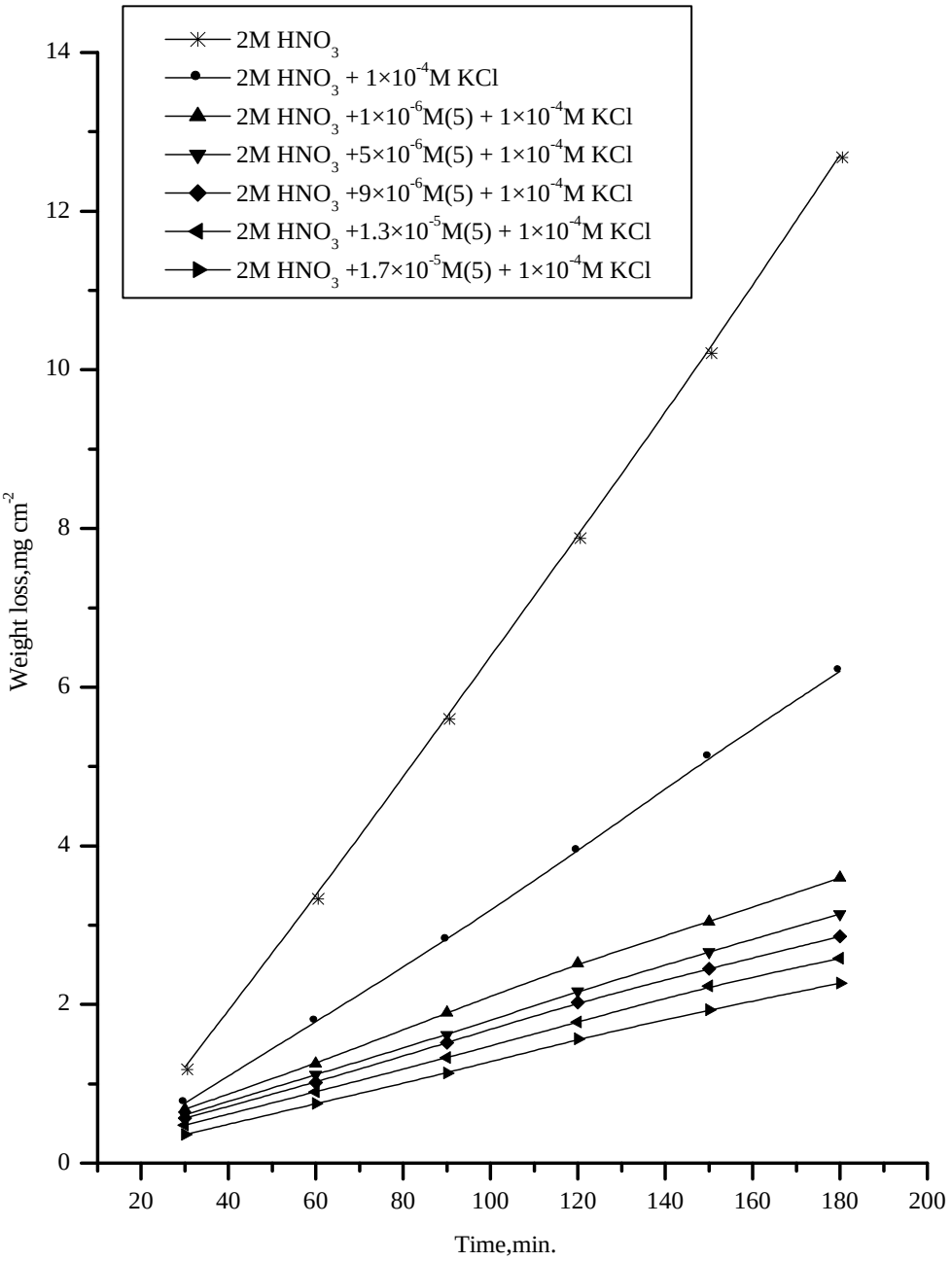

Fig.(3.15): Weight loss-time curves for copper in 2M HNO_3 in absence and presence of different concentrations of compound (5) and $1X10^{-4}$ M KCl at 30°C.

Table (3.4): Inhibition efficiency at different concentrations of inhibitors + 1 x 10^{-4} M KCl as determined from weight loss method at 30°C.

Conc., M	%Inhibition				
	Compound (1)	**Compound (2)**	**Compound (3)**	**Compound (4)**	**Compound (5)**
$1x10^{-6}$	59.77	61.88	64.51	65.56	68.20
$5x10^{-6}$	63.13	65.21	66.80	68.38	72.59
$9x10^{-6}$	66.97	68.55	70.13	71.71	74.35
$1.3x10^{-5}$	70.11	70.66	72.24	74.88	77.51
$1.7x10^{-5}$	73.91	74.96	75.21	78.65	80.23

Table.(3.5): Synergistic parameter (S_θ) at different concentrations of all investigated inhibitors in 2M HNO_3 in presence of $1x10^{-4}$ M of KCl.

Conc., M	S_θ				
	Compound (1)	**Compound (2)**	**Compound (3)**	**Compound (4)**	**Compound (5)**
$1x10^{-6}$	0.81	0.93	0.96	0.95	0.61
$5x10^{-6}$	0.82	0.94	0.98	0.96	0.85
$9x10^{-6}$	0.85	0.97	1.00	0.99	0.89
$1.3x10^{-5}$	0.84	0.98	0.96	1.00	0.86
$1.7x10^{-5}$	0.87	1.03	0.99	1.06	0.87

3.3-ADSORPTION ISOTHERM

Organic molecules as quinazoline molecules inhibit the corrosion of copper in 2M HNO_3 by the adsorption on metal surface. Theoretically, the adsorption process can be regarded as a single substitutional process in which an inhibitor molecule, I, in the aqueous phase substitutes an "x" number of water molecules adsorbed on the metal surface [55] vis,

$$I_{(aq)} + xH_2O_{(sur)} \longrightarrow I_{(sur)} + xH_2O_{(aq)} \qquad (3.3)$$

where x is known as the size ratio and simply equals the number of adsorbed water molecules replaced by a single inhibitor molecule. The adsorption depends on the structure of the inhibitor, the type of the metal and the nature of its surface, the nature of the corrosion medium and its pH value, the temperature and the electrochemical potential of the metal-solution interface. Also, the adsorption provides information about the interaction among the adsorbed molecules themselves as well as their interaction with the metal surface. Actually an adsorbed molecule may make the surface more difficult or less difficult for another molecule to become attached to a neighboring site and multilayer adsorption may take place. There may be more or less than one inhibitor molecule per surface site. Finally, various surface sites could have varying degrees of activation. For these reasons a number of mathematical adsorption isotherm expressions have been developed to take into consideration some of non-ideal effects (see appendix I).

Adsorption isotherm equations are generally of the form [56]:

$$f(\theta, x) \exp(-a, \theta) = KC \qquad (3.4)$$

where f (θ, x) is the configurational factor that depends essentially on the physical model and assumptions underlying the derivation of the isotherm a is a molecular interaction parameter depending upon molecular interactions in the adsorption layer and the degree of heterogeneity of the surface. All adsorption expressions include the equilibrium constant of the adsorption process, K, which is related to the standard free energy of adsorption ($\Delta G^{\circ}_{ads.}$) by:

$$K = 1/55.5 \exp (-\Delta G^{\circ}_{ads.} / RT) \qquad (3.5)$$

where R is the universal gas constant and T is the absolute temperature.

A number of mathematical relationships for the adsorption isotherms have been suggested to fit the experiment data of the present work. The Frumkin adsorption isotherm [57] is given by the following equation:

$$K C = \theta / 1 - \theta \exp (-2 a \theta) \qquad (3.6)$$

where K is the equilibrium constant of the adsorption reaction, C is the inhibitor concentration in the bulk of the solution and θ is the surface coverage. The surface coverage, i.e., the fraction of the surface covered by the inhibitor molecules, θ were calculated as before (eqn. 2.3):

The plot of θ against log C for all additives gives S shaped curves and this can be shown in Fig (3.16). This indicates that these compounds are adsorbed on the surface of copper electrode according to frumkin adsorption isotherm.

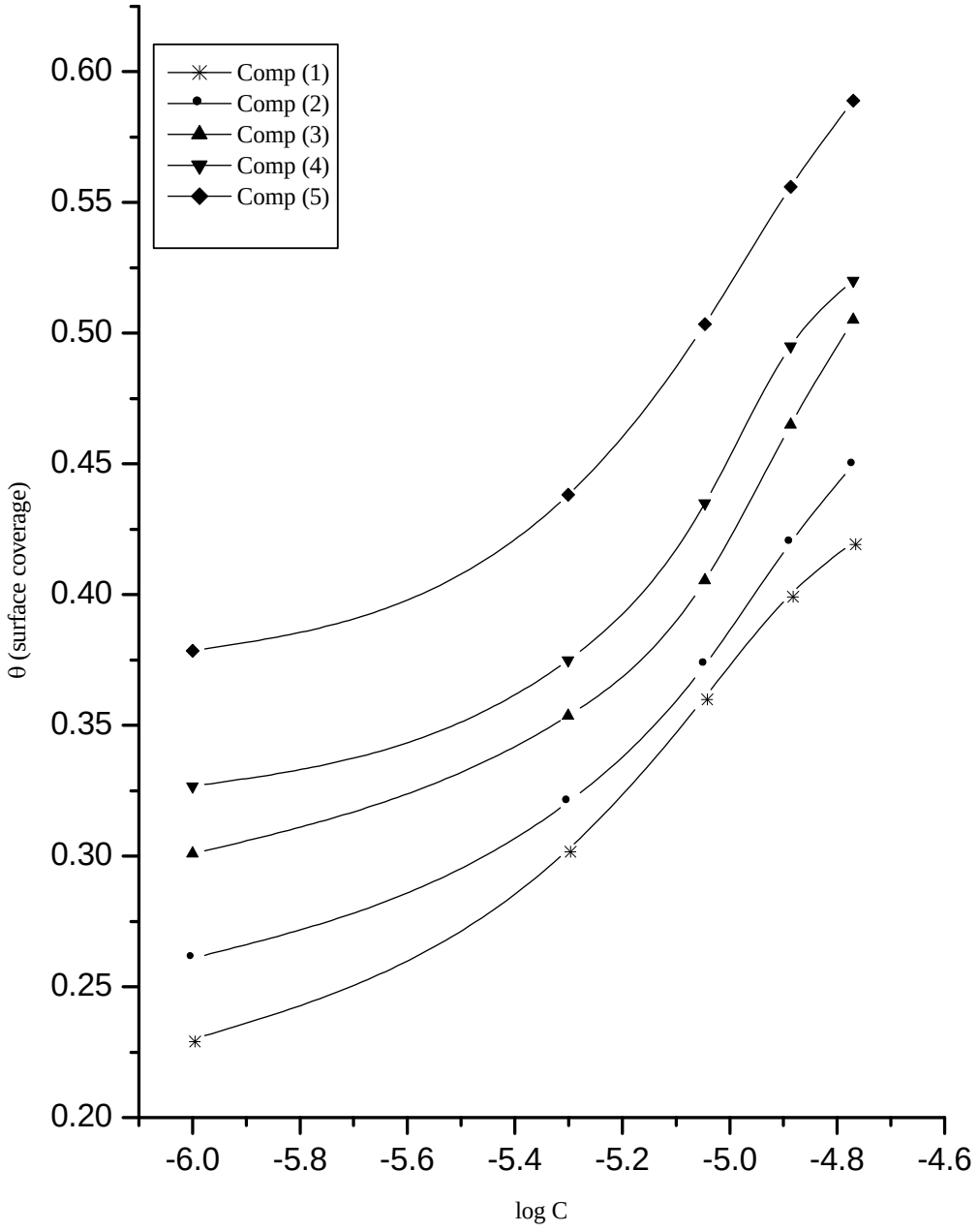

Fig.(3.16): Frumkin adsorption isotherms for copper in 2M HNO_3 in presence of all inhibitors from weight loss measurments at30°C.

3.4- EFFECT OF TEMPERATURES

In this part the effect of temperature on the corrosion rate of copper in 2M HNO_3 solution in absence and presence of $1x10^{-6}$ – $1.7x10^{-5}$M of quinazoline compounds was studied at different temperatures (35-50^{o}C) by weight loss method Figs.(3.17-3.36). It is clear that from these figures the weight loss values increase at all concentrations with raising temperature. This may be attributed to desorption of quinazoline derivatives from the surface at higher temperatures. The increase in weight loss values with increasing temperature is suggestive of physical adsorption of these compounds on the surface of copper.

Tables (3.6-3.9) show the effect of temperature on the percentage inhibition at different concentrations for all the tested compounds. Inspection of these tables it is found that the percentage inhibition efficiency decreases with rising temperature. Also, the percentage inhibition efficiency increases with increasing the concentration of quinazoline compounds. The order of inhibition efficiency is:

5 > 4 > 3 > 2 >1

3.5- ACTIVATION PARAMETERS OF CORROSION PROCESS

The apparent activation energy E_a^*, the enthalpy of activation ΔH^* and the entropy of activation ΔS^* for the corrosion of copper samples in 2M HNO_3 solutions in the absence and presence of different concentrations of quinazoline compounds at 30,35, 40, 45, 50°C were calculated from Arrhenius-type equation:

$$\text{Rate} = A \exp(-E_a^*/RT) \quad (3.10)$$

and transition-state equation:

$$\text{Rate} = RT/Nh \exp(\Delta S^*/R) \exp(-\Delta H^*/RT) \quad (3.11)$$

where A is the frequency factor, h is the Planck's constant, N is Avogadro's number and R is the universal gas constant. A plots of log Rate vs. 1/T and log (Rate/T) vs. 1/T give straight lines with slope of $-E_a^*/2.303R$, and $-\Delta H^*/2.303R$, respectively. The intercepts will be A and log $R/Nh + \Delta S^*/2.303R$ for Arrhenius and transition state equations, respectively.

Figure (3.37) represents plots of the log rate vs. 1/T and Figure (3.38) log (rate/T) vs. 1/T. The calculated values of the apparent activation energy, E_a^*, activation entropies, $\Delta S^*$and activation enthalpies, ΔH^* are given in Table (3.10).

The almost similar values of E_a^* suggest that the inhibitors are similar in the mechanism of action and the order of efficiency may be related to the preexponential factor A in equation (3.10). This is further related to concentration, steric effects and metal surface characters.

The value of activation energy obtained in free acid solution is equal to 71.99 kJ mol^{-1} which is of the same order of magnitude as those observed by Mansour et al., 72.4 kJ mol^{-1} [58]

From the results of Table(3.10), it is clear that the presence of tested compounds increased the activation energy values and consequently decreased the corrosion rate of the copper. Also, activation energy increased by increasing the concentration of the inhibitors. These results indicate that these tested compounds act as inhibitors through increasing

activation energy of copper dissolution by making a barrier to mass and charge transfer by their adsorption on copper surface. The positive signs of ΔH^* reflect the endothermic nature of the copper dissolution process. The values of ΔH^* are different for studied compounds which means that their structure affect the strength of its adsorption on the metal surface.

The negative values of ΔS^* in the absence and presence of the inhibitors implies that, the activated complex is the rate determining step and represents association rather than dissociation. It also reveals that an increase in the order takes place in going from reactants to the activated complex.

The order of the inhibition efficiencies of quinazoline compounds as gathered from the increase in E_a^* and ΔH^* values and decrease in ΔS^* values are as follow:

5 > 4 > 3 > 2 >1

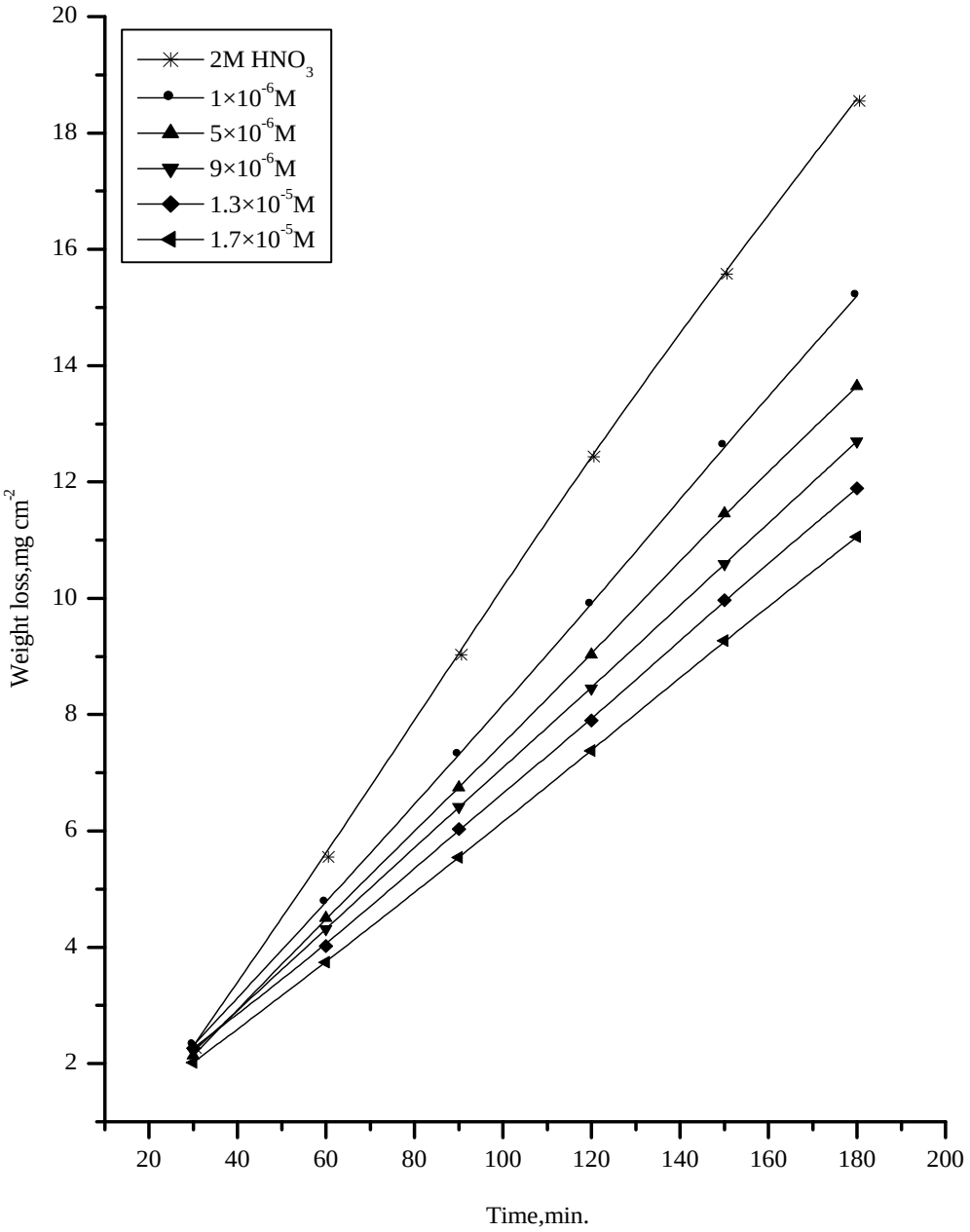

Fig.(3.17): Weight loss-time curves for copper in 2M HNO_3 in absence and presence of different concentrations of compound (1) at 35°C.

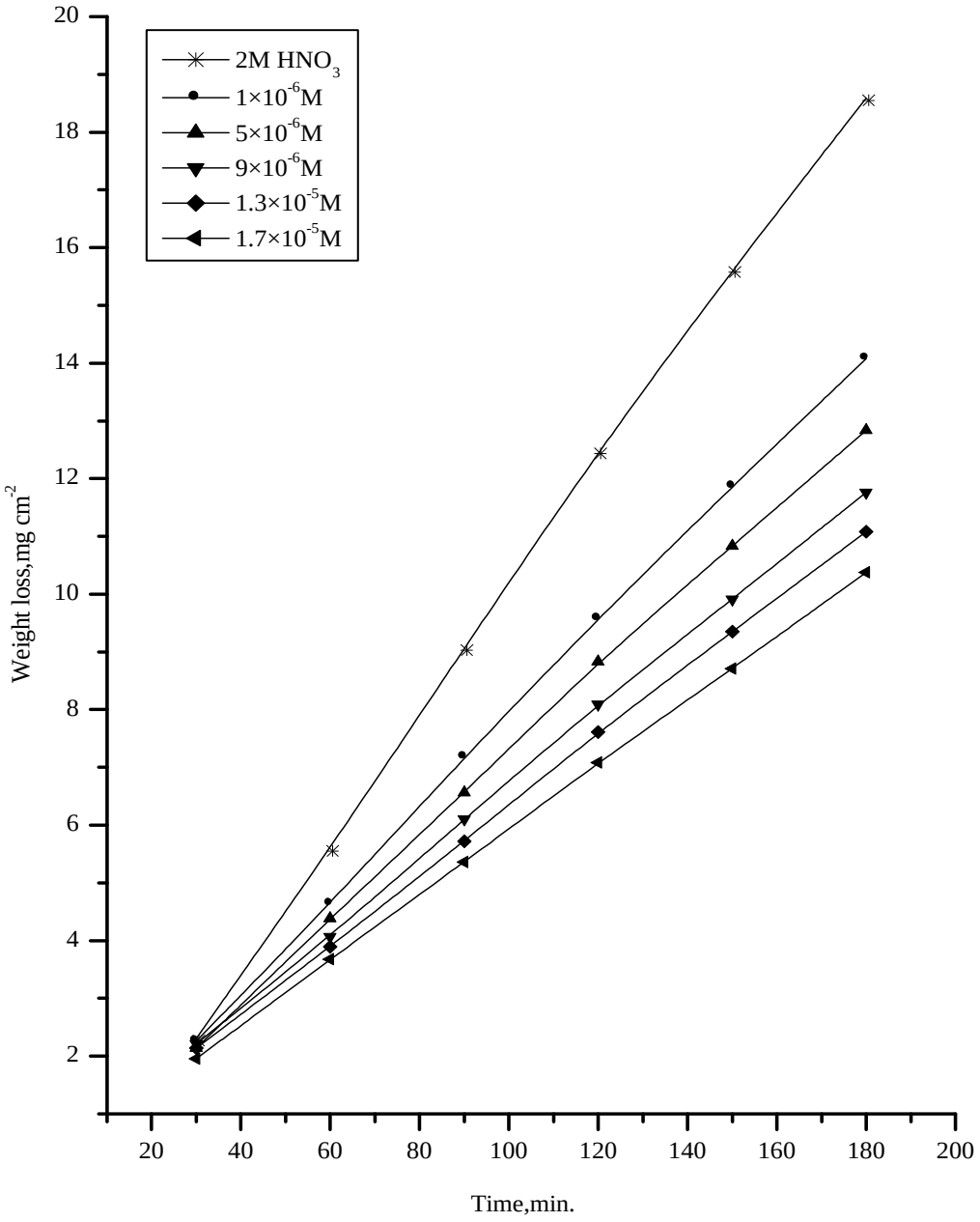

Fig.(3.18): Weight loss-time curves for copper in 2M HNO_3 in absence and presence of different concentrations of compound (2) at 35°C.

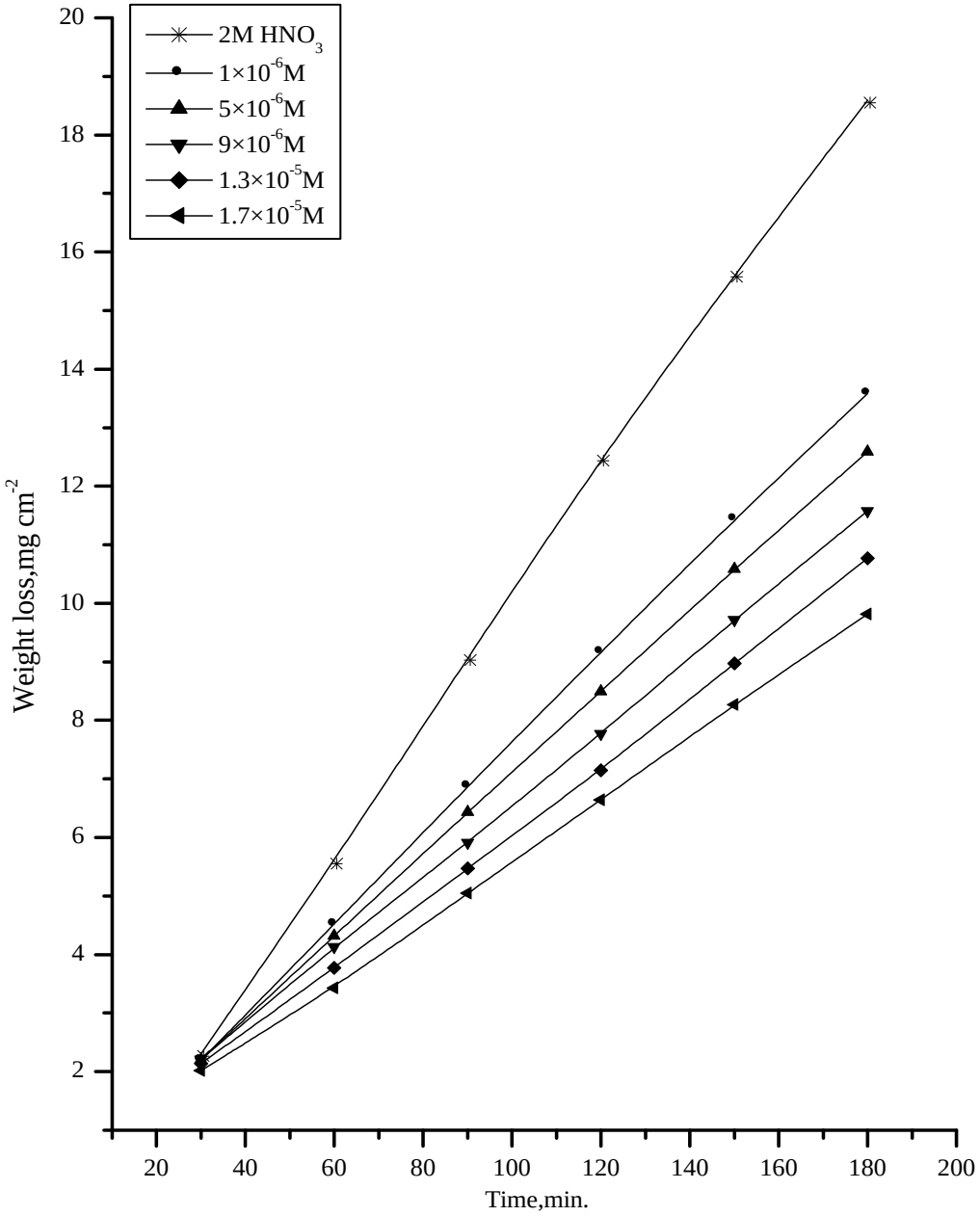

Fig.(3.19): Weight loss-time curves for copper in 2M HNO_3 in absence and presence of different concentrations of compound (3) at 35°C.

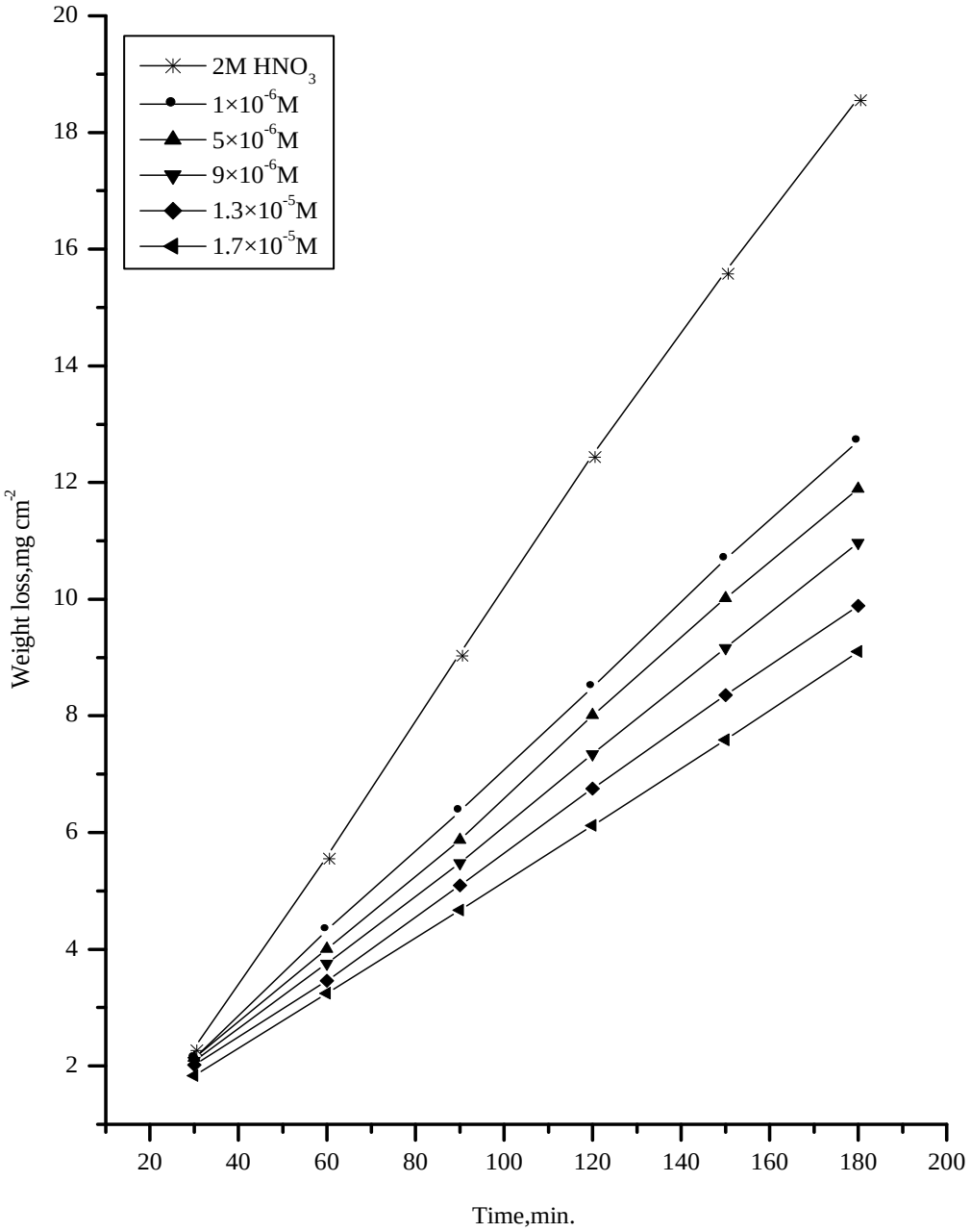

Fig.(3.20): Weight loss-time curves for copper in 2M HNO_3 in absence and presence of different concentrations of compound (4) at 35°C.

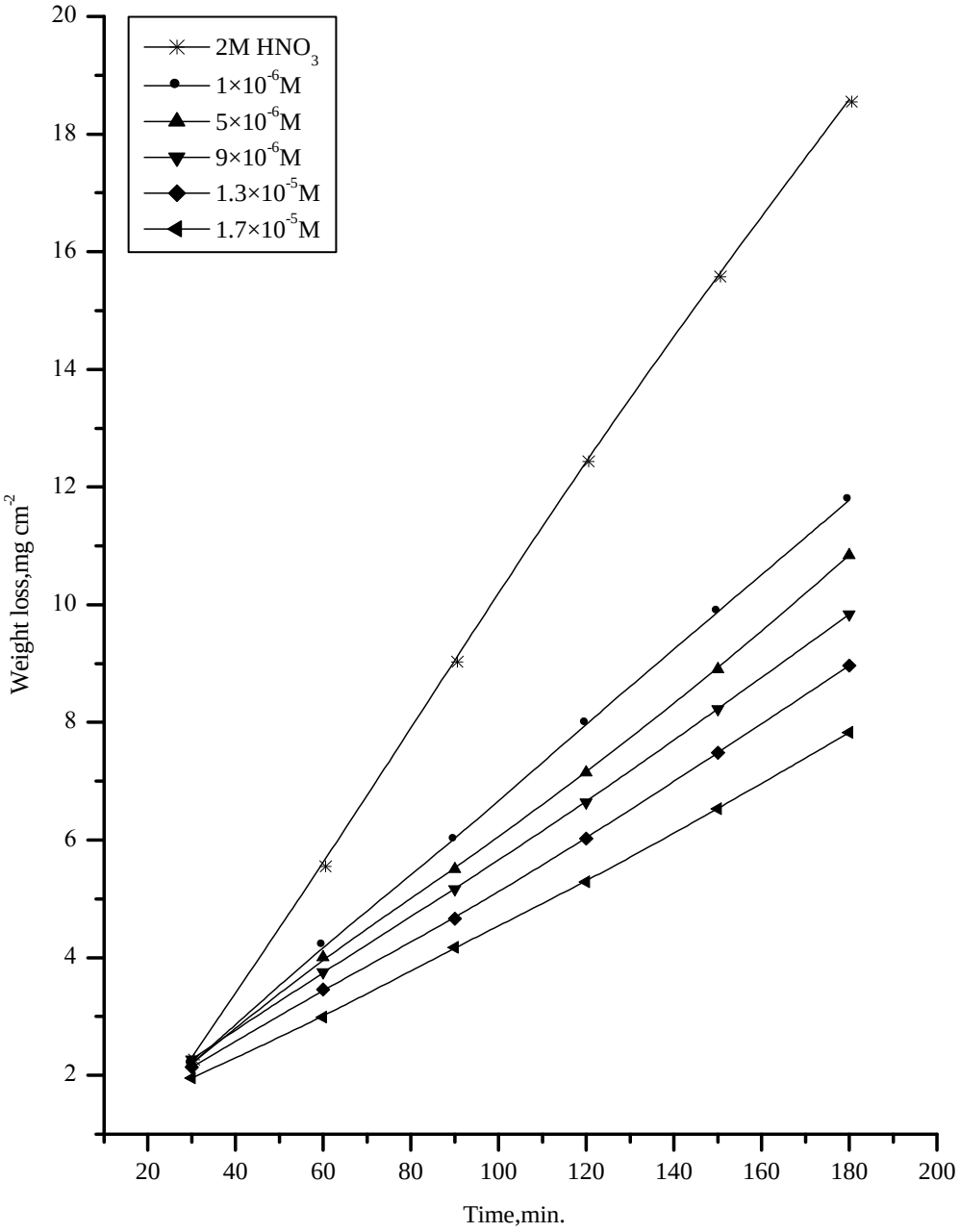

Fig.(3.21): Weight loss-time curves for copper in 2M HNO_3 in absence and presence of different concentrations of compound (5) at 35°C.

Table (3.6): Inhibition efficiency at different concentrations of inhibitors as determined from weight loss method at 35°C.

Conc., M	%Inhibition				
	Compound (1)	**Compound (2)**	**Compound (3)**	**Compound (4)**	**Compound (5)**
$1x10^{-6}$	20.73	23.22	26.55	31.95	36.00
$5x10^{-6}$	27.64	29.21	31.93	35.78	42.74
$9x10^{-6}$	32.26	35.12	37.68	41.10	46.78
$1.3x10^{-5}$	36.66	39.02	42.73	45.87	51.71
$1.7x10^{-5}$	40.83	43.21	46.73	50.91	57.60

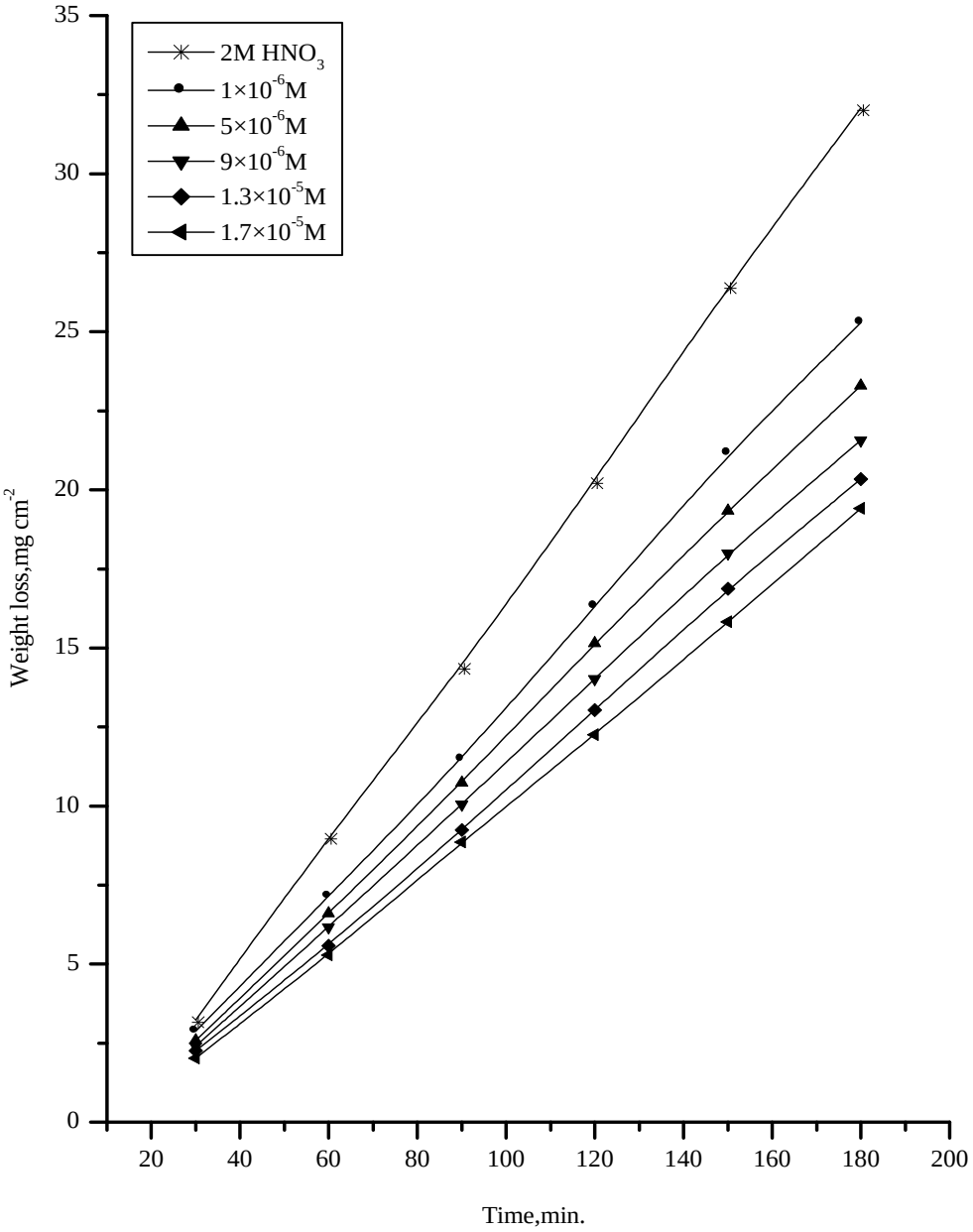

Fig.(3.22): Weight loss-time curves for copper in 2M HNO_3 in absence and presence of different concentrations of compound (1) at 40°C.

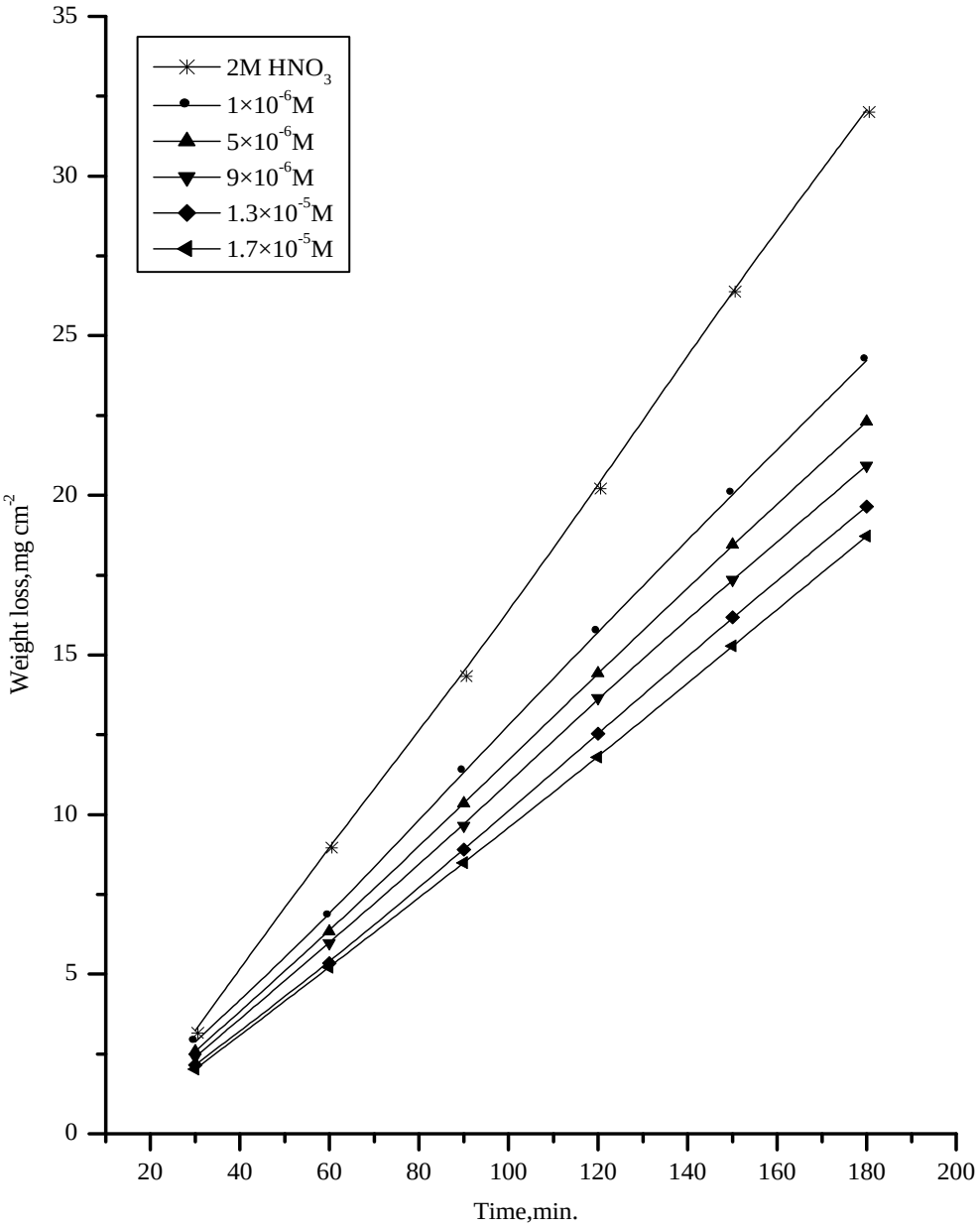

Fig.(3.23): Weight loss-time curves for copper in 2M HNO_3 in absence and presence of different concentrations of compound (2) at 40°C.

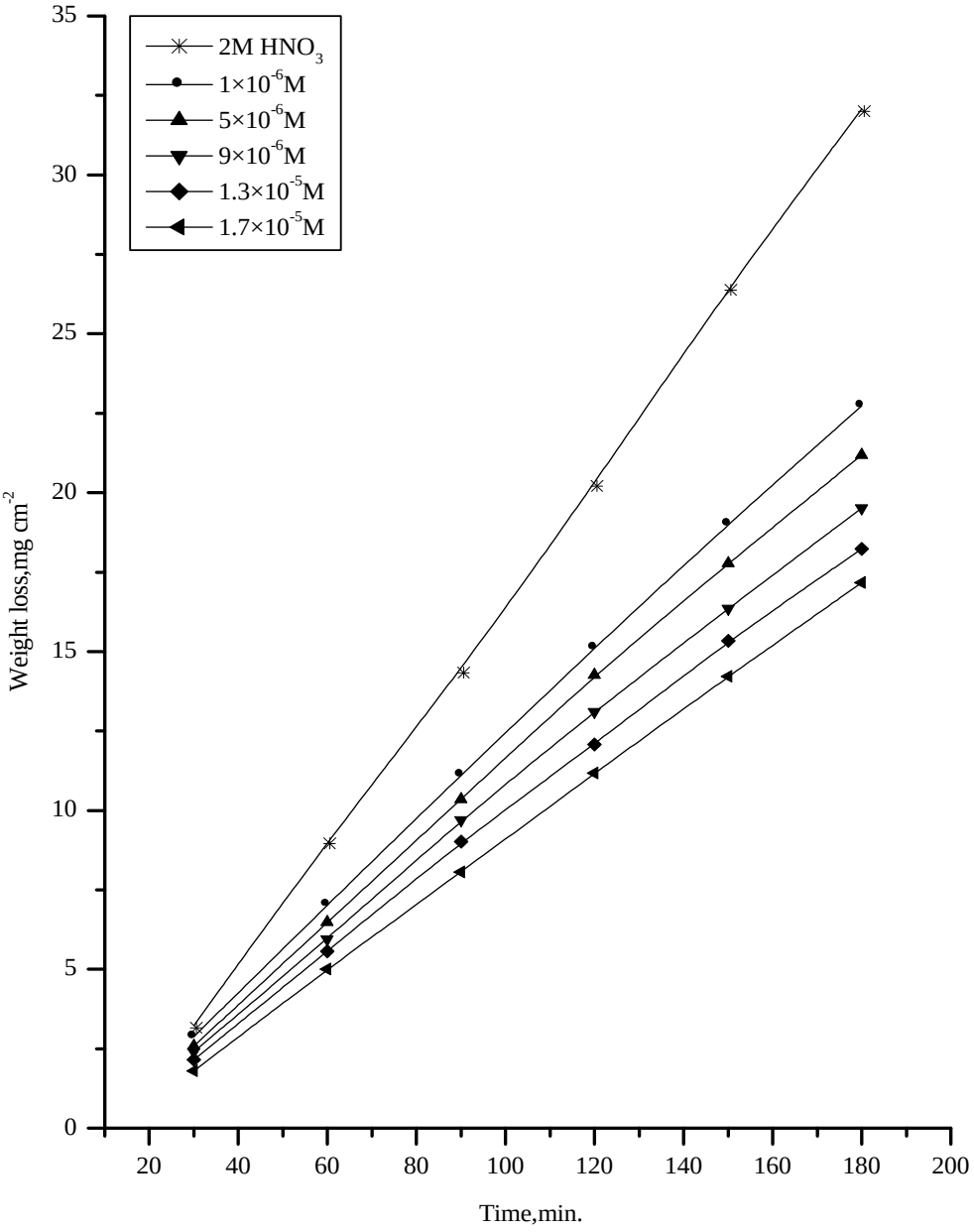

Fig.(3.24): Weight loss-time curves for copper in 2M HNO_3 in absence and presence of different concentrations of compound (3) at 40°C.

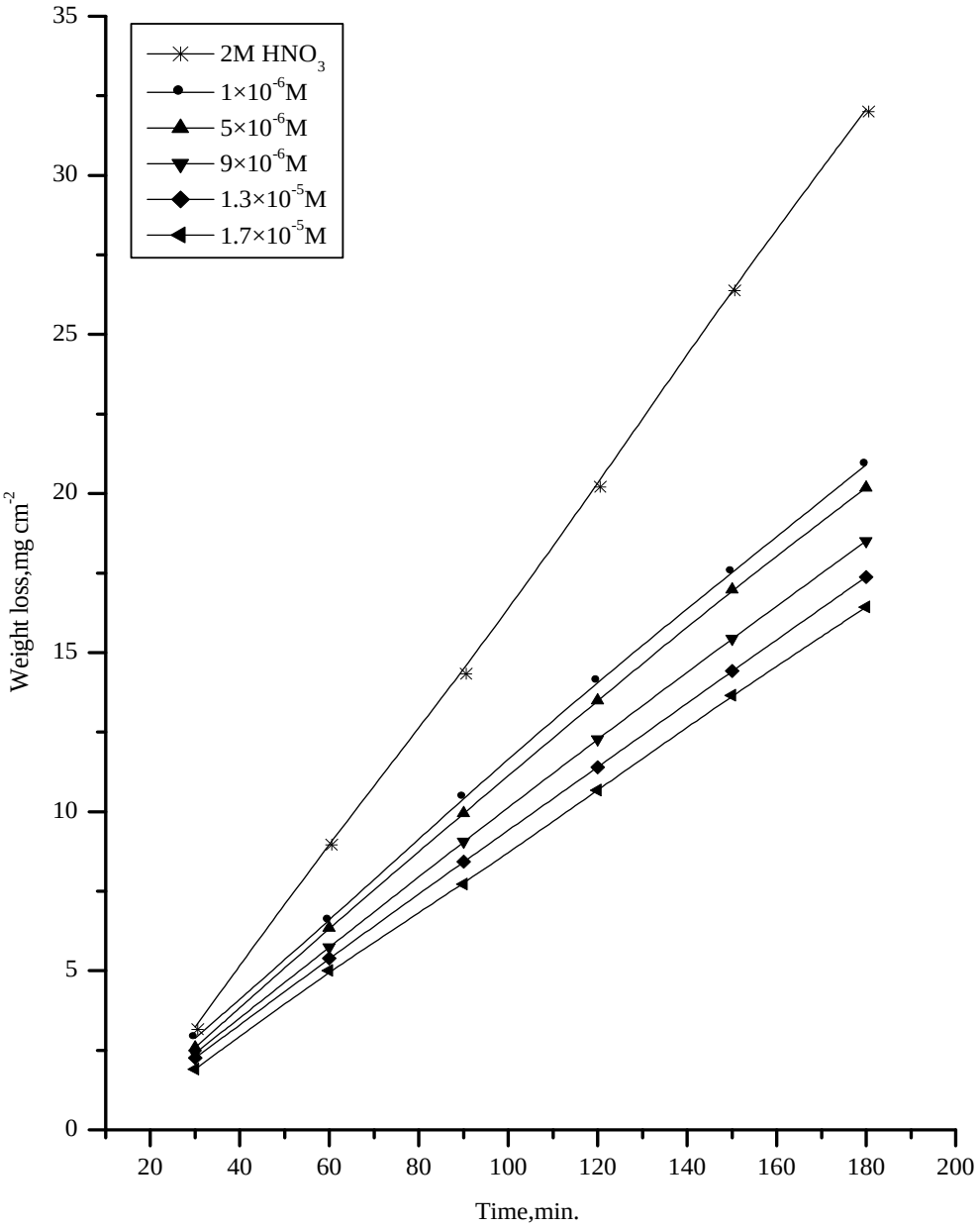

Fig.(3.25): Weight loss-time curves for copper in 2M HNO_3 in absence and presence of different concentrations of compound (4) at 40°C.

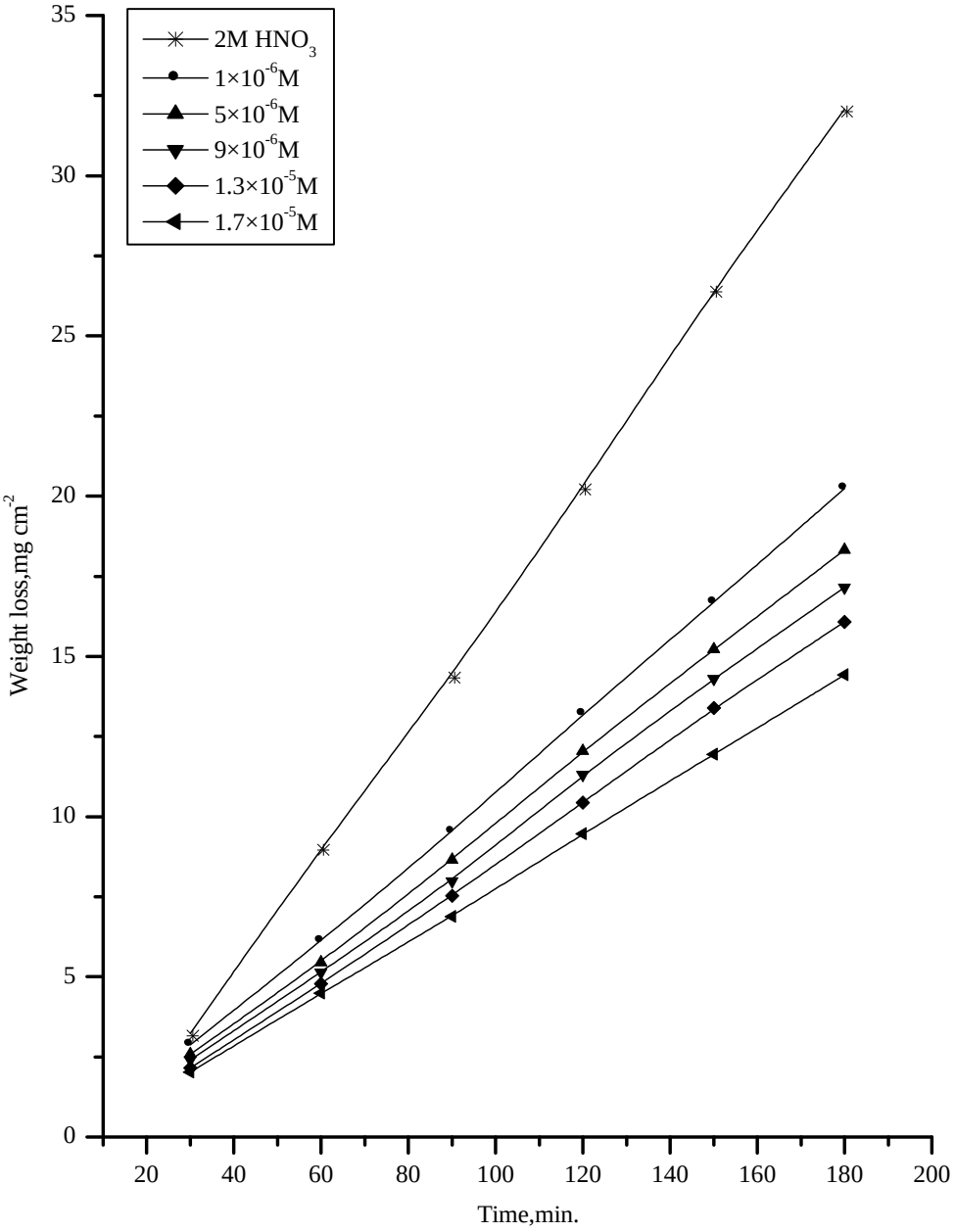

Fig.(3.26): Weight loss-time curves for copper in 2M HNO_3 in absence and presence of different concentrations of compound (5) at 40°C.

Table (3.7): Inhibition efficiency at different concentrations of inhibitors as determined from weight loss method at 40°C.

Conc., M	%Inhibition				
	Compound (1)	**Compound (2)**	**Compound (3)**	**Compound (4)**	**Compound (5)**
$1x10^{-6}$	19.57	22.46	25.47	30.46	34.91
$5x10^{-6}$	25.32	28.85	29.68	33.45	40.63
$9x10^{-6}$	30.88	32.66	35.36	39.44	44.25
$1.3x10^{-5}$	35.75	38.20	40.48	43.77	48.54
$1.7x10^{-5}$	39.61	41.87	44.90	47.36	53.37

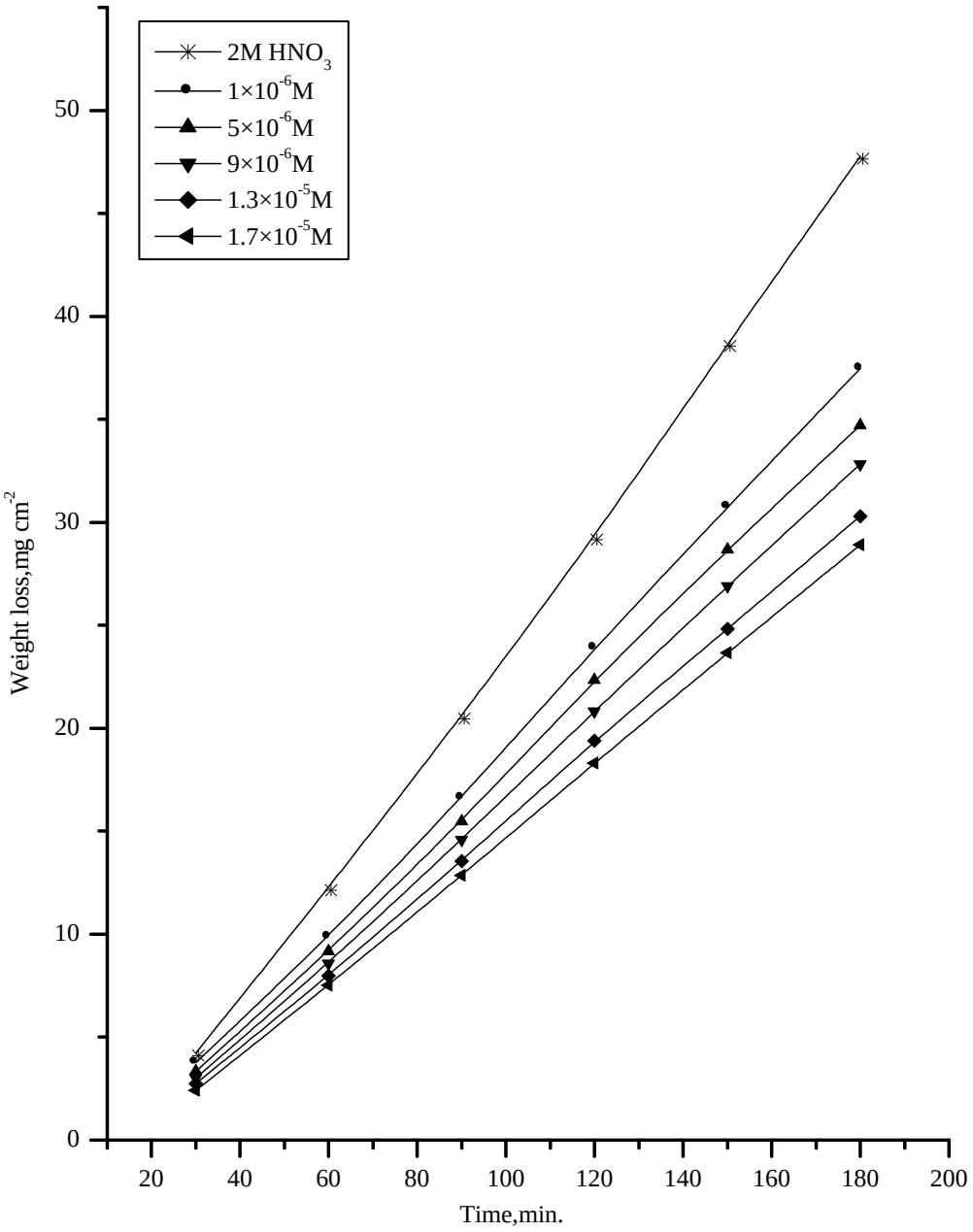

Fig.(3.27): Weight loss-time curves for copper in 2M HNO_3 in absence and presence of different concentrations of compound (1) at 45°C.

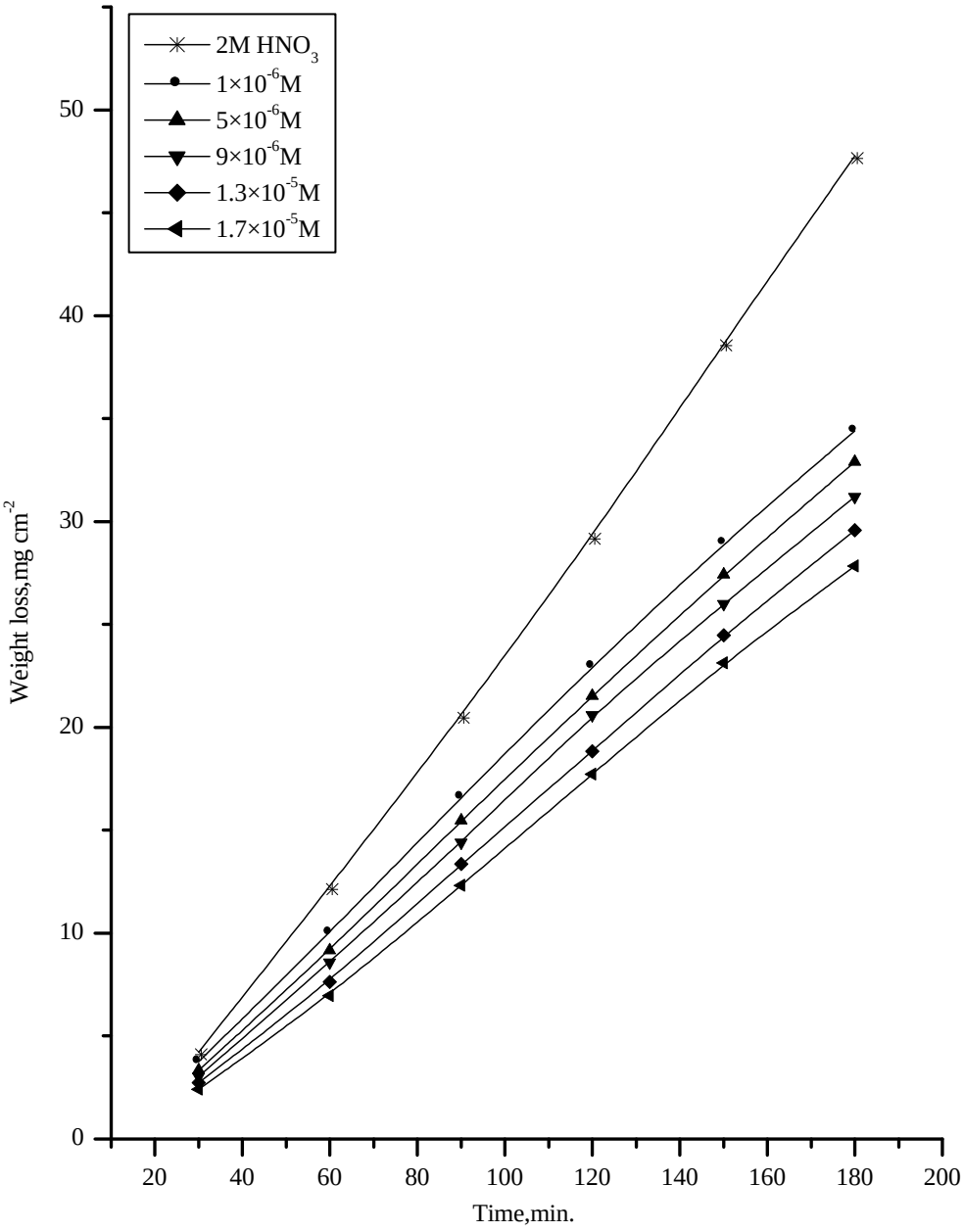

Fig.(3.28): Weight loss-time curves for copper in 2M HNO_3 in absence and presence of different concentrations of compound (2) at 45°C.

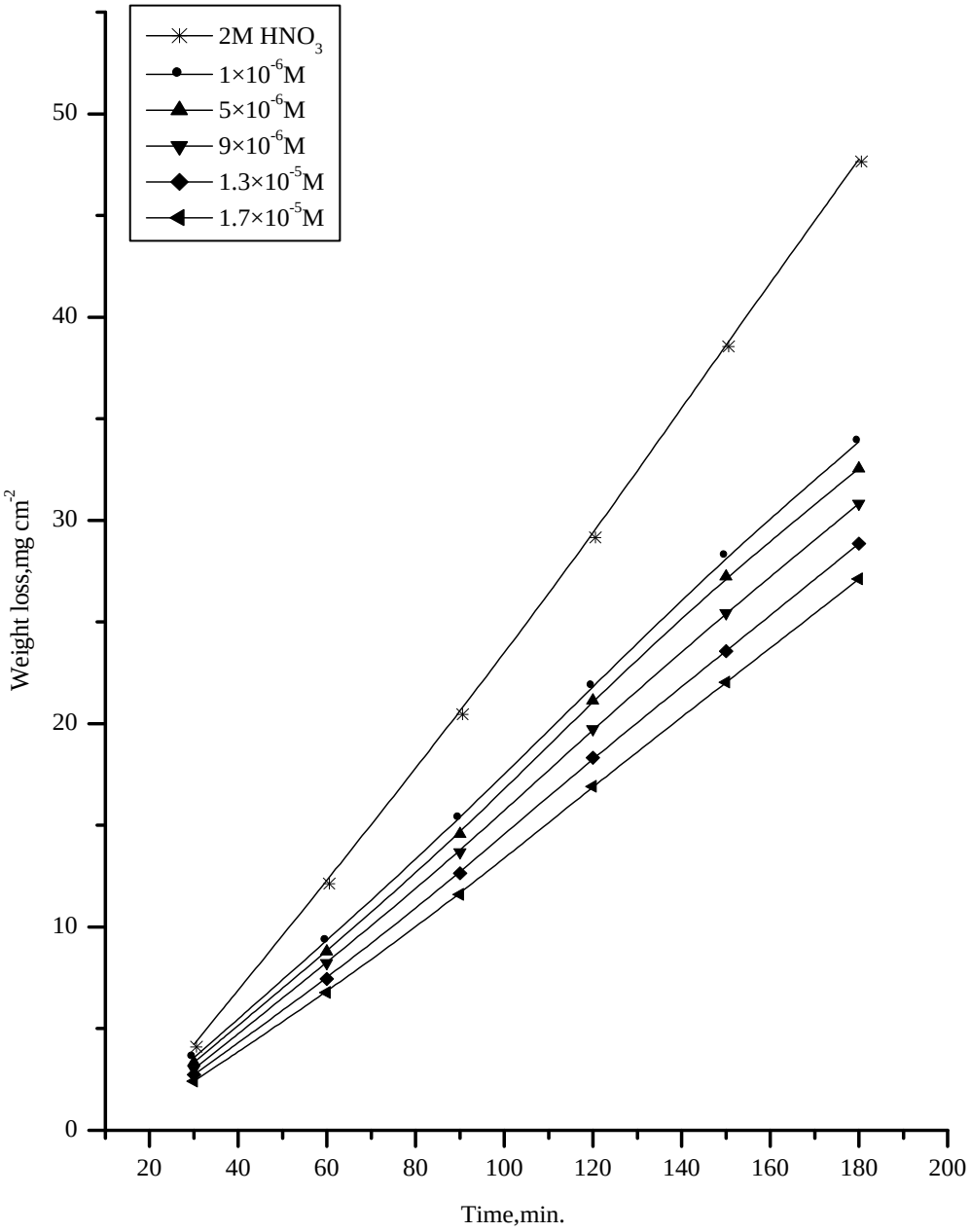

Fig.(3.29): Weight loss-time curves for copper in 2M HNO_3 in absence and presence of different concentrations of compound (3) at 45°C.

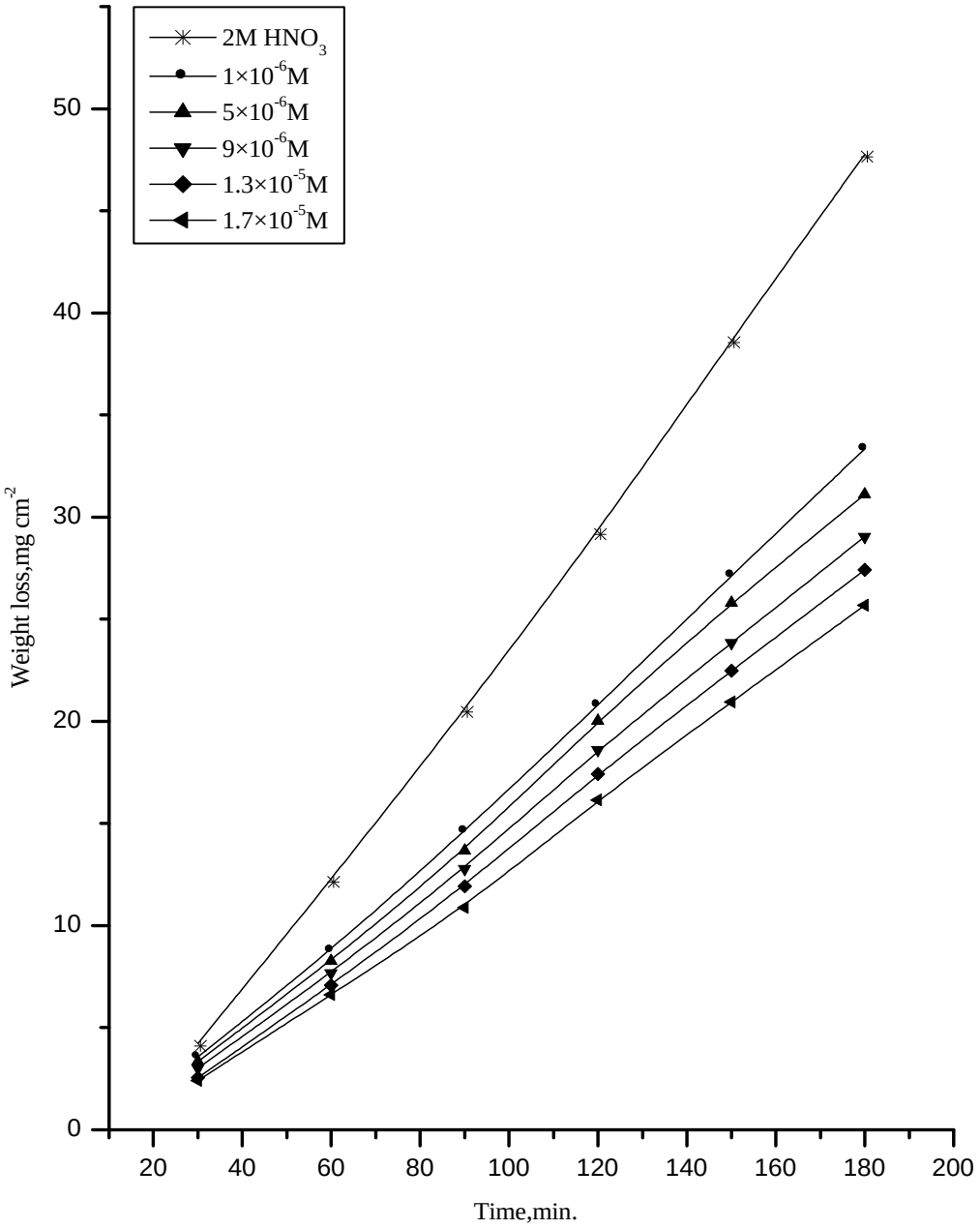

Fig.(3.30): Weight loss-time curves for copper in 2M HNO_3 in absence and presence of different concentrations of compound (4) at 45°C.

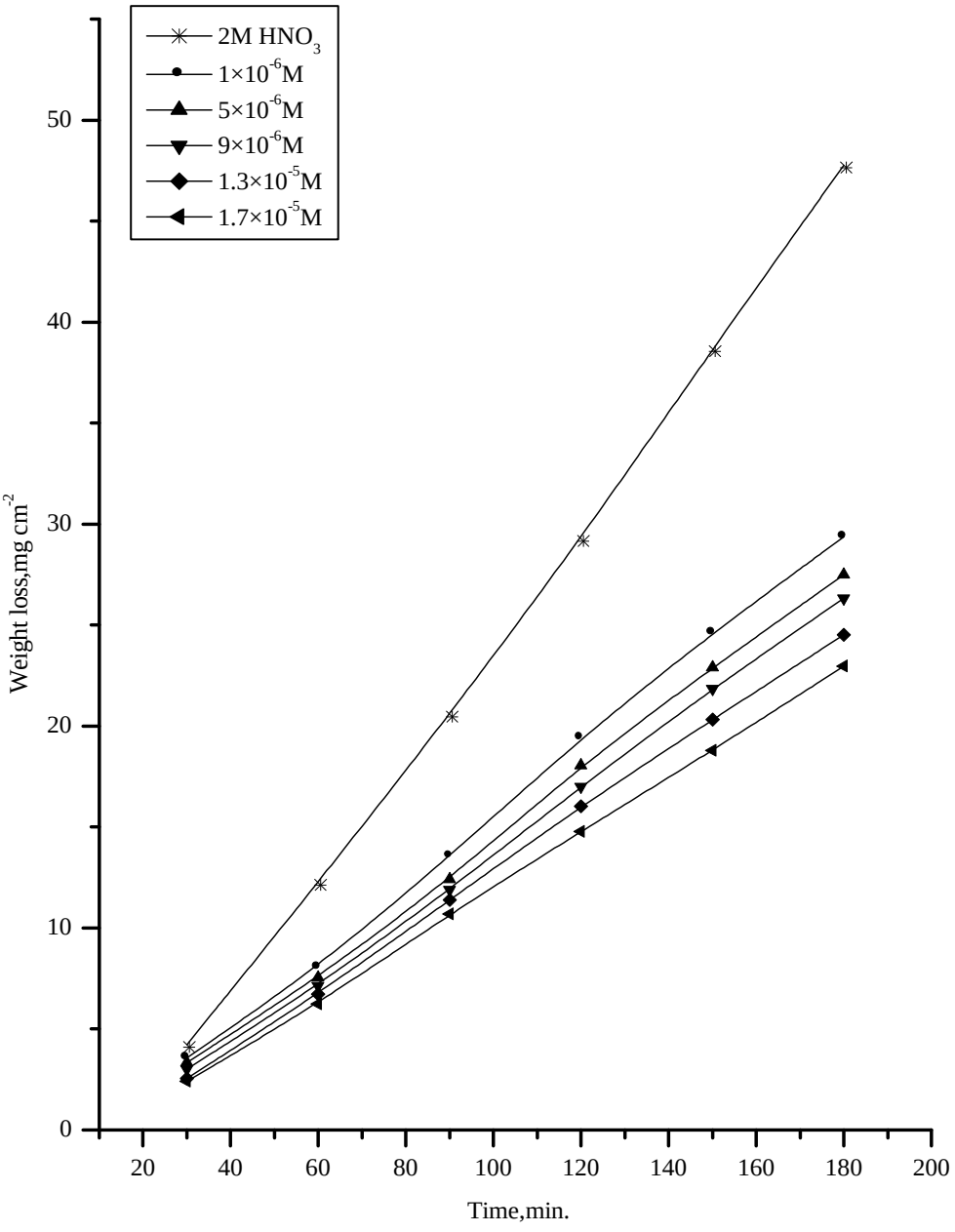

Fig.(3.31): Weight loss-time curves for copper in 2M HNO_3 in absence and presence of different concentrations of compound (5) at 45°C.

Table (3.8): Inhibition efficiency at different concentrations of inhibitors as determined from weight loss method at 45°C.

Conc., M	%Inhibition				
	Compound (1)	**Compound (2)**	**Compound (3)**	**Compound (4)**	**Compound (5)**
$1x10^{-6}$	18.36	21.57	25.47	28.98	33.66
$5x10^{-6}$	23.70	26.48	27.79	31.65	38.37
$9x10^{-6}$	28.85	29.67	32.56	36.49	41.96
$1.3x10^{-5}$	33.80	35.69	37.37	40.47	45.22
$1.7x10^{-5}$	37.47	39.44	42.26	44.83	49.55

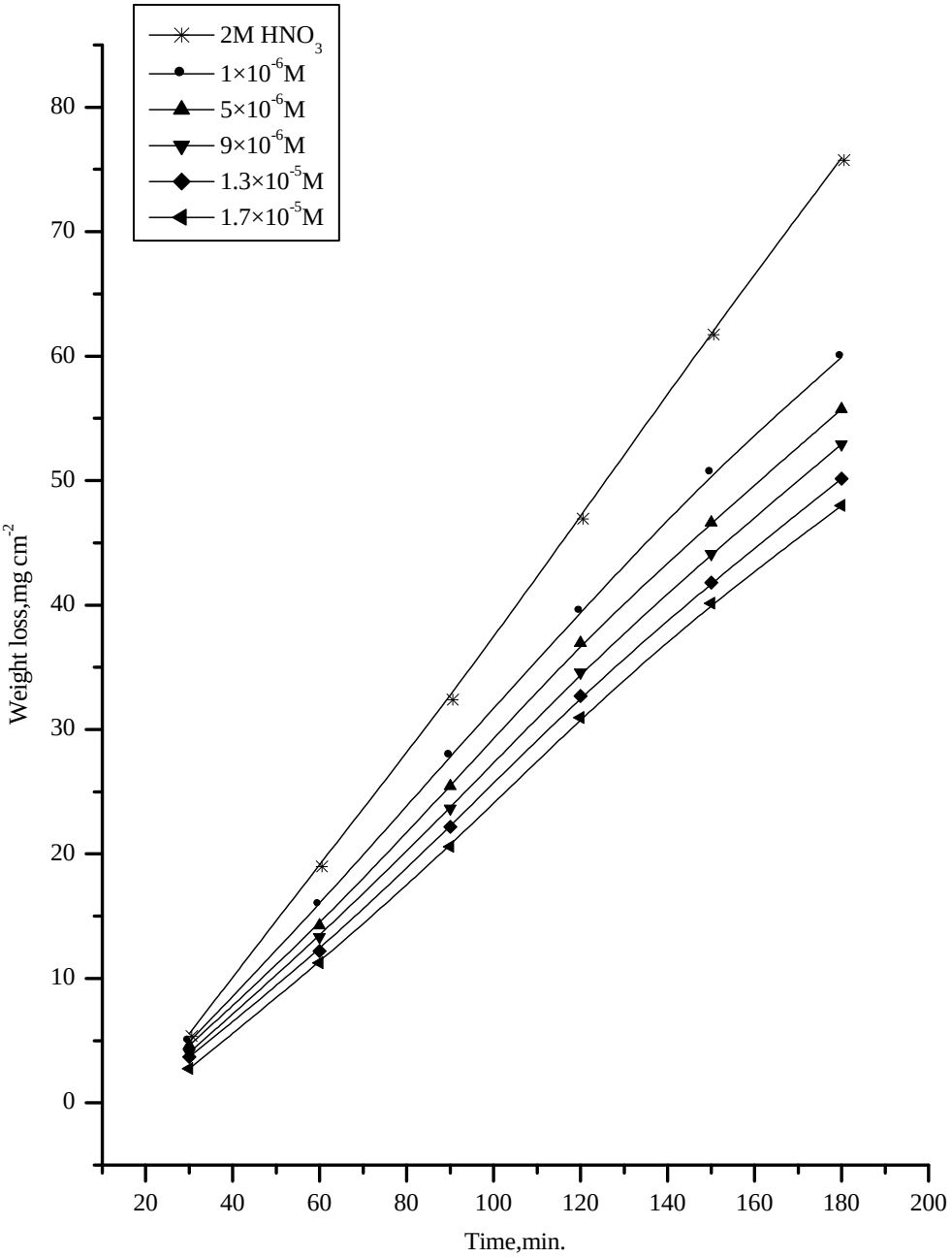

Fig.(3.32): Weight loss-time curves for copper in 2M HNO_3 in absence and presence of different concentrations of compound (1) at 50°C.

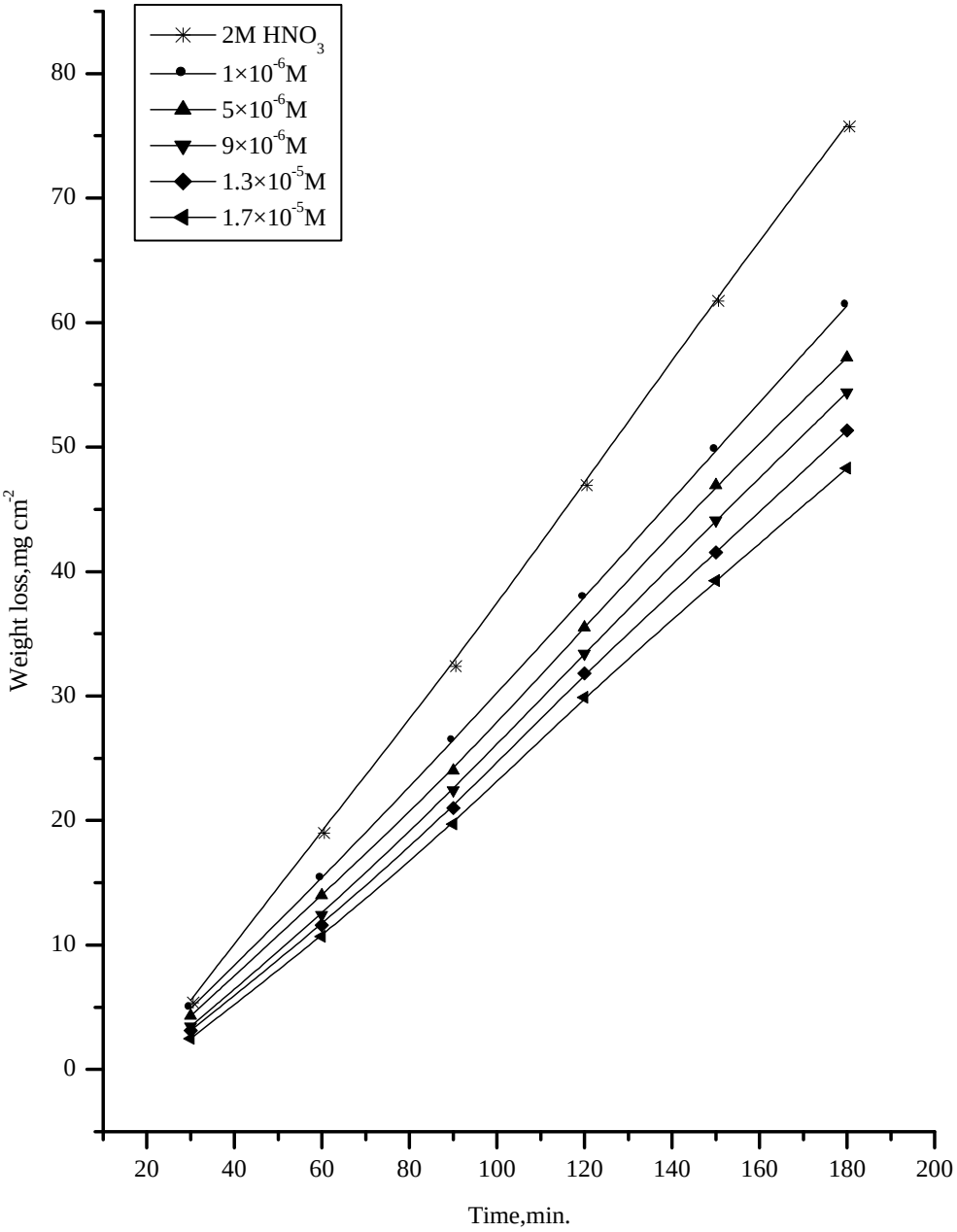

Fig.(3.33): Weight loss-time curves for copper in 2M HNO_3 in absence and presence of different concentrations of compound (2) at 50°C.

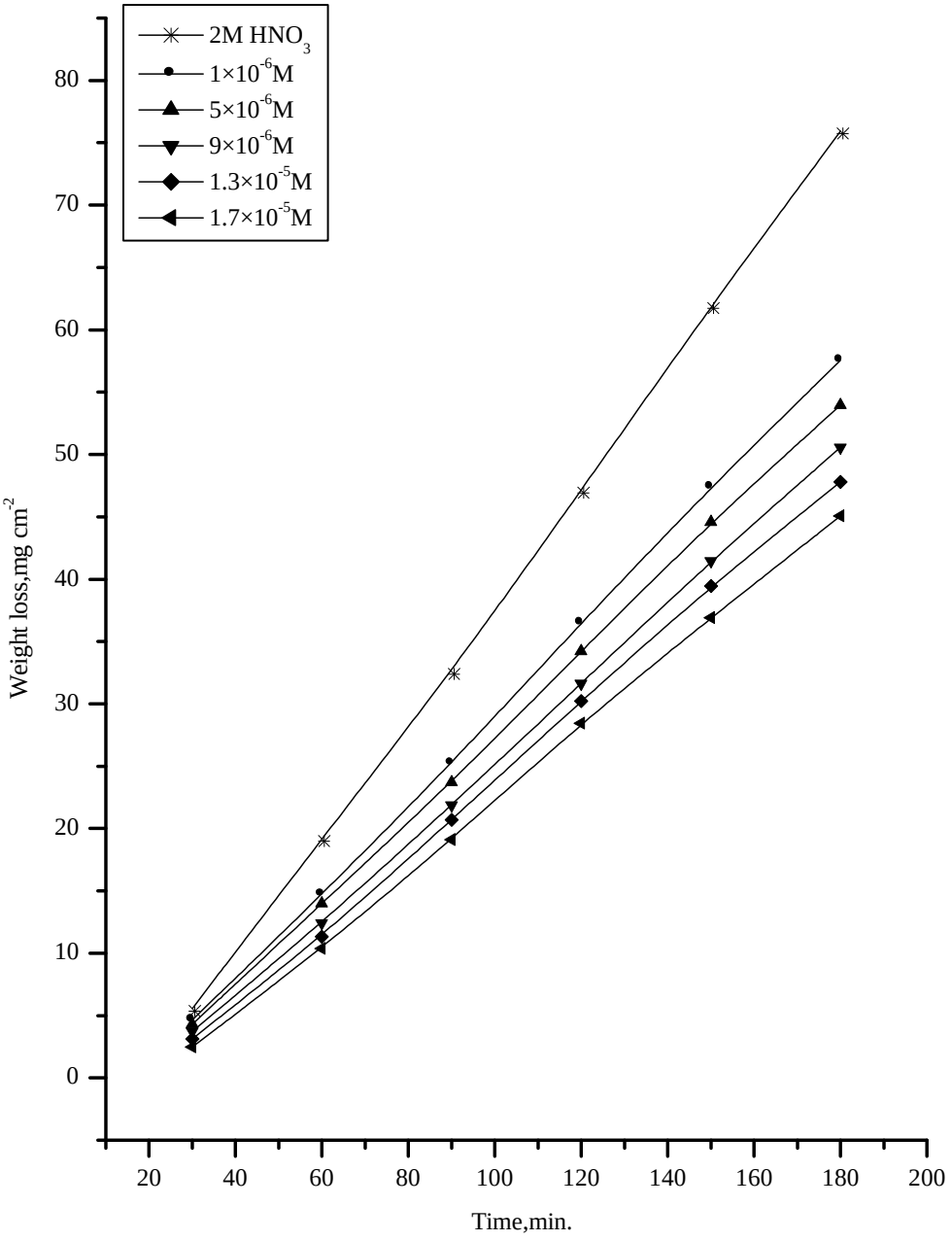

Fig.(3.34): Weight loss-time curves for copper in 2M HNO_3 in absence and presence of different concentrations of compound (3) at 50°C.

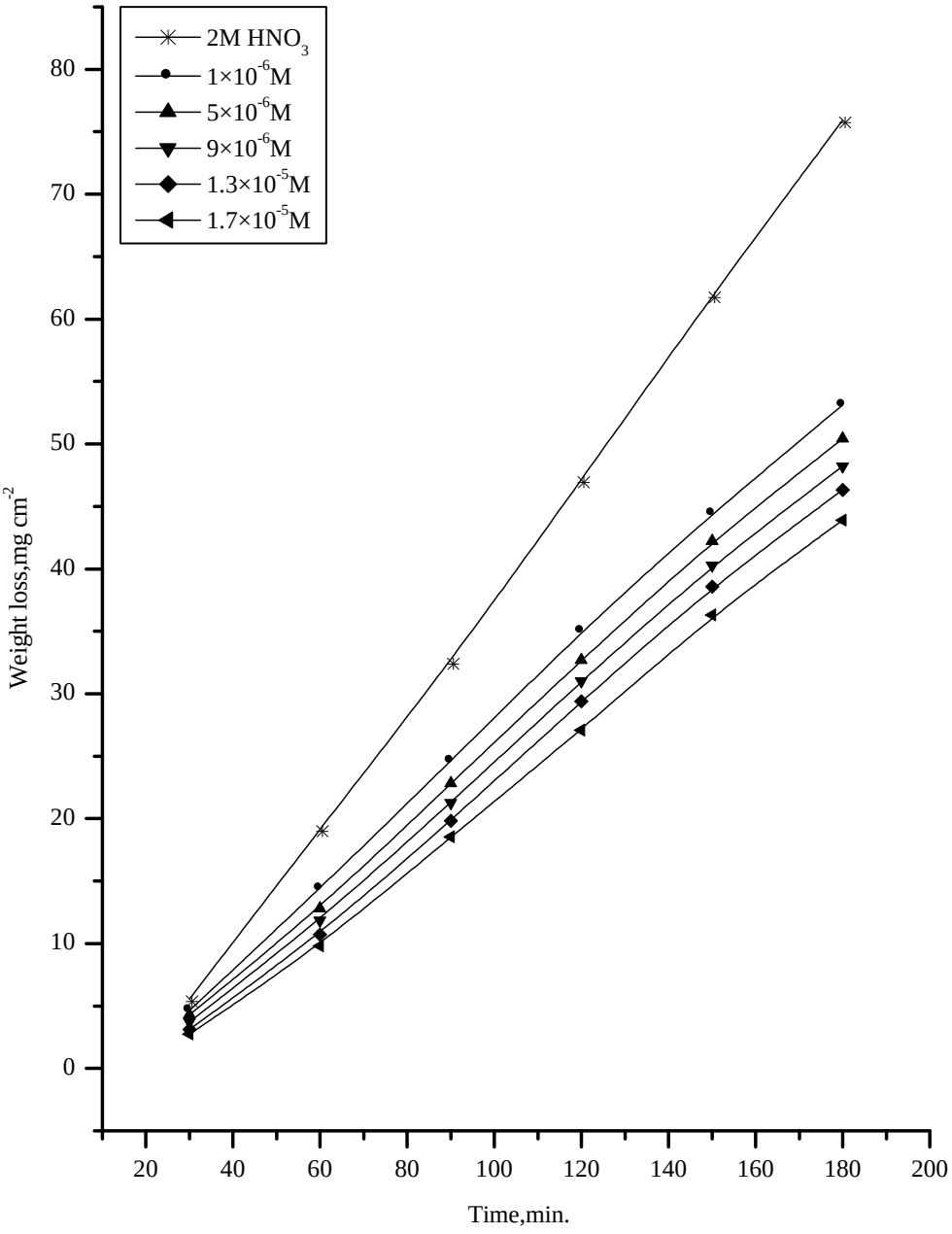

Fig.(3.35): Weight loss-time curves for copper in 2M HNO_3 in absence and presence of different concentrations of compound (4) at 50°C.

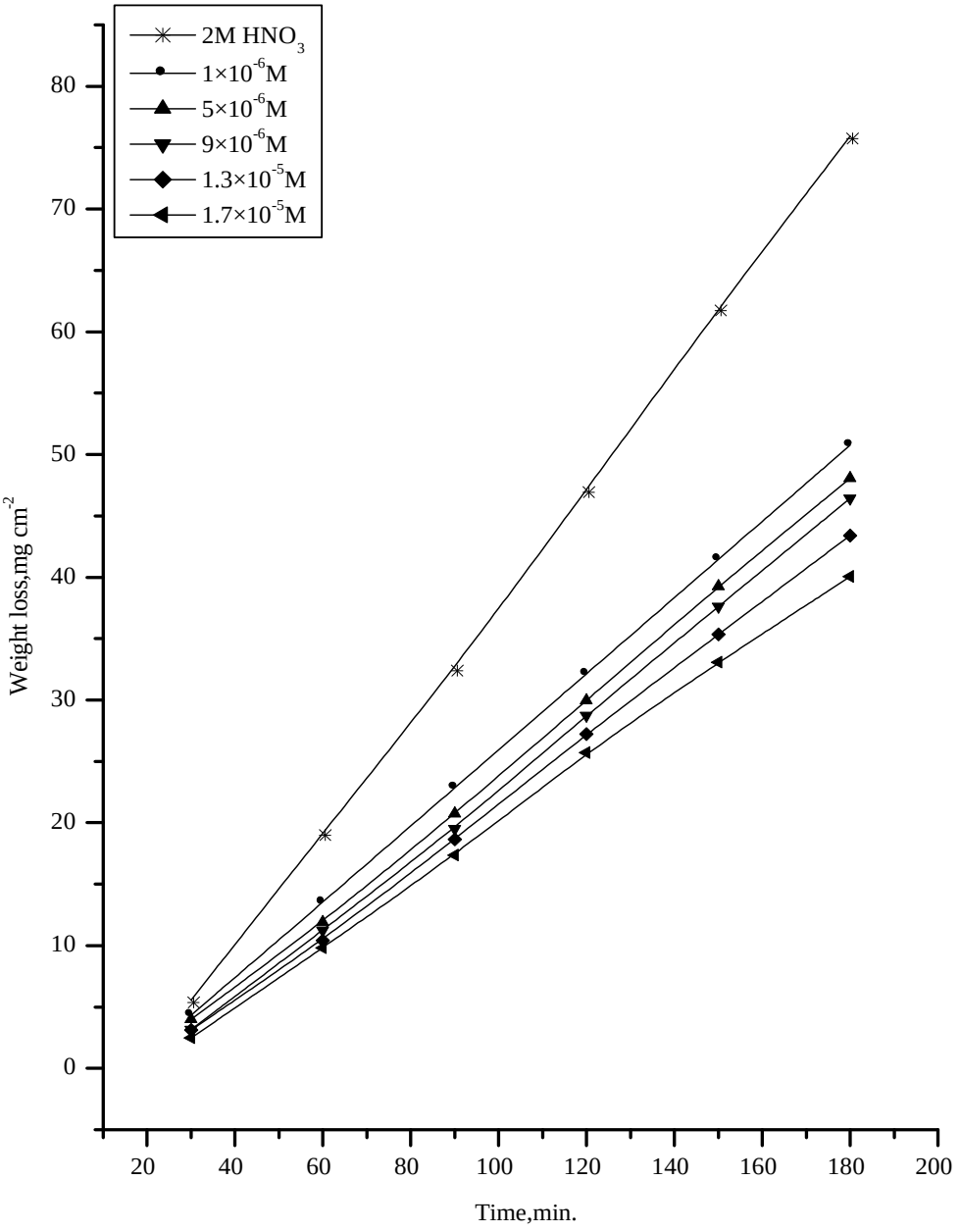

Fig.(3.36): Weight loss-time curves for copper in 2M HNO_3 in absence and presence of different concentrations of compound (5) at 50°C.

Table (3.9): Inhibition efficiency at different concentrations of inhibitors as determined from weight loss method at 50°C.

Conc., M	%Inhibition				
	Compound (1)	**Compound (2)**	**Compound (3)**	**Compound (4)**	**Compound (5)**
$1x10^{-6}$	16.25	19.55	22.57	25.69	31.79
$5x10^{-6}$	21.57	24.66	27.41	30.64	36.38
$9x10^{-6}$	26.57	29.12	32.84	34.19	38.98
$1.3x10^{-5}$	30.64	32.46	35.88	37.62	42.21
$1.7x10^{-5}$	34.35	36.55	39.66	42.53	45.45

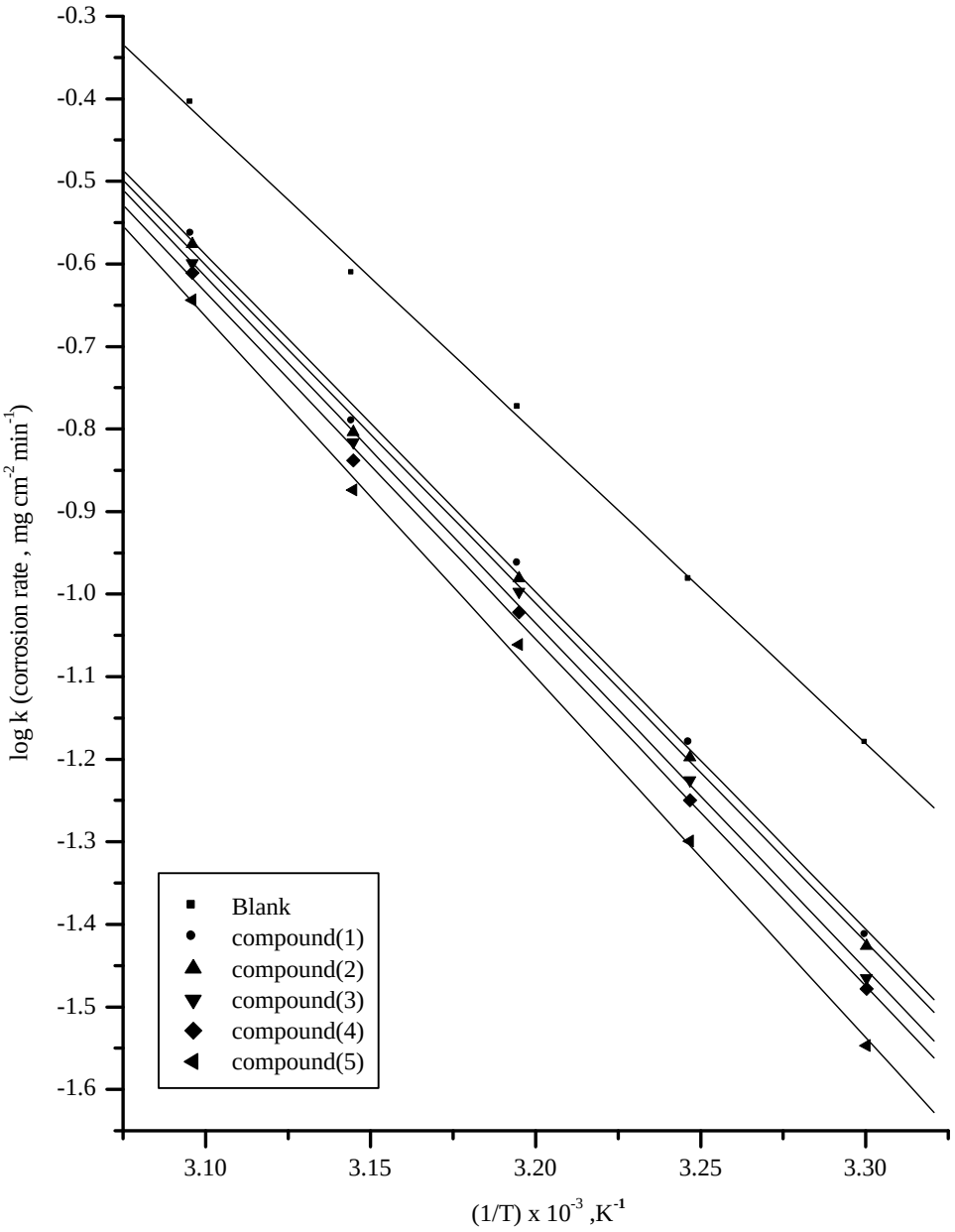

Fig.(3.37): log k vs.1/T curves for copper dissolution in absence and presence of $1.3x10^{-5}$M inhibitors

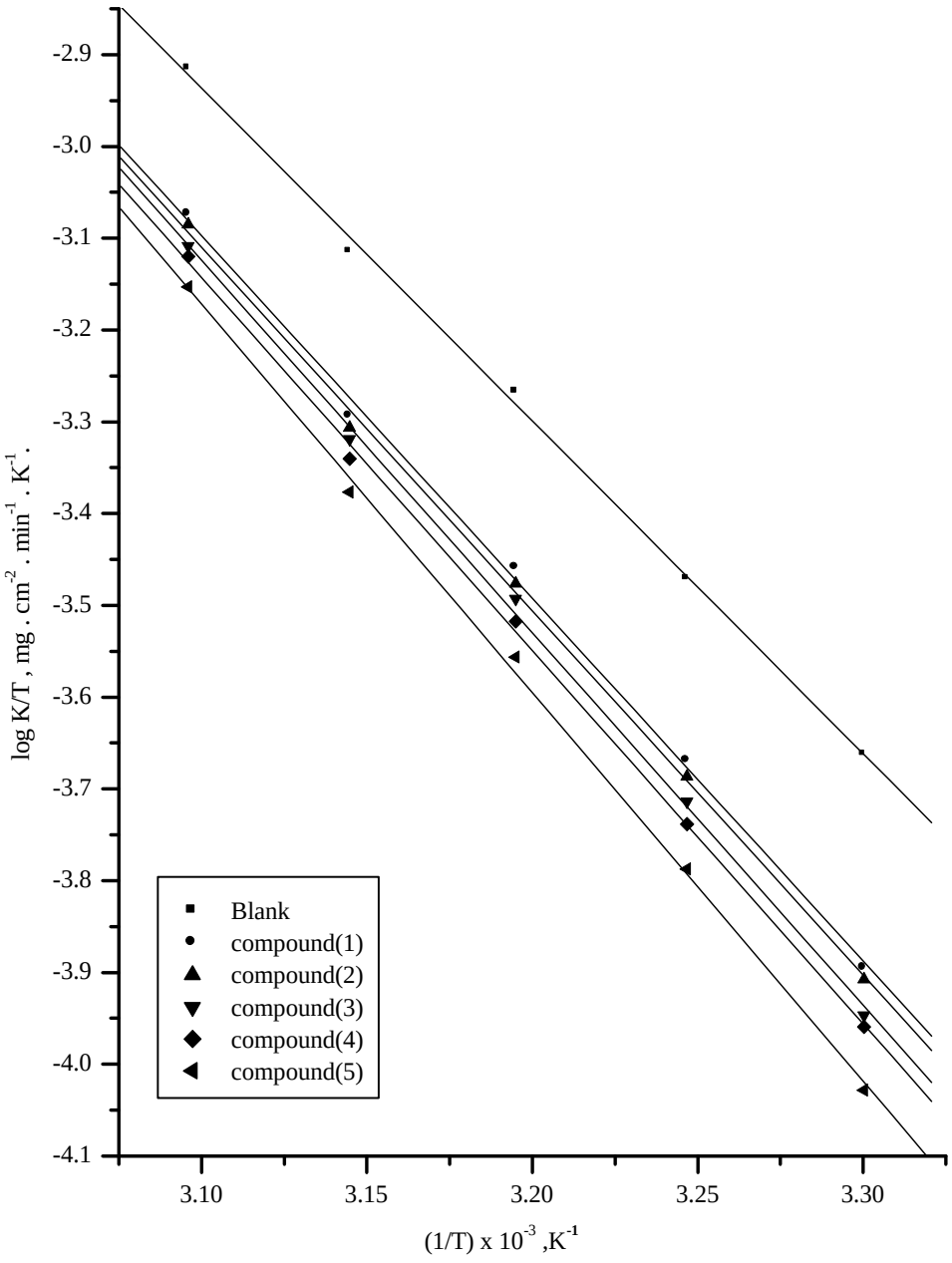

Fig.(3.38): log k/T vs.1/T curves for copper dissolution in absence and presence of $1.3x10^{-5}$M inhibitors

Table (3.10): Activation parameters of copper in 2M HNO_3 in absence and presence of $1.3x10^{-5}$ M of different inhibitors.

Inhibitors	Activation parameter		
	E_a^* ,k J mol^{-1}	ΔH^* , k J mol $^{-1}$	$-\Delta S^*$, J mol^{-1} K^{-1}
Free acid	71.99	69.39	38.58
Compound (1)	78.22	75.62	22.34
compound (2)	78.47	75.87	21.8
Compound (3)	80.26	77.66	16.52
Compound (4)	80.42	77.83	16.36
compound (5)	83.62	81.02	7.02

SECTION (B)

STUDYING THE CORROSION BEHAVIOR OF COPPER BY THE ELECTROCHEMICAL TECHNIQUE

Electrochemical techniques are based on current and potential measurements. According to the choice of the technique accurate and confidential data, concerning the corrosion process can be obtained.

3.6- GALVANOSTATIC POLARIZATION

The technique of anodic and cathodic polarization of metals are frequently used to study the phenomena of metal corrosion and passivation. It yields useful information on the electrode behavior, action of inhibitive and aggressive anions and the effect of the environmental conditions. In this technique an external applied current is used and can be varied as will, the experiments can be performed in relatively short time. When a Tafel equation as applicable for both anodic and cathodic polarization, the point of intersection of the two Tafel lines corresponding to the stationary conditions of corrosion. The function of a substance as an inhibitor or stimulator could be shown from its effect on the polarization curves and the consequent displacement of the point of interaction.

The effect of increasing concentration of quinazoline compounds on the anodic and cathodic polarization curves of copper in 2M HNO_3 are illustrated in Figs.(3.39-3.43).

Inspection of the curves of these Figures, one can observe at first a transition region in which the potential increases (anodic polarization) or decreases (cathodic polarization) slowly with current density following the region there is a rapid linear build up of potential with current density (Tafel region).

Further inspection of the curves of Figs.(3.39-3.43) reveals that, the presence of increasing concentrations of quinazoline compounds cause a decrease in the rate of anodic dissolution reaction i.e. shifting the anodic current - potential curves in the anodic direction. This may be ascribed to a parallel adsorption of the organic molecules over the corroding surface.

From the cathodic polarization curves illustrated in Figs.(3.39-3.43), its clear that the increase of the additives concentration shifts the current- potential curves towards less cathodic potentials. Quinazoline compounds like other adsorption inhibitors, are known to undergo specific adsorption I.e. they adsorb in the inner part of the double layer. In doing so the adsorbed species replace some of the H_3O^+ ion i.e. the additives blocks part of the surface and hence decrease the rate of hydrogen evolution reaction and consequently the rate of the overall corrosion reaction is produced.

The numerical values of the variation of corrosion current density (i_{corr}), corrosion potential (E_{corr}), Tafel slopes (β_a and β_c), degree of surface coverage (θ) and protection efficiency (%IE) with the concentrations of different quinazoline compounds are given in Tables (3.11-3.15).

This indicates that:

1- The cathodic and anodic curves obtained exhibit Tafel-type behavior. Addition of quinazoline compounds increased both cathodic and anodic overvoltages and caused mainly parallel displacement to the more negative and positive values, respectively. This indicates that there is no change in the mechanism of inhibition process.

2- The corrosion current density ($I_{corr.}$) decreases with increasing the concentration of quinazoline compounds, which indicates that the presence of these compounds retards the dissolution of copper in 2M HNO_3 solution and the degree of inhibition depends on the concentration and type of the inhibitors present.

3- The order of increased inhibition efficiency for the additives is:

$$5 > 4 > 3 > 2 > ١ .$$

This is also in agreement with the observed order of corrosion inhibition by the weight-loss method.

4-The data suggest that these compounds act as mixed type inhibitors because they enhance both the anodic and cathodic potentials by the same amount.

5- The corrosion potential ($E_{corr.}$) values shifted to less negative and positive values by increasing the concentration of compounds.

The values of inhibition efficiencies were evaluated using the galvanostatic polarization and weight loss measurements show an agreement and conformity of the experimental results. However,

there are small differences in the values obtained from the two techniques. These difference may be due to the short time taken by the electrochemical measurements.

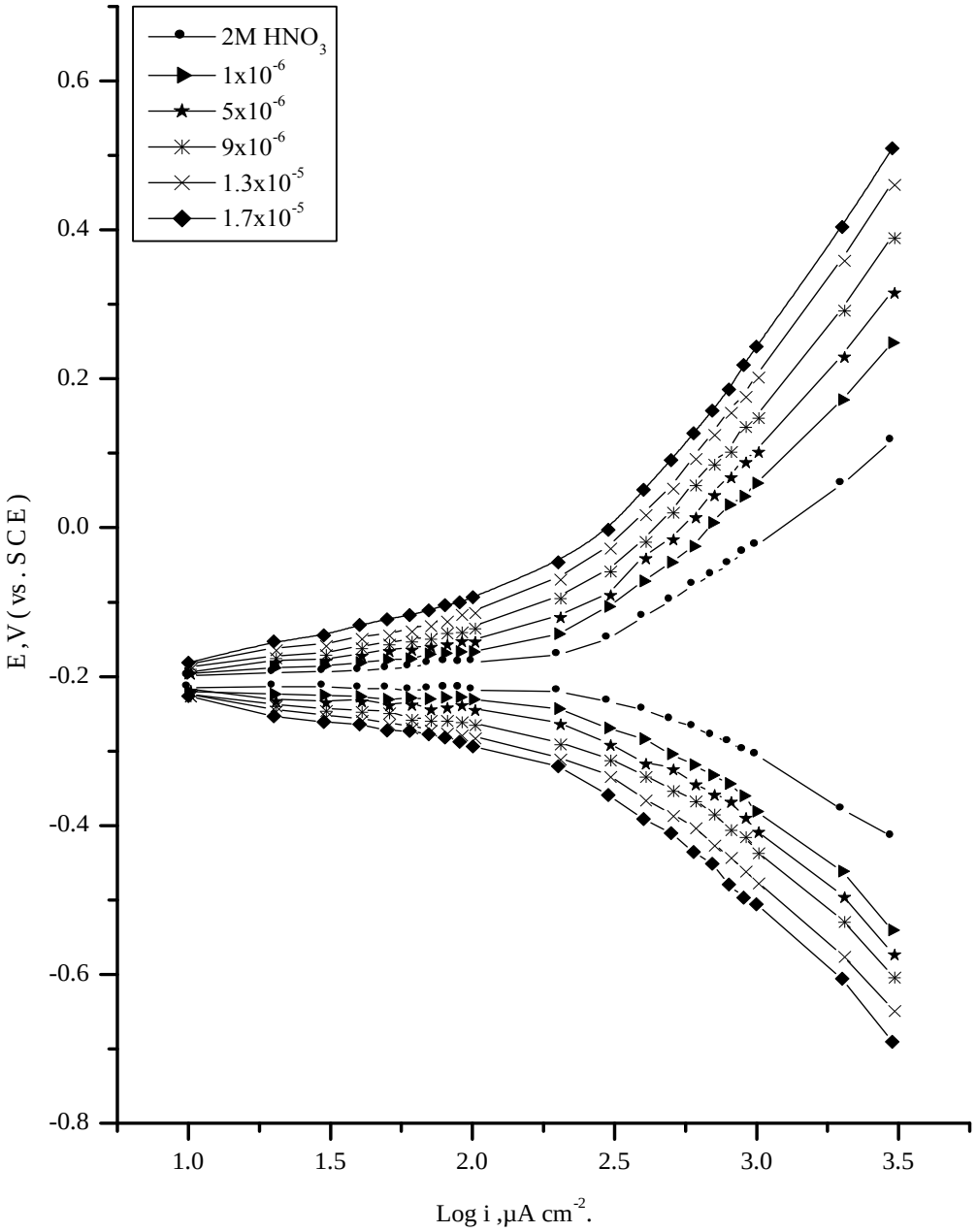

Fig.(3.39): Galvanostatic polarization curves of copper in 2M HNO_3 alone and containing different concentrations of compound (1) at 30°C

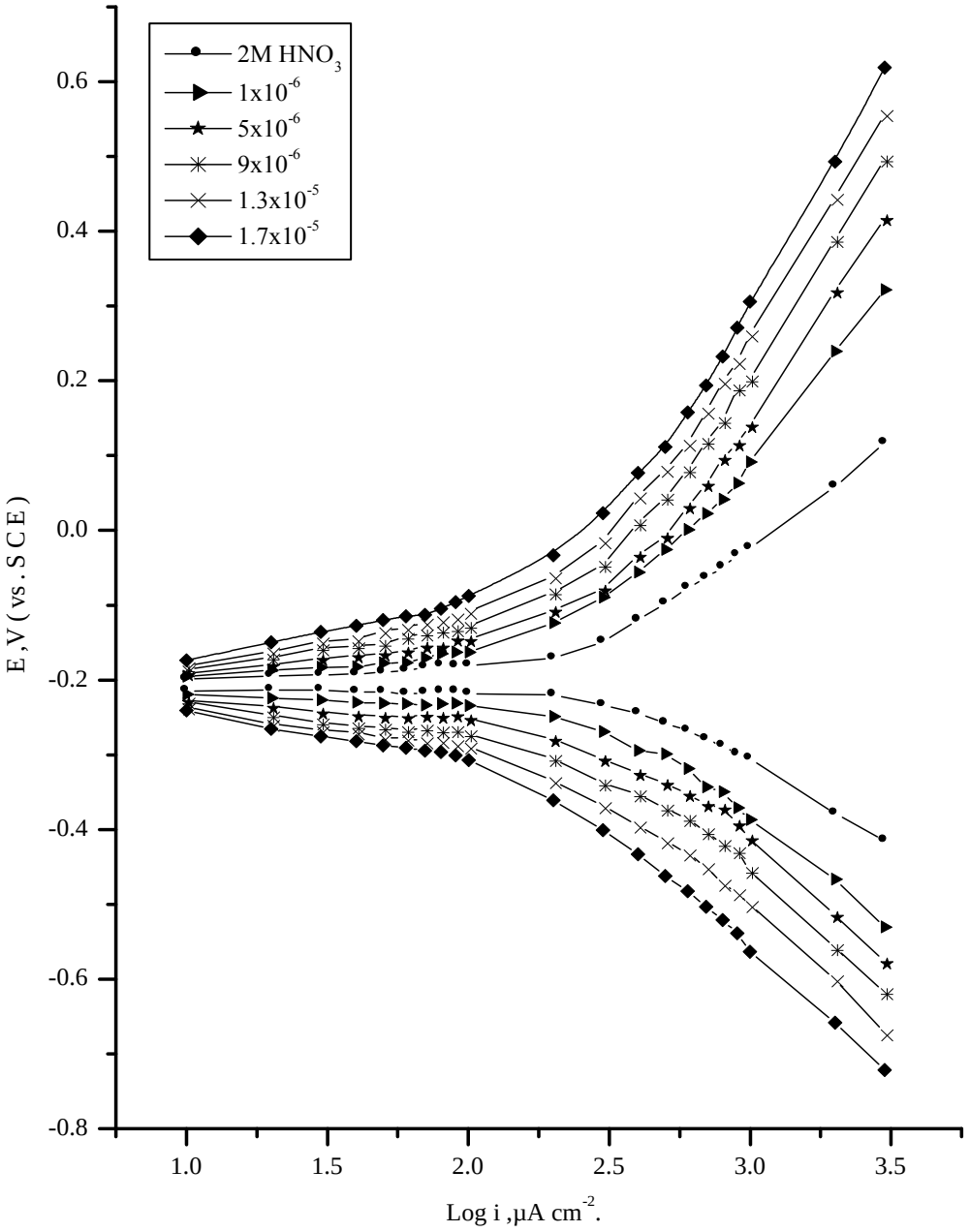

Fig.(3.40): Galvanostatic polarization curves of copper in 2M HNO_3 alone and containing different concentrations of compound (2) at 30°C

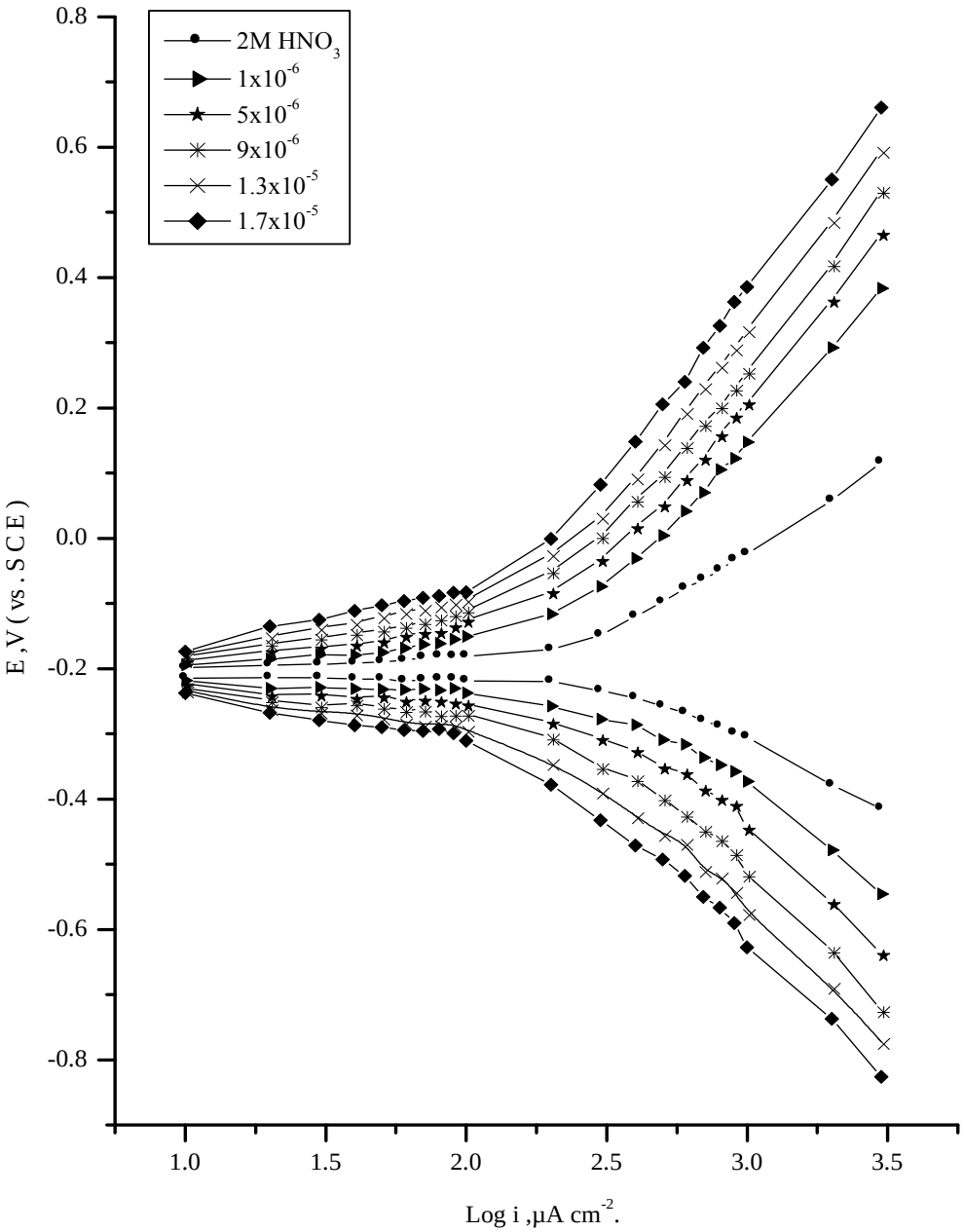

Fig.(3.41): Galvanostatic polarization curves of copper in 2M HNO_3 alone and containing different concentrations of compound (3) at 30°C

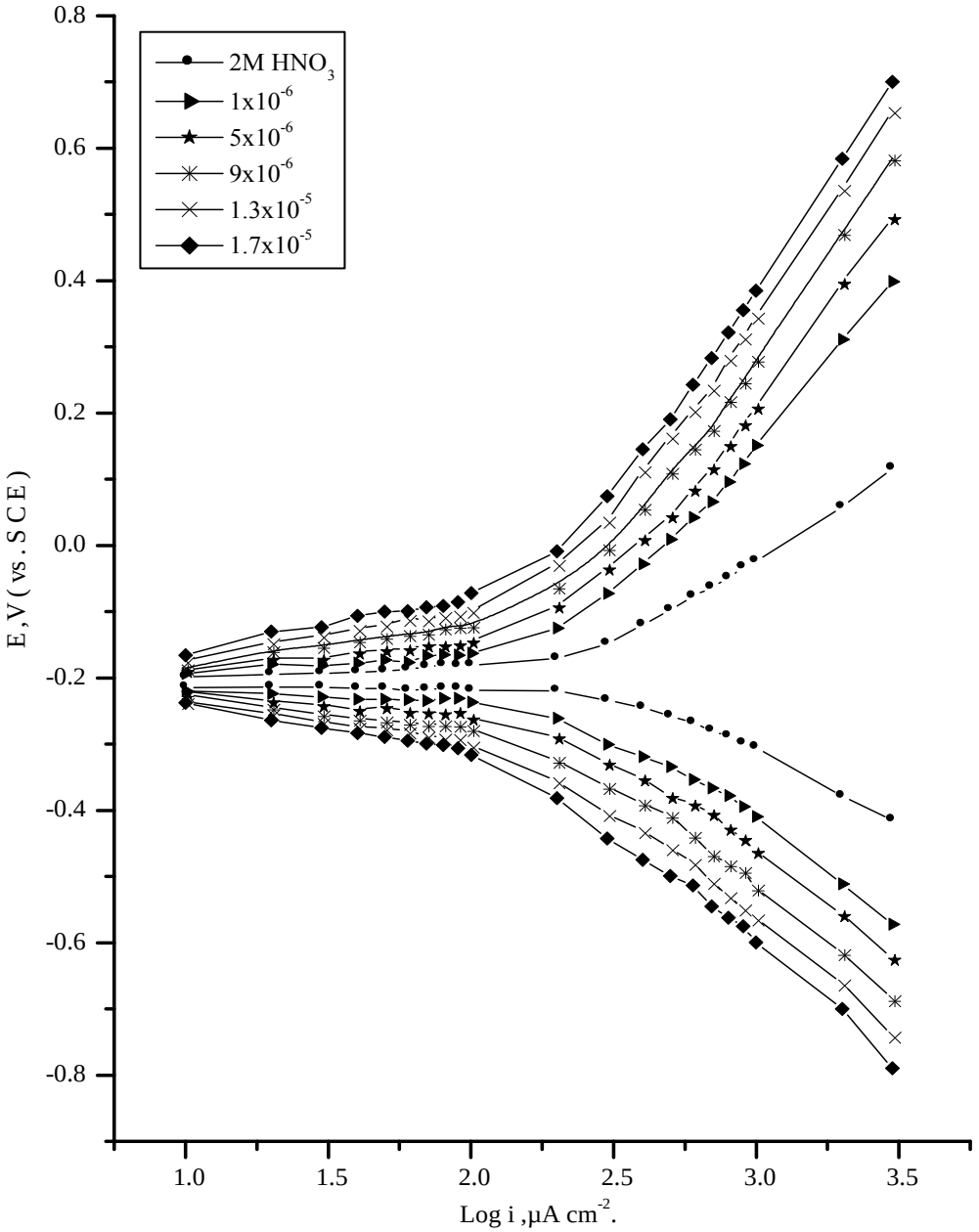

Fig.(3.42): Galvanostatic polarization curves of copper in 2M HNO_3 alone and containing different concentrations of compound (4) at 30°C

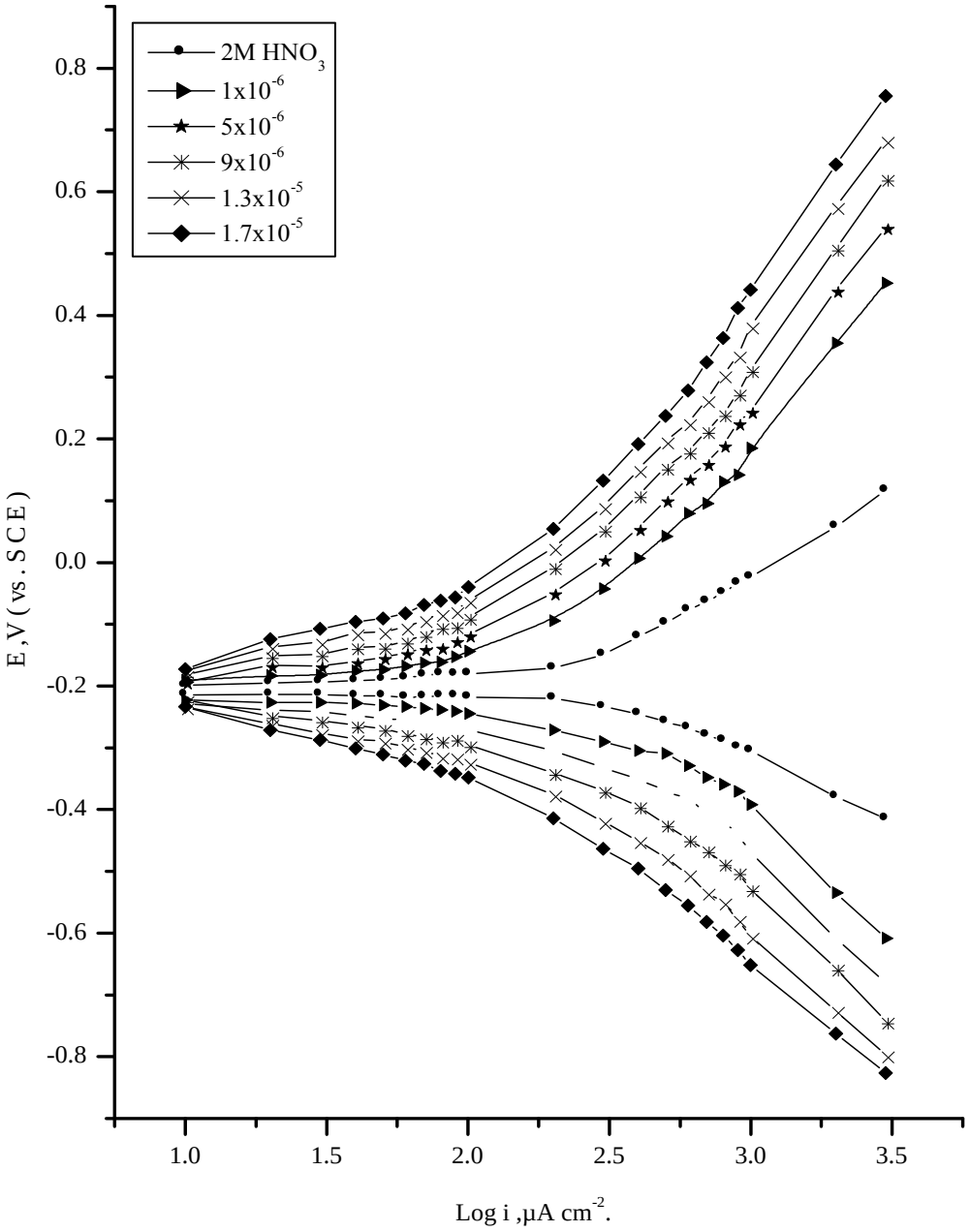

Fig.(3.43): Galvanostatic polarization curves of copper in 2M HNO_3 alone and containing different concentrations of compound (5) at 30°C

Table. (3.11): Corrosion parameters obtained from galvanostatic polarization of copper in 2M HNO_3 containing various concentrations of inhibitor (1) at 30° C.

Conc., M	$-E_{corr}$, m V, (SCE)	I_{corr}, μ A cm^{-2}	βa m V dec^{-1}	-βc m V dec^{-1}	θ	% IE
0.0	0.20	1.92	244	142	---	------
$1x10^{-6}$	0.21	1.44	300	193	0.25	24.85
$5x10^{-6}$	0.22	1.31	359	193	0.32	31.67
$9x10^{-6}$	0.22	1.22	453	275	0.36	36.14
$1.3x10^{-5}$	0.24	1.13	509	261	0.41	40.86
$1.7x10^{-5}$	0.26	1.09	563	302	0.43	42.83

Table. (3.12): Corrosion parameters obtained from galvanostatic polarization of copper in 2M HNO_3 containing various concentrations of inhibitor (2) at 30° C.

Conc., M	$-E_{corr}$, m V, (SCE)	I_{corr}, μ A cm^{-2}	βa m V dec^{-1}	-βc m V dec^{-1}	θ	% IE
0.0	0.20	1.92	244	142	---	------
$1x10^{-6}$	0.19	1.35	303	205	0.29	29.44
$5x10^{-6}$	0.22	1.27	365	199	0.33	33.43
$9x10^{-6}$	0.22	1.17	432	232	0.39	38.56
$1.3x10^{-5}$	0.25	1.11	509	266	0.42	41.86
$1.7x10^{-5}$	0.25	1.02	548	301	0.47	46.59

Table. (3.13): Corrosion parameters obtained from galvanostatic polarization of copper in 2M HNO_3 containing various concentrations of inhibitor (3) at 30° C.

Conc., M	$-E_{corr}$, m V, (SCE)	I_{corr}, μ A cm^{-2}	βa m V dec^{-1}	-βc m V dec^{-1}	θ	% IE
0.0	0.20	1.92	244	142	---	------
$1x10^{-6}$	0.20	1.37	377	234	0.28	28.34
$5x10^{-6}$	0.22	1.26	452	249	0.34	34.09
$9x10^{-6}$	0.22	1.12	501	303	0.42	41.59
$1.3x10^{-5}$	0.22	1.00	550	343	0.48	47.65
$1.7x10^{-5}$	0.26	0.95	627	331	0.50	50.21

Table. (3.14): Corrosion parameters obtained from galvanostatic polarization of copper in 2M HNO_3 containing various concentrations of inhibitor (4) at 30° C.

Conc., M	$-E_{corr}$, m V, (SCE)	I_{corr}, μ A cm^{-2}	βa m V dec^{-1}	-βc m V dec^{-1}	θ	% IE
0.0	0.20	1.92	244	142	---	------
$1x10^{-6}$	0.20	1.24	360	180	0.35	35.19
$5x10^{-6}$	0.20	1.16	408	226	0.39	39.10
$9x10^{-6}$	0.21	1.07	468	297	0.44	43.78
$1.3x10^{-5}$	0.22	0.95	517	312	0.50	50.05
$1.7x10^{-5}$	0.24	0.88	577	334	0.54	53.82

Table. (3.15): Corrosion parameters obtained from galvanostatic polarization of copper in 2M HNO_3 containing various concentrations of inhibitor (5) at 30° C.

Conc., M	$-E_{corr}$, m V, (SCE)	I_{corr}, μ A cm^{-2}	βa m V dec^{-1}	-βc m V dec^{-1}	θ	% IE
0.0	0.20	1.92	244	142	---	------
$1x10^{-6}$	0.20	1.18	388	193	0.38	38.36
$5x10^{-6}$	0.20	1.02	426	249	0.47	46.54
$9x10^{-6}$	0.18	0.92	450	320	0.52	52.00
$1.3x10^{-5}$	0.22	0.85	527	346	0.55	55.27
$1.7x10^{-5}$	0.25	0.75	579	343	0.61	60.93

SECTION (C)

INITIATION AND INHIBITION

OF PITTING CORROSION OF COPPER

3.7-Introduction

Pitting corrosion is the major factor limiting the use of major industrial materials such as stainless steels, copper and aluminum alloys, causing significant damages both in terms of material loss and resultant accidents.

Pitting corrosion is probably the most insidious corrosion since it concentrates on a very small area of materials and often leads to serious accidents without any indication.

Copper have a good anti-corrosion properties in atmosphere and some acidic and alkaline solutions. However, they are subject to localized corrosion problems such as pitting corrosion, intergranular corrosion and stress corrosion cracking. Among these forms of corrosion, pitting corrosion is the most dangerous one.

It is generally believed that although there are still controversies about the pitting mechanisms, pitting is initiated through the local breakdown of the protective passive film due to specific interaction of the film and the corrosive ions in the environment. Once the destruction of the passive film exposes the vulnerable base copper, the dissolution of bare metal is confined to this small region, resulting in the formation of pits of

various geometries. The composition and structure of the passive film are of great importance in the pitting process. Correspondingly, much work has been done to improve the performance of the passive film and increase the resistance of copper to pitting corrosion. The aim of the present work is to initiate the pitting corrosion of copper in 0.1M HNO_3 by addition of NaCl and its inhibition by quinazoline compounds.

3.8- Susceptibility of copper to pitting corrosion by chloride ions

Pitting corrosion of copper as other metal and alloys occurs when passivity break down takes place points on the surface exposed to the corrosive environments at which anodic dissolution proceeds whilst the major part of the surface remains passive.

Fig .(3.44) represents the potentiodynamic anodic polarization curves of copper electrode in 0.1M HNO_3 containing different concentrations of NaCl as a pitting corrosion agents at a scanning rate 1mV/sec.

The slow scan rate permits that the pitting initiation occurs at less positive potential [59]

Its clear that from Fig.(3.2٠) ,the higher Cl^- ion concentration results in a sudden and marked increase of current density at some definite potentials denoting the destruction of the passive film and initiation of visible pits [60]. This potential is known a critical pitting potential (E_{pitt}) as the chloride ion concentrations increases the pitting potential is shifted to

more negative (active) direction. This indicates that the destruction of passive film and initiation of pitting corrosion. This effect could be attributed to adsorption of the aggressive anions on the bare metal surface [61,62].

Examination of the electrode surface often polarization experiments showed visible pits whose number per unit area increase with the increase of Cl^- ion content in the solution. The break down of passivity could be attribute to the adsorption of chloride ions on the passive film formed on the copper surface, which create an electrostatic field across film/solution interface [63,64] .Thus, when the electrostatic field reaches a certain value, the adsorbed anions begin to penetrate into the passive film and the pitting corrosion is initiated.

The depended of the pitting corrosion potential of copper electrode on the concentration of Cl^- ion can be clearly seen in Fig.(3.45). This figure represents the plot of pitting potential $E_{pitt.}$ Vs. the logarithm of chloride ion concentration. Straight line relationships were obtained satisfying the following equation:

$$E_{pitt.} = a_1 - b_1 \log C_{Cl^-} \qquad (3.12)$$

Where a_1 and b_1 are constants which depend on both the nature of the electrode and type of aggressive anions. As the concentration of chloride ions increases the pitting potential is shifted to more negative direction indicating the destruction of passive film and initiation of pitting corrosion.

The differentiation between pit initiation and pit propagation is well explained by Aziz and Godard [65]. A pit can be started by artificial

stimulation at otherwise normal sites on the metal surface. Yet continue to propagate if given the right environmental conditions. This concept has been widely used to explain pitting corrosion phenomena.

Hoars et al. [66] related pit initiation on a supposed oxide film, followed by their penetration through the film (without exchange) under the influence of an electrostatic field across the film solution interface. When the latter field reaches a certain critical value, corresponding to the pitting potential, pitting occurs, and the oxide film is presumably undetermined either by vacancy condensation at the metal interface, or it releases cations rapidly at the electrolyte interface so that in either cases pitting proceeds. The introduction period for pitting to occur is related to the time required for supposed penetration of the ions through the oxide film. Regarding this mechanism Leckie and Uhlig[67] argued that, if this is correct, either anion of large molecular size than the halogen ions e.g. SO_4^{2-}, ClO_4^-, NO_3^- and OH^-, which are practically having no pitting tendency, can also penetrate the passive oxide film causing the formation of pit.

The later author [67] proposed another model based on the visible competitive adsorption of the aggressive ions with oxygen for adsorption sites on the metal surface. This model is based on the assumption that adsorbed oxygen rather than oxide is the cause of passive formation. Oxygen has normally higher affinity than Cl^- ions for adsorption sites on the metal surface, but as the potential of the working electrode is shifted into the passive direction, higher Cl^- ions move into the double layer when the concentration of the latter reaches a certain definite value,

corresponding to the pitting potential, it succeeds at favored sites in destroying passivity by displacing adsorbed O_2 ions. The introduction time for pitting is attributed here to the slow process of competitive adsorption. It is of interest to mention that similar view were also, reported by Kolotryrkin[60], Rosenfeld[68] and Schwenk et al[69].

It contrast to the model of competitive adsorption, Foroulis and Thubriker[70] based their argument on the findings that, the critical pitting potential of the polarized depends on the thickness of oxide film at the metal surface. They concluded that, if competitive adsorption at the metal surface the controlling mechanism, then the thickness of any overlying oxide would have no influence on the critical potential at which the Cl^- ions displace the adsorbed oxygen on the metal bare.

Abd El-Haleem [71] assumed that the initiation of pitting on Zn-Ti-Cu alloy involves, as a rate controlling step, the adsorption of chloride ions on a layer of mixed oxide/hydroxide of Zn, Ti and or Cu followed by the formation of the corresponding chloro-metal oxide or hydroxide complexes. The deadly soluble of these complexes can go into solution, most probably the Zn complexes as soluble Zn^{2+}. These result in pit initiation with the continues anodic dissolution of Zn^{2+} at the point of attack. This latter model was confirmed by the use of the electron microscope analyzer of performed pits.

3.9-Inhibition of Pitting Corrosion of Copper

Organic compounds have been successfully applied for the inhibition of general corrosion of materials, inhibition efficiency is assumed to be proportional to the adsorption density of organics present. The pitting corrosion, however, is a complicated localized corrosion phenomenon and the relationship between adsorption and inhibition is not obvious. The adsorption of organic molecules on metal surfaces has been studied by various methods such as potential current step technique, electrochemical impedance spectroscopy, radiotracer, scanning tunneling microscopy, atomic force microscopy and batch adsorption with powder .However, to elucidate the relationship between adsorption and corrosion inhibition, direct and quantitative measurement of adsorption density of organic compounds is needed.

Besides, in developing the mechanisms of corrosion inhibition, the role of changes in the interfacial charge of the material due to adsorption of organic compounds has been largely neglected. However, the interfacial charge can determine the adsorption of charged organic molecules and inorganic ions therefore affect the corrosion or corrosion inhibition significantly.

3.10-Inhipition of pitting corrosion of copper by quinazoline compounds.

The primary step in the action of corrosion inhibitors in NaCl solution usually is adsorption of inhibitors on the metal surface [72]. The

adsorption process depends upon electronic characteristic of the inhibitors, the nature of surface, temperature and pressure of the reaction, steric effect, multiplayer adsorption and adsorption and the degree of surface activity.

Figs.(3.46-3.50) represent the effect of the addition of increasing concentrations of some quinazoline derivatives on the potentiodynamic anodic polarization curve of copper electrode in 0.1M HNO_3 + 0.001M NaCl at a scanning rate of 1mV/sec. It was found that the pitting potential of the copper electrode is shifted to more positive (noble) direction with increasing the concentration of additives. This indicates that increased resistance to pitting attack.

Fig. (3.51) represents the relationship between pitting potential and the logarithmic of the molar concentration of the added compounds. Straight lines were obtained and the following conclusion can be drawn:

a) An increase of inhibitor concentration causes the shift of the pitting potential into more positive values in accordance with the following equation:

$$E_{pitt.} = a_2 + b_2 \log C_{inh.} \qquad (3.13)$$

where a_2 and b_2 are constants which depend on both the composition of additives and the nature of the electrode.

b) Inhibition afforded by these compounds using the same different concentrations of the additives decreases in the following order:

٥ >4 > 3 > 2 > 1

The adsorption of organic compounds may be due to:

I) Electrostatic attraction between charged metal.

II) Interaction of unshared electron pair in the molecule with the metal.

III) Interaction of electron with the metal.

IV) Or a combination of the above.

The adsorbed molecule can then retarded the anodic and cathodic corrosion reaction. Also, the adsorbed molecule may be inhibit the pitting corrosion by shifted the critical pitting potential to more noble value by one or a combination of the following mechanisms:

I) Forming a physical barrier layer between metal and coordinate.

II) Reducing the metal reacting through an alteration in the nature of metal surface.

III) Changing the structure of the metal solution interface.

However, inhibition efficiency of additive compounds depends on many factors, including the number of adsorption active centers in the molecule and their charge density, molecular size, mode of adsorption, heat of hydrogenation and formation of metallic complexes.

The results obtained in this part revealed that inhibition of pitting corrosion of copper by quinazoline derivatives as indicated from potentiodynamic anodic polarization was found to depend on the concentration and nature of inhibitor. The values of pitting corrosion potential ($E_{pitt.}$) were shifted to more noble value as the concentration of inhibitor increases. These results indicated the inhibiting effect of such compounds toward the pitting corrosion.

Also, the inhibition of pitting corrosion by organic compounds is assumed to occur as a result of the following processes:

a) Competitive adsorption sites on the metal surface occurs, a shift of the pitting potential to noble direction which required to enable the chloride ions to reach a concentration in the double layer sufficient to overcome the inhibiting action of amino group, there by destroying the passivity and initiation of pitting corrosion occurs.

b) The presence of nitrogen and oxygen atoms makes the adsorption take place through the transfer of its lone pair of electron to the metal surface forming coordinate type linkage.

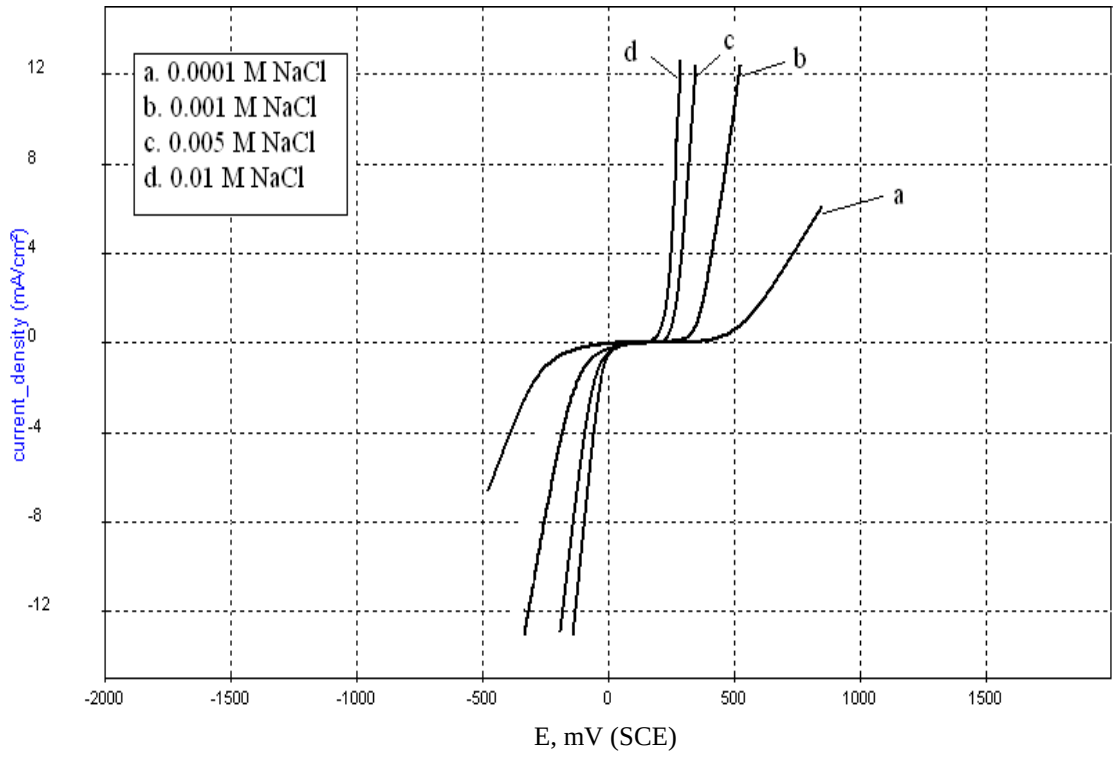

Fig.(3.44): Potentiodynamic anodic polarization curves of copper in 0.1M HNO_3 + different concentrations of NaCl.

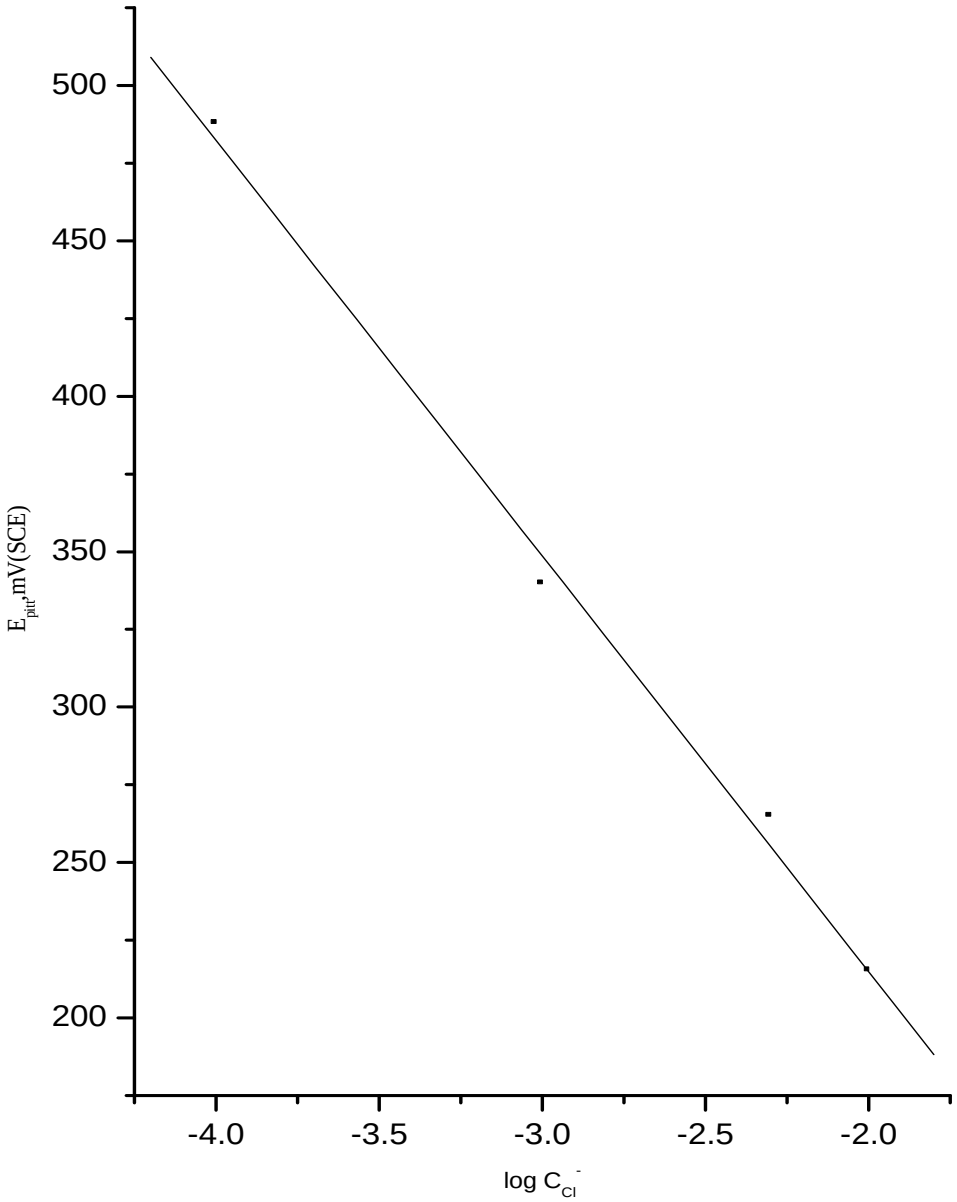

Fig.(3.45): The relationship between pitting corrosion potential of copper and logarithm concentration of NaCl

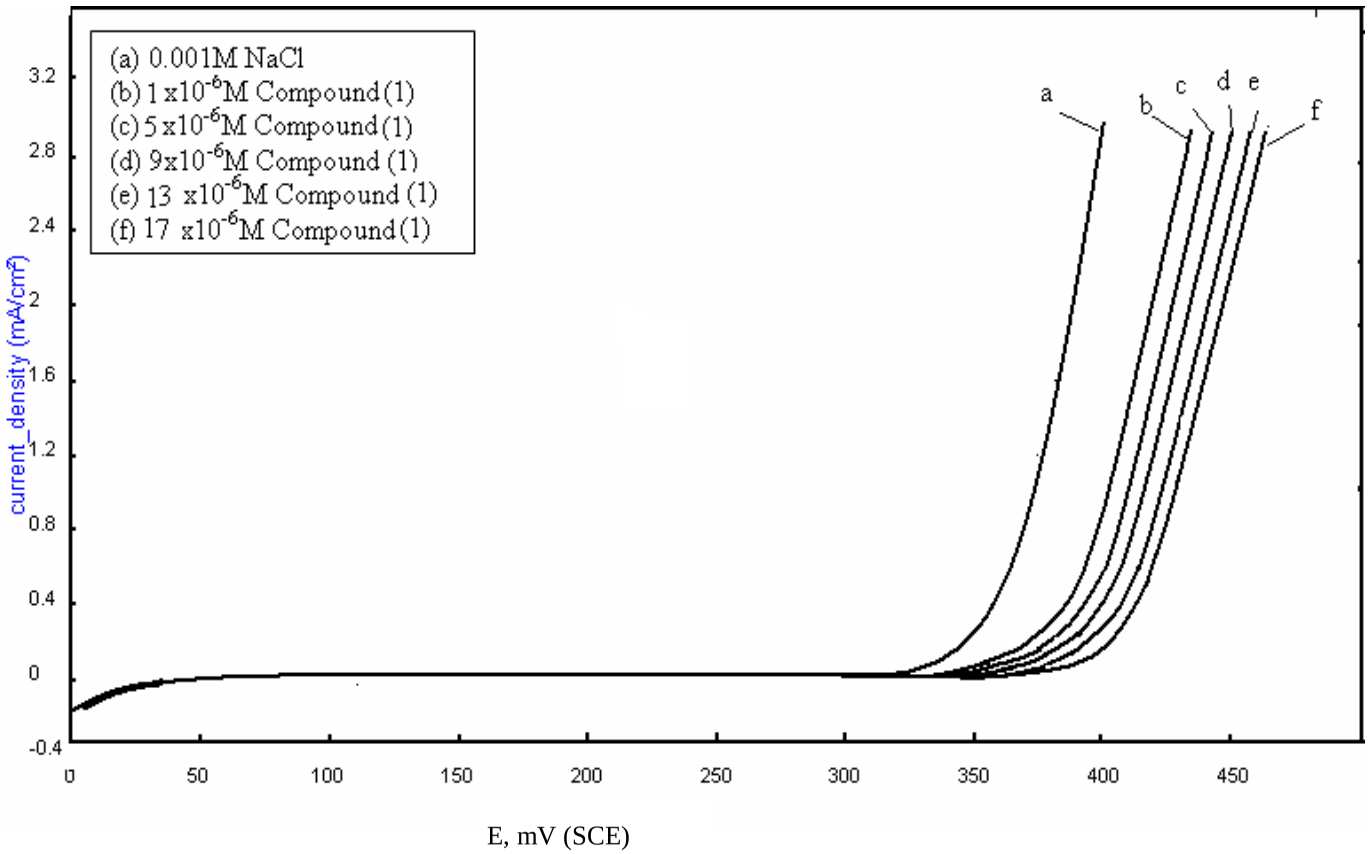

Fig .(3.46): Potentiodynamic anodic polarization curves of copper in 0.1M HNO_3 + 0.001M NaCl containing different concentrations of compound (1)

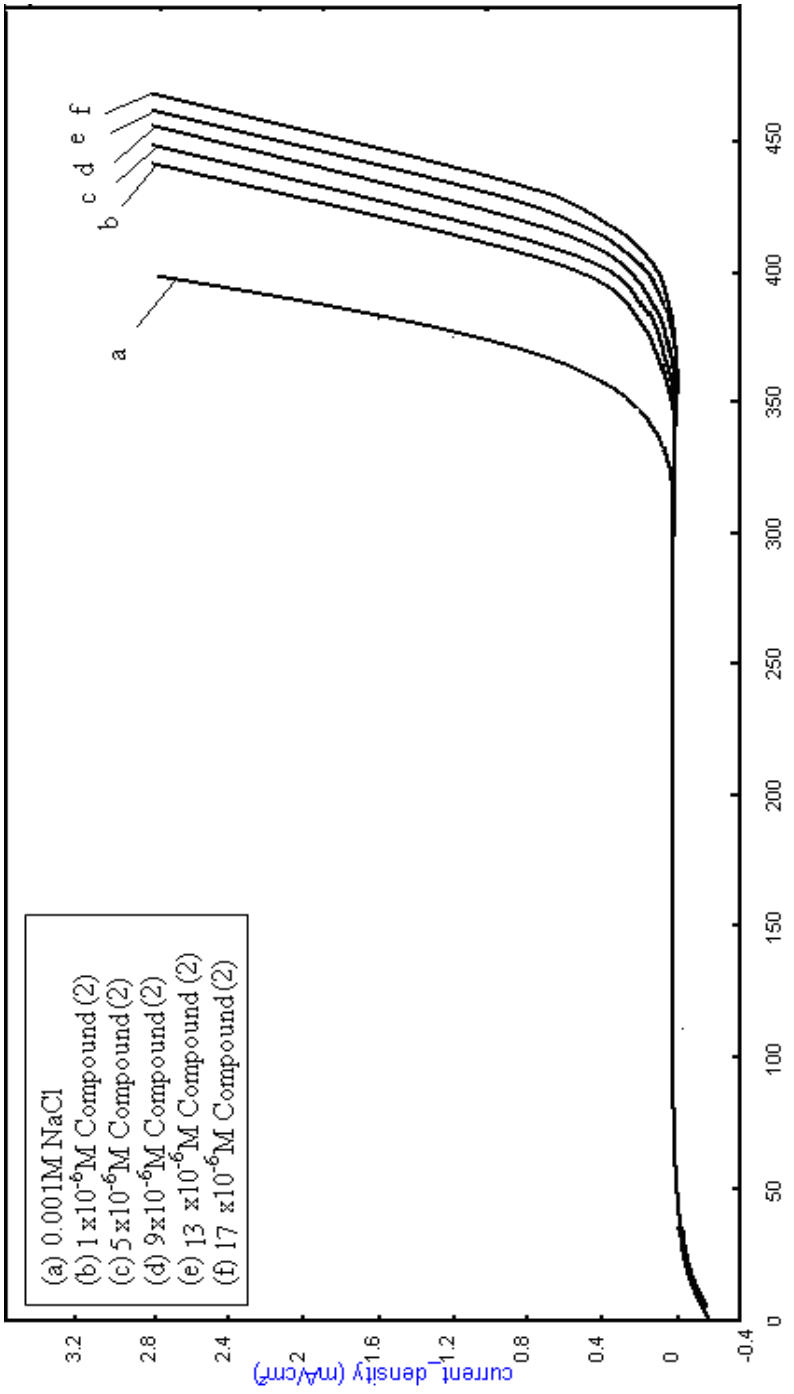

Fig .(3.47): Potentiodynamic anodic polarization curves of copper in 0.1M HNO_3 + 0.001M NaCl containing different concentrations of compound (2)

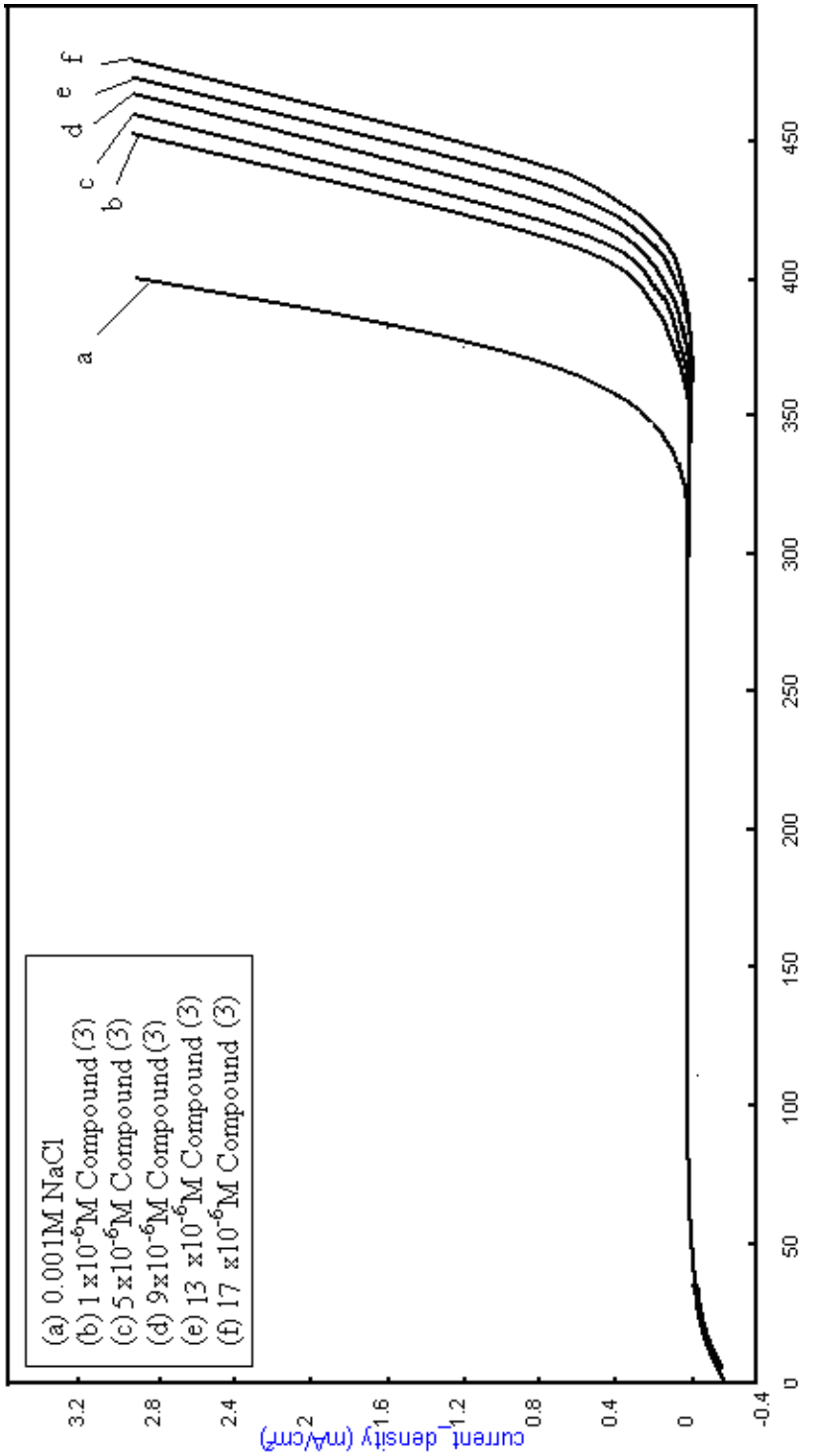

Fig .(3.48): Potentiodynamic anodic polarization curves of copper in 0.001M NaCl + 0.1M HNO_3 containing different concentrations of compound (3)

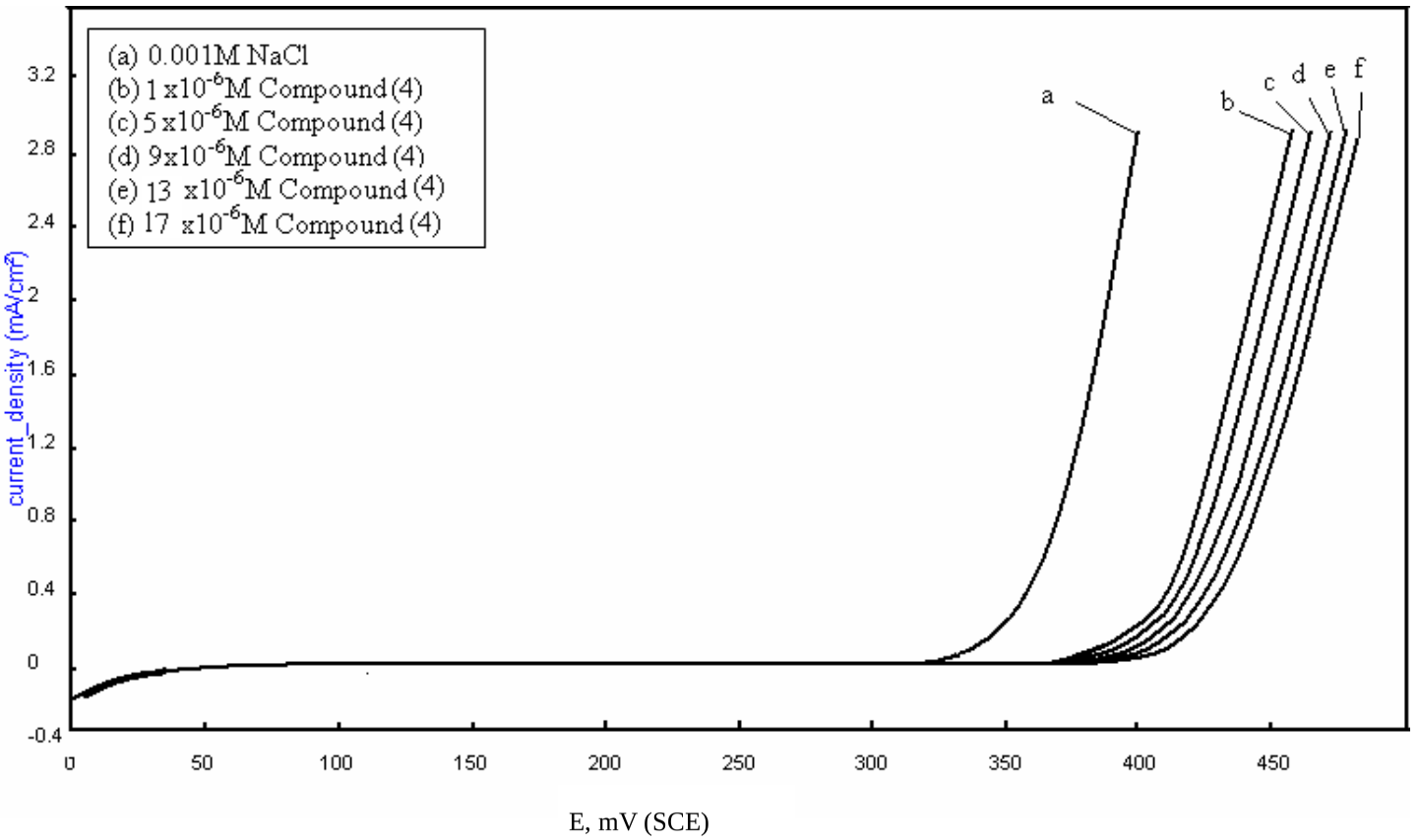

Fig .(3.49): Potentiodynamic anodic polarization curves of copper in 0.1M HNO_3 + 0.001M NaCl containing different concentrations of compound (4)

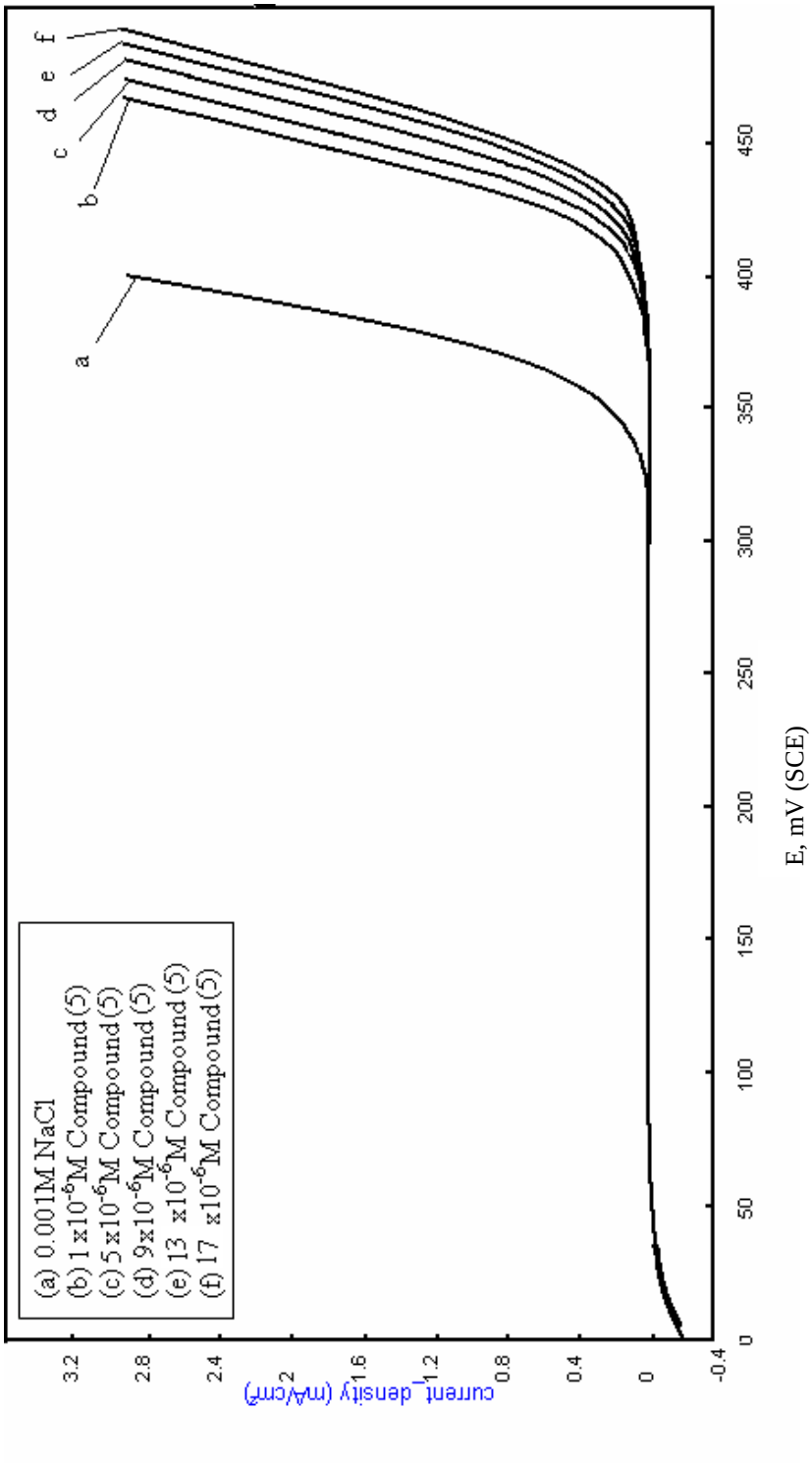

Fig .(3.50): Potentiodynamic anodic polarization curves of copper in 0.1M HNO_3 + 0.001M NaCl containing different concentrations of compound (5)

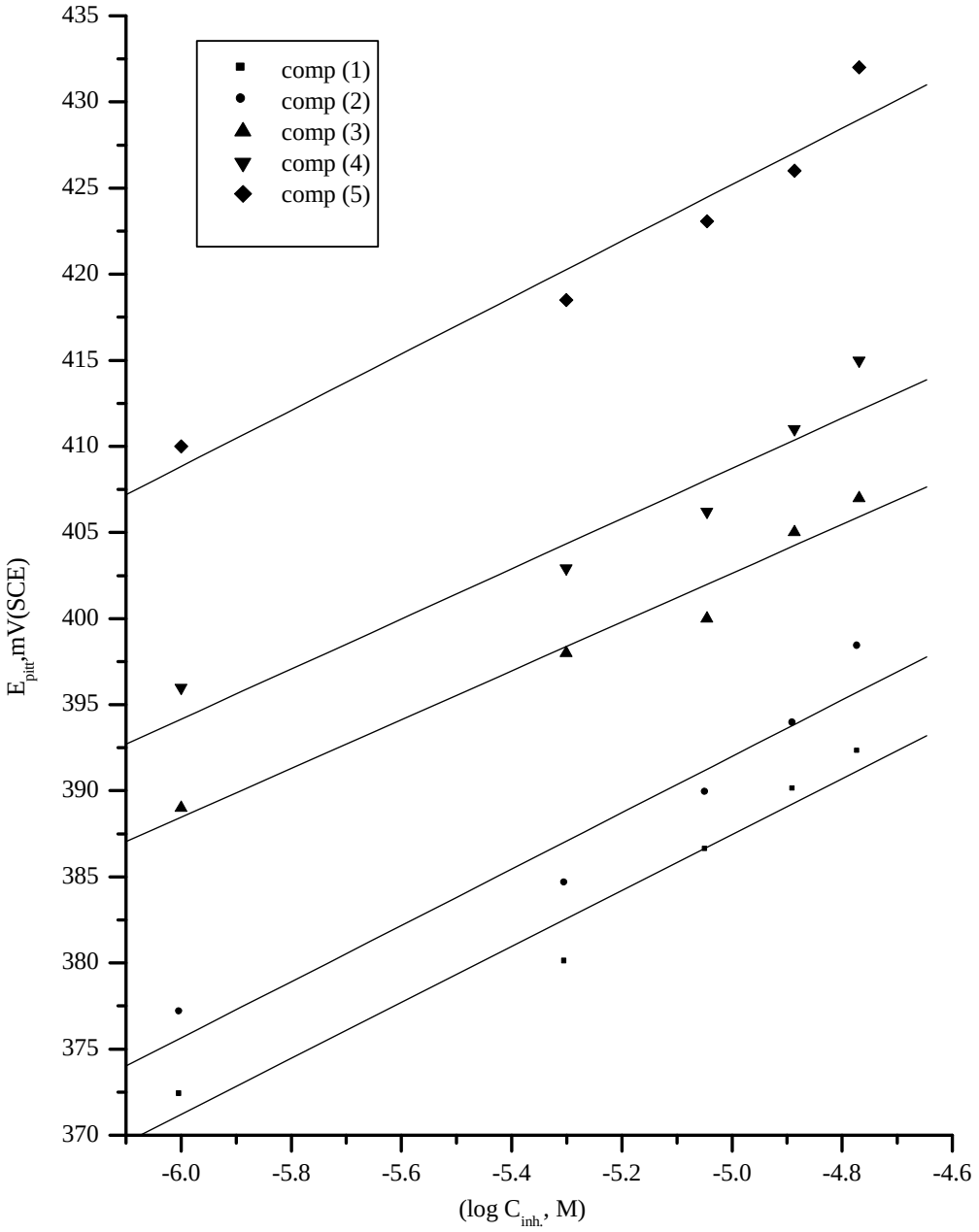

Fig(3.51): The relationship between pitting corrosion potential of copper and logarithm concentration of the inhibitors in presence of 0.001M NaCl

3.11- CHEMICAL STRUCTURE OF THE INHIBITORS AND CORROSION INHIBITION

Inhibition of the corrosion of copper in nitric acid solutions by some quinazoline compounds is determined by weight loss, galvanostatic polarization and by potentiodynamic anodic polarization measurements, was found to depend on the concentrations, the mode of adsorption of the inhibitors, stability of these derivatives in acidic solution, nature of metal and surface conditions.

Skeletal representation of the proposed mode of adsorption of the investigated quinazoline compounds as shown in Fig.(3.52) and clearly indicates the active adsorption centers in the quinazoline derivatives.

The surface coordination is through the oxygen and nitrogen atom attached to the ring. It was concluded that the mode of adsorption depends on the affinity of the metal towards the π-electron clouds of the ring system [73]. Metals such as Cu and Fe, which have a greater affinity towards aromatic moieties, were found to adsorb benzene rings in flat orientation. Thus, it is reasonable to assume that the tested inhibitors are adsorbed in a flat orientation through the n and o atoms as shown in Fig.(3.52).

The order of decreasing the percentage inhibition efficiency of the investigated inhibitors in the corrosive solutions was as follow:

5 > 4 > 3 > 2 > ١

All compounds have two adsorption active centers, so, the number of active center has no effect. Compound (5) is the most efficient inhibitor because of increased molecular size (318) and presence of one more benzene ring in the molecule. Compound (4) comes next in the sequence of decreased inhibition efficiency, because of its lower molecular size (232). Compound (3) comes after compound (4) in the sequence of decreased inhibition efficiency. This is due to its lower molecular size (230) and N atom less basic than s atom in compound (4). Compound (2) has lower molecular size (216) than compound (3), so, it comes after it in inhibition efficiency . Compound (1) is the least effective inhibitor. This is due to its lower molecular size (217) and O atom is less basic than N atom.

The order of inhibition efficiency of the investigated compounds was revealed by the weight loss and further confirmed by galvanostatic polarization measurements. The agreement among these techniques proves the validity of results obtained and supports the explanation given for the effect of chemical structure on the inhibition action of the investigated compounds, which contributes л electrons to the adsorption active centers and hence increases the electron density on the adsorption centers.

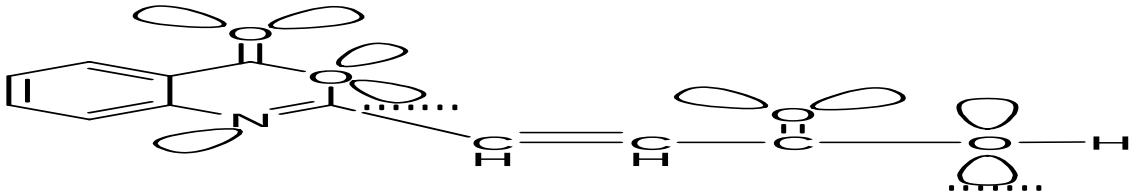

Comp. (1)

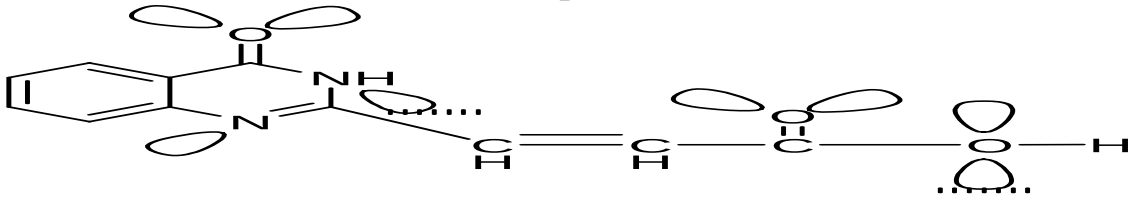

Comp. (2)

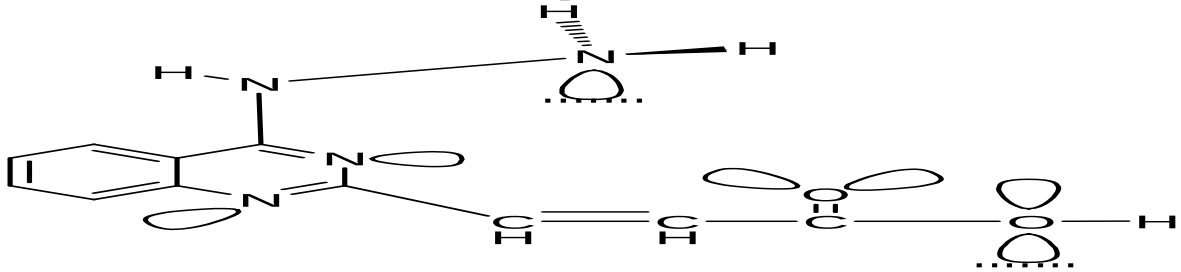

Comp. (3)

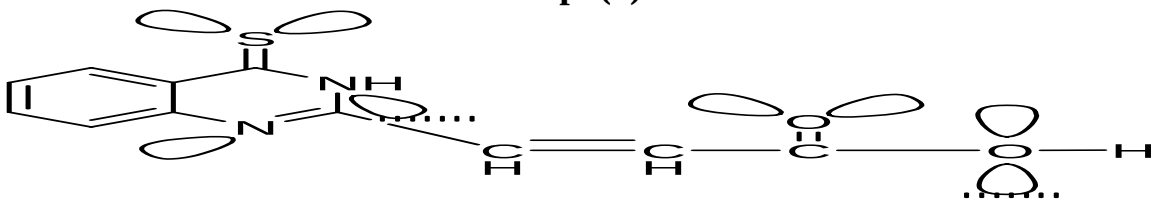

Comp. (4)

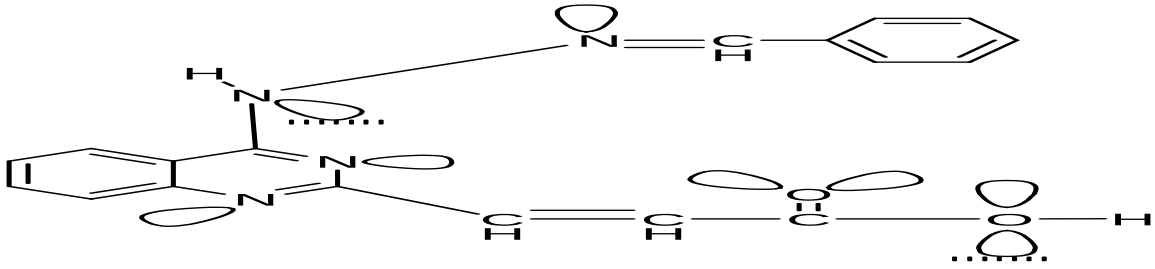

Comp. (5)

Fig .(3.52): Skeletal representation of the mode of adsorption of all quinazoline compounds.